BEDROCK STRENGTH CONTROLS ON THE VALLEY MORPHOMETRY OF BIG CREEK, VALLEY AND IDAHO COUNTIES, CENTRAL IDAHO

ZACHERY M. LIFTON

In presenting this thesis in partial fulfillment of the requirements for an advanced degree at Idaho State University, I agree that the Library shall make it freely available for inspection. I further state that permission for extensive copying of my thesis for scholarly purposes may be granted by the Dean of Graduate Studies, Dean of my academic division, or by the University Librarian. It is understood that any copying or publication of this thesis for financial gain shall not be allowed without my written permission.

Signature Zach Tifton

Date 9-15-05

BEDROCK STRENGTH CONTROLS ON THE VALLEY MORPHOMETRY OF BIG CREEK, VALLEY AND IDAHO COUNTIES, CENTRAL IDAHO.

by

Zachery M. Lifton

A thesis submitted in partial fulfillment

of the requirements for the degree of

Master of Science in Geology

Idaho State University

2005

To the Graduate Faculty:

The members of the committee appointed to examine the thesis of ZACHERY M. LIFTON find it satisfactory and recommend that it be accepted.

Dr. Glenn D. Thackray, Major Advisor

Dr. Nancy F. Glenn, Committee Member

Dr. Paul K. Link, Committee Member

Dr. Robert Van Kirk, Graduate Faculty Representative

ACKNOWLEDGEMENTS

Many people have influenced and helped me on my way to this point. My parents, Alan and Susan Lifton, have supported and guided me more than I can describe here. I could not imagine having cooler, more loving, or more understanding parents. They showed me that the world is a crazy place and a sense of humor will help you get through it. My older brother, Josh Lifton, has been my friend, companion, and role model since I can remember. I will always look up to him. My grandparents, Leo and Ruth Lifton, have always helped me put things into proper perspective.

Sifu Gary Mitchell has taught me what hard work really is and how much potential a human has. His commitment to kung fu is amazing. Sensei Sami Tadehara and Sensei Nobuhiro Imanaka shared their knowledge of Judo with me and helped me live a fuller life.

Thanks to my long-time friends Benny, Dorje, Anneli, and Schwam for always being around, and to all my friends here in the department: Sean, Steve, Martin, Luke, Nagendra, Adrian, Sharon, John, Renee, Brad, Andrew, Charlie, and Garrett – it was fun sharing graduate school with you.

Glenn Thackray, despite having many irons in the fire, always provided conversations that got to the core of this research project. Paul Link first suggested working on Big Creek and has been enthusiastic about the project every since then. He was also the first to convince me to come to ISU, and I haven't regretted it! If it wasn't for his enthusiasm and sense of humor, I may not have lasted long in school. Nancy Glenn always had time to talk to me and answer questions, despite living 250 miles away! Her work ethic is inspiring and difficult to live up to. Rob Van Kirk patiently helped me with data analysis and greatly strengthened the project.

Thanks also to the crew in the office: Melissa, Connie, Bobbie, and Dawn, who always watched out for me and helped me when I didn't have a clue.

Jim and Holly Akenson made me feel welcome at Taylor Ranch and provided important local insight on Big Creek. I was assisted in the field by Cody McCoy, Josh Lifton, and Cinnamon Robinson. Dave Stewart and Reed Lewis know the geology of Big Creek better than anyone and kindly allowed me to use their maps. Discussions with them helped me very much. Thanks to Carol, Ray, and Walt at Arnold Aviation in Cascade for flying me around the heart of the wilderness; they are skilled professionals.

Funding for this project was provided by the NASA Idaho Space Grant Consortium Experimental Program to Stimulate Competitive Research (EPSCoR) Grant #FPK302-02. I was supported during my time at ISU by a research assistantship from the Idaho Department of Water Resources and a graduate fellowship from the National Science Foundation GK-12 Project. Their support is greatly appreciated.

TABLE OF CONTENTS

Photocopy and Use Authorization	i
Title Page	ii
Committee Approval	iii
Acknowledgements	iv
Table of Contents	v
List of Figures	vii
List of Tables	viii
Abstract	ix
Chapter 1: Introduction	1
1.1 Problem Statement	1
1.2 Background	1
1.2.1 Processes and Mechanisms of Fluvial Erosion	1
1.2.2 Formation of Valley Floor Width	6
1.2.2.1 Erosive Processes of Valley Widening	7
1.2.3 Rock Strength and the Schmidt Hammer	9
1.2.4 Spatial and Temporal Scales	13
1.3 Approach	14
Chapter 2: Study Area	16
2.1 Regional Setting	16
2.1.1 Topography and Tectonics	16
2.2 Big Creek Drainage Basin	20
2.2.1 Basin Parameters	20
2.2.2 Geology	20
2.2.2.1 Description of Map Units	23
2.2.2.1.1 Mesoproterozoic quartzites and siltites	23
2.2.2.1.2 Neoproterozoic mafic intrusions	25
2.2.2.1.3 Tertiary intrusive granodiorites	25
2.2.2.1.4 Tertiary Challis Volcanic Group tuffs and porphyry dikes	28
2.3 Reach Descriptions	29
2.3.1 Little Ramey Creek (Reach #1)	31
2.3.2 Bar Creek Reach (Reach #2)	32
2.3.3 Acorn Creek Reach (Reach #3)	32
2.3.4 Soft Boil Bar Reach (Reach #4)	33
2.3.5 Dacite Gorge Reach (Reach #5)	33
2.3.6 Vines Reach (Reach #6)	34
2.3.7 Doe Creek Reach (Reach #7)	34
2.3.8 Cabin Creek Reach (Reach #8)	35
2.3.9 Lobauer Reach (Reach #9)	36
2.3.10 Cougar Creek Reach (Reach #10)	37
2.3.11 Big Creek Gorge Reach (Reach #11)	37
2.3.12 Breeching Creek Reach (Reach #12)	38

2.3.13 Bighorn Bridge Reach (Reach #13) 39

Chapter 3: Methods 40
3.1 Introduction 40
3.2 Reach Delineation 40
3.3 Rock Strength 41
3.3.1 In Situ Measurements Using the Schmidt Hammer 41
3.4 Valley Morphometry 45
3.4.1 Valley Floor Width 45
3.4.2 Stream Gradient 47
3.4.3 Hillslope Gradient 47
3.4.4 Hypsometric Analysis 48
3.5 Data Analysis 49

Chapter 4: Results and Interpretation 51
4.1 Schmidt Hammer Rebound Data 51
4.2 Valley Floor Width 56
4.3 Stream Gradient 61
4.4 Hillslope Gradient 65
4.5 Hypsometric Analysis 69
4.6 Summary of Results 71

Chapter 5: Discussion 73
5.1 Introduction 73
5.2 Bedrock Strength 73
5.2.1 Aspect Variability 73
5.2.2 Lithology 74
5.3 Valley Floor Width 75
5.4 Stream Gradient 77
5.5 Hillslope Gradient 82
5.6 Implications for the Use of the Schmidt Hammer in a Geomorphic Context 83
5.7 Conclusions 84
5.8 Future Work 85

Appendix A: GIS Methods 88
Appendix B: Schmidt Hammer Rebound Data 93
Appendix C: Alternative Stream Gradients 114

References 120

LIST OF FIGURES

Figure 1. Diagram of plucking	5
Figure 2. Diagram of abrasion	6
Figure 3. Photo Big Creek valley	8
Figure 4. Diagram of the Schmidt hammer	10
Figure 5. Location map of Idaho	17
Figure 6. Big Creek Drainage basin	22
Figure 7. Geologic map of Big Creek	23
Figure 8. Photo of granodiorite	28
Figure 9. Photo of weathered granodiorite	28
Figure 10. Reach location map	30
Figure 11. Channel longitudinal profile	31
Figure 12. Photo of Cabin Creek reach	36
Figure 13. Photo of Big Creek Gorge	38
Figure 14. Photo of Schmidt hammer in use	43
Figure 15. Diagram of a river valley	46
Figure 16. Graph of rebound vs. valley width	58
Figure 17. Graph of rebound vs. valley width	59
Figure 18. Graph of rebound vs. valley width	60
Figure 19. Graph of rebound vs. valley width	60
Figure 20. Graph of rebound vs. valley width	61
Figure 21. Graph of rebound vs. topo-derived stream gradient	63
Figure 22. Graph of rebound vs. topo-derived stream gradient	64
Figure 23. Graph of rebound vs. topo-derived stream gradient (bedrock only)	65
Figure 24. Graph of rebound vs. hillslope gradient	66
Figure 25. Graph of rebound vs. hillslope gradient	67
Figure 26. Graph of rebound vs. hillslope gradient	67
Figure 27. Graph of valley width vs. hillslope gradient	68
Figure 28. Hypsometric curve for Big Creek basin	69
Figure 29. Graph of rebound vs. hypsometric integral	70
Figure 30. Graph of rebound vs. hypsometric integral	71
Figure 31. Diagram of valley floor widening	77
Figure 32. Photo of lake bed deposits	86
Figure 33. Photo of fluvial terraces	87
Figure 34. ArcMap image of basin delineation	90
Figure 35. ArcMap image of hillslope facets	92
Figure 36. Graph of rebound vs. gross stream gradient	114
Figure 37. Graph of rebound vs. gross stream gradient	115
Figure 38. Graph of rebound vs. buffered stream gradient	117
Figure 39. Graph of rebound vs. buffered stream gradient	117
Figure 40. Graph of rebound vs. moving average stream gradient	118
Figure 41. Graph of rebound vs. moving average stream gradient	119

LIST OF TABLES

Table 1. Rebound and Morphometric Data 52
Table 2. T-test results 54
Table 3. Schmidt hammer joint spacing test data 55
Table 4. Reach data 62
Table 5. Stream gradient data 62

Abstract

Rock strength exerts important influences on the geomorphology of Big Creek, a tributary to the Middle Fork Salmon River in central Idaho. Big Creek flows through Neoproterozoic metamorphic rocks and Eocene plutonic rocks in a narrow, actively eroding canyon.

Thirteen reaches, ranging from 200 m to 1700 m in length, were studied. The Schmidt hammer was used to measure relative *in situ* rebound values of exposed bedrock on both sides of the valley adjacent to the river and field and digital techniques were used to determine geomorphic characteristics.

A strong negative correlation ($r^2 = 0.8394$, $P = 1.08 \times 10^{-5}$) exists between Schmidt hammer rebound and valley floor width (i.e. weaker rock coincides with wider valley floor). The valley floor width is most strongly correlated to the rebound value on the weaker of the two valley sides. A proposed model of valley floor widening explains the strong correlation. Bedrock with high strength is resistant to lateral fluvial erosion and can hold an oversteepened slope, preventing further widening. Bedrock with low strength is less resistant to lateral fluvial erosion and easily fails when oversteepened, thus facilitating valley floor widening.

A moderate correlation exists between Schmidt hammer rebound and hillslope gradient ($r^2 = 0.5153$, $P = 0.0057$). A weak correlation exists between Schmidt hammer rebound and stream gradient; a stronger correlation is likely inhibited by high sediment load in the channel and by a fault and knickpoint. A statistically significant difference between north- and south-facing slopes indicates that aspect influences bedrock strength.

Data from four Schmidt hammer tests demonstrate a systematic decrease in rebound value with the presence of joints.

CHAPTER 1: INTRODUCTION

1.1 Problem Statement

Rock strength is an important parameter in the study of geomorphology. Intuitively, the strength of bedrock must have some control on weathering, erosion, channel initiation, channel incision, valley morphometry, and drainage development, but the degree to which bedrock strength influences these and other factors is not well known. Relatively little is known about which properties of rock strength (e.g. unconfined compressive strength, tensile strength, shear strength, or Young's modulus of elasticity) actually control valley development. Furthermore, it is not explicitly clear which fluvial and hillslope processes (e.g. abrasion, plucking, shear failure, or mass wasting) are involved in valley formation or how those processes are affected by rock strength. This study has several objectives: 1) to determine what, if any, relationships exist between the relative *in situ* bedrock strength and the morphometry of the valley of Big Creek, a tributary to the Middle Fork of the Salmon River, in central Idaho and through which mechanisms or processes they might be related; 2) to clarify the principles by which the Schmidt hammer operates and how those apply to measuring rock properties relevant to fluvial geomorphology; and 3) to increase the understanding of fluvial geomorphology as related to bedrock geology in the Big Creek drainage basin.

1.2 Background

1.2.1 Processes and Mechanisms of Fluvial Erosion

Two types of processes affect the morphometry of river valleys: hillslope processes and fluvial processes. A variety of weathering and erosional processes occur on the hillslopes of a drainage basin, weakening rock material and moving the products to lower elevations. These processes include mechanical, physical, and biological weathering, and erosional processes such as water erosion, creep, slides, flows, topples, and avalanches, all of which help deliver a sediment load to the stream. Fluvial processes are those occurring in channels, where flowing water interacts directly with sediment derived from bedrock or sediment delivered by hillslope processes. These fluvial processes include bedload transport, suspended load transport, saltation, dissolution, cavitation, plucking, and abrasion. Depending on the balance between resisting forces (sediment flux and grain size, stream bed roughness) and driving forces (slope and discharge), all of these processes can contribute to downward incision of the river and/or lateral erosion of the river by meander migration (Wohl, 1999; Whipple et al., 2000).

Hillslope and fluvial processes do not operate independently of each other. The relationship between sediment supply and transport capacity describes the relationship between the hillslope domain and the fluvial domain: sediment is supplied to the channel by the hillslopes and then transported through the channel via fluvial processes. If the sediment supply from the hillslopes or from tributary streams exceeds the transport capacity of the river, sediment is deposited and stored in the floodplain, and the channel bed aggrades. If the transport capacity of the river exceeds the sediment supply from the hillslopes, sediment in the channel is evacuated and the river runs directly over bedrock, resulting in incision and lowering of the river elevation. Equilibrium between sediment supply and transport capacity will maintain the bed elevation and fluvial morphometry of the river.

As alluvial sediment accumulates on a bedrock bed, it covers and protects the bed below (Howard et al., 1994; Sklar and Dietrich, 1998; 2001). This reflects a change from a bedrock channel where rock strength should be related to valley floor width and stream gradient, to an alluvial channel, which is more complex. This transition from a bedrock channel to an alluvial channel can significantly alter the processes and rates of erosion occurring in the river. The distinction between a bedrock channel and an alluvial channel is somewhat indistinct in the literature (Howard et al., 1994; Sklar and Dietrich, 1997; 2001; Wohl, 1998;1999; Whipple et al., 2000; Ritter et al., 2002). Various definitions depend on temporal and spatial scale, hydrologic regime, geologic structure, and sediment supply. The difference between a wide river valley filled with a large volume of alluvial sediment and a narrow river valley composed of bedrock and with little sediment is straightforward. However, virtually all rivers, including bedrock rivers, have some sediment in the channel.

Bedrock channels are commonly defined as those in which only a thin, discontinuous bed of sediment may exist, all of which can be mobilized during flood events (Ritter et al., 2002). Whipple et al. (2000) adopt the Howard et al. (1994) characterization of bedrock channels as having, "minimal and/or transient alluvial sediment storage and thus occur wherever sediment transport capacity exceeds sediment supply over the long term." This is a logical conclusion and lends itself to the idea that bedrock channels commonly occur in regions of high relief because rivers in those areas typically have high gradients and thus high transport capacity (Wohl, 1999). Wohl (1999) offers perhaps the most comprehensive definition. A bedrock channel can either be one in which at least half of its length is exposed bedrock, one in which the bed morphology is primarily erosional (e.g. flutes, potholes, and longitudinal grooves) or one that has a thin, continuous veneer of alluvial sediment that can be completely mobilized during large discharges.

The choice of definition for a bedrock channel could have important implications in this study. For my purposes I will adopt Wohl's (1998, 1999) definition stated above. While the definition used by Whipple et al. (2000) and Howard et al. (1994) is conceptually the most basic and correct, it is difficult to apply to Big Creek. Sediment supply and transport capacity are difficult to quantify; both the rate of sediment supply from the hillslopes to the channel and the long term discharge of Big Creek are unknown. Even recent, short-term discharge data are unavailable for Big Creek as it has not been gauged since the 1970s. Classifying an entire river as either alluvial or bedrock is difficult because characteristics of the river can change over space and time. Observations of the steep, deeply incised canyon of Big Creek suggest that it is primarily a bedrock river. However, for this study, it is more useful to classify each reach separately based on the current conditions.

Several types of physical processes occur in a bedrock channel. Incision of a river into bedrock occurs through abrasion, plucking, dissolution, and cavitation (Figures 1 and 2). The type of process occurring in a given reach must be dictated by many factors, though my data suggest jointing is the most important. Whipple et al. (2000) and Hancock et al. (1998) argue that jointing has the greatest influence on the type of erosional processes that occur. A bedrock bed with little or no jointing has high cohesion overall and will be eroded mainly by abrasion of bedload or suspended load. However, if the bedrock bed is densely jointed there are many planes of non-cohesion, increasing the surface area available to be weathered or abraded and allowing joint blocks to be removed in a process known as plucking.

Plucking is the dominant erosion process occurring on the bed where the joints are spaced close enough to create joint blocks small enough to be transported by the river. Where jointing is widely spaced and joint blocks are too large to be transported, erosion will occur by abrasion, as described above. Cavitation and dissolution can also erode a bedrock channel: however, these processes probably do not occur at the same rate as abrasion and plucking. Cavitation requires very high energy, and dissolution is typically only significant in calcium carbonate rocks, which are not found in the Big Creek drainage.

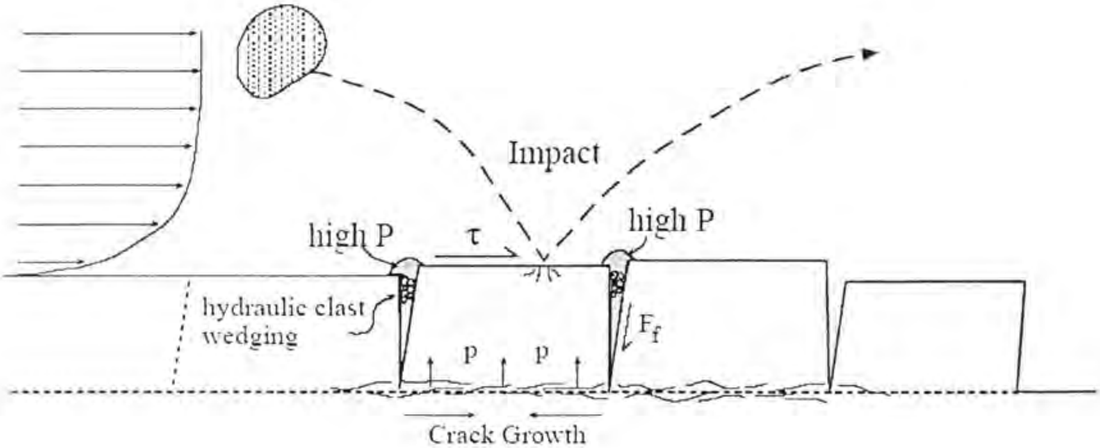

Figure 1. Schematic diagram of the process of plucking. Large saltating grains can cause abrasion, but also generate stresses that drive crack propagation. Smaller sediment can be hydraulically wedged into existing cracks. Joint blocks bounded by cracks can be lifted out of place and moved by surface drag and differential pressures across the block (from Whipple et al., 2000).

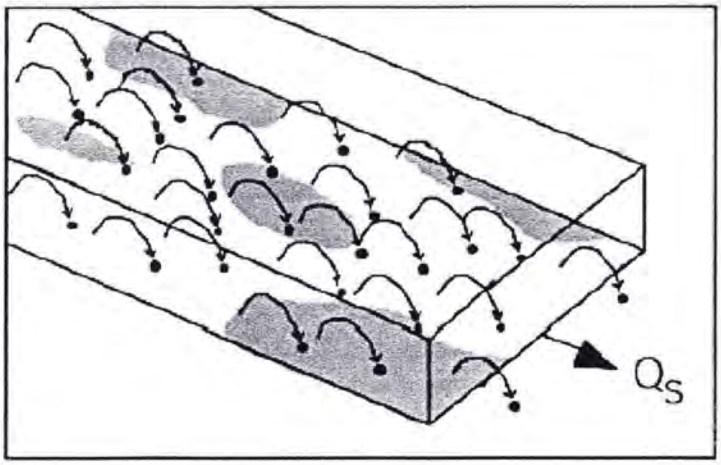

Figure 2. Schematic diagram of a channel bed being abraded by the impacts of saltating bedload. Shaded patches are areas of the channel bed covered by alluvium; alluvial deposits can act to shield the bedrock bed from bedload impacts, greatly reducing erosion (from Sklar and Dietrich, 2004).

1.2.2 Formation of Valley Floor Width

Several studies have explored the mechanisms of lateral bank erosion in unconsolidated alluvial material (e.g. Simon et al., 1999; Thorne, 1982) in an effort to understand valley floor processes. However, there is a dearth of literature dealing with the physical processes and mechanisms that widen the valley floor in bedrock.

Convexity of the hillslopes adjacent to the river channel can reveal information about the relationship between hillslope and fluvial processes. For example, if a slope is convex, fluvial erosion is occurring at a greater rate than hillslope erosion. This may be due to high incision rates (uplift or base-level drop) or hillslope stability (high rock strength). Concave hillslopes, on the other hand, suggest that hillslope erosion is occurring at a greater rate than fluvial erosion. This may be due to an aggrading stream (stable base-level or net subsidence) or to unstable hillslopes (low rock strength).

Straight hillslopes ideally indicate that hillslope and fluvial erosion are in equilibrium (Strahler, 1952; Ritter et al., 2002).

Hypsometric analysis (Strahler, 1952) is often used to estimate the relative maturity of a drainage basin. Basins with a high proportion of area at relatively high elevations (i.e. convex slopes) are considered immature because hillslope erosion has not moved material from the high elevations to the low elevations. Conversely, basins with a high proportion of area at relatively low elevations (i.e. concave slopes) are considered mature because hillslope erosion has moved material from high elevations to low elevations.

1.2.2.1 Erosive Processes of Valley Widening

In cases where a floodplain or terrace exists, the river will meander through the alluvial sediment, occasionally coming into contact with the bedrock of the valley walls. Lateral erosion is thus the primary mechanism for oversteepening and widening the valley walls. Meanders can shift over time scales as short as years or decades, so on the time scale of valley development (10^4 to 10^7 years) the river appears to "bounce" back and forth off the bedrock valley walls and apply equal erosive work to the length of the valley. Alluvial and colluvial sediment must be removed before any direct erosion of bedrock valley walls occurs.

In cases where no floodplain exists and the valley floor width is the same as the channel width, both vertical and lateral erosion act to oversteepen the valley walls and widen the valley floor, with vertical erosion being the primary mechanism. As the river incises, the valley walls oversteepen and the channel gets narrower.

Figure 3. Photograph of a moderately wide valley floor along Big Creek, near Taylor Ranch (between reaches 9 and 10). The valley wall on the left side is oversteepened bedrock and illustrates the processes of valley widening.

If discharge is constant, then a narrower channel will increase the unit stream power of the river and more erosive energy will be applied in both the vertical and lateral directions. Focusing of unit stream power also occurs regularly during periods of flooding and is especially important to bedrock erosion.

If the above assumptions about the formation of valley floor width are correct, then rock strength should affect the width of the valley floor. Bedrock strength and joint spacing dictate whether erosion occurs by abrasion or plucking, and therefore the relative rates of erosion. Erosion by plucking occurs less frequently but at a greater magnitude, whereas erosion by abrasion occurs more frequently but at a smaller magnitude. Lateral erosion of bedrock valley walls by abrasion and plucking oversteepen hillslopes and widen the valley floor. Measurements of the rock strength in the valley walls are expected to be negatively correlated to the valley floor width.

1.2.3 Rock Strength and the Schmidt Hammer

Resistance to erosion is often attributed to rock strength. Rock with low strength erodes at greater rates than rock with high strength (e.g. Gilbert, 1877). These assumptions are logical, yet lack quantitative support and are insufficient in a rigorous study of geomorphology. With that in mind, several methods have been developed for quantitatively measuring the strength of bedrock. The most practical and efficient method is the use of the Schmidt hammer, a portable tool that rapidly measures the energy rebounded by a rock when impacted. Other methods require core samples to be drilled from the bedrock and tested in the laboratory for unconfined compression strength, tensile strength, and shear strength. The Schmidt hammer is convenient because strength of *in situ* bedrock can be measured without arduous sample collection and destruction.

The Schmidt hammer was developed in the early 1950s as a tool for quick, non-destructive testing of the strength of concrete (Schmidt, 1951; Figure 4). The hammer weighs about 2.5 kg and is about 30 cm long. It is easily carried in the field, and a single measurement can be performed in just a few seconds. The hammer consists of a cylinder containing a plunger, spring, and mass. When the mass is loaded against the compressed spring, the plunger is released. The tip of the plunger, which has a diameter of 1.5 cm, is placed normal to the surface being tested. When the hammer is depressed, the plunger retracts into the cylinder and releases the spring-loaded mass. The mass strikes the plunger, which then transmits the impact energy (2.207 Nm) onto the surface being tested.

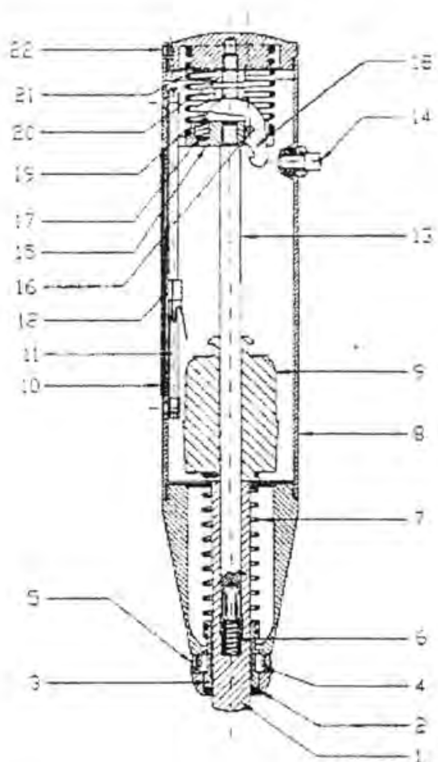

1 – Impact Plunger
2 – Felt Washer
3 – Guide Sleeve
4 – Two Part Ring
5 – Cap
6 – Retaining Spring
7 – Impact Spring
8 – Housing
9 – Hammer Mass
10 – Graduated Scale
11 – Guide Rod
12 – Indicator
13 – Hammer Guide Bar
14 – Push-button
15 – Disk
16 – Pin
17 – Pawl Spring
18 – Pawl
19 – Trip Screw
20 – Lock Nut
21 – Compression Spring
22 – Rear Cover

Figure 4. Cut-away diagram of a Schmidt hammer.

Energy is elastically rebounded by the surface material back through the plunger and the mass bounces back. The distance that the mass bounces back is measured by a scale on the side of the hammer; this is the rebound value (R) of the surface. Rebound values are simply relative measures, but they can be converted to a variety of mechanical properties, including uniaxial compressive strength (MPa, N/mm^2 or lb/in^2), using several available empirical conversion charts (Yaşar and Erdoğan, 2004; Katz et al., 2000). Variability in rebound value occurs depending on the orientation of the hammer; measurements taken vertically downward will give slightly higher rebound values than those taken vertically upward (Basu and Aydin, 2004; Day, 1980).

One type of erosion is abrasion. Sklar and Dietrich (2001) assert that tensile strength is the rock strength parameter that controls rock resistance to abrasion because rock fails in tension when impacted by saltating grains. The Brazilian tension splitting test (Vutukuri et al., 1974) is a typical laboratory test for measuring tensile strength and involves the destruction of a sample. The Schmidt hammer is a non-destructive, *in situ* tool for estimating physical properties of rock related to tensile strength. Schmidt hammer rebound measurements are very strongly correlated to Young's modulus of elasticity (Katz et al., 2000). Young's modulus of elasticity is directly related to the spring constant of molecular bonds in the rock and therefore is related to tensile strength (Knight, 2004).

Plucking is another type of erosion. The Schmidt hammer measurement is sensitive to weathering, surface roughness, microfractures, joints, and other discontinuities (Williams and Robinson, 1983; McCarroll, 1991; Sumner and Nel, 2002). Measuring the rebound of this unweathered and unfractured rock sample with a Schmidt hammer would give the intact rock strength. Intact rock strength describes the virgin mechanical strength properties of the material, but is fairly unrealistic because rocks in the field are almost always modified by weathering, strain, or discontinuities, especially at the scale of river valleys.

Selby (1980) developed a measure called Rock Mass Strength Index for incorporating a variety of modifications (weathering, joint spacing, joint orientation, joint width, joint continuity, and outflow of groundwater) into the intact rock strength of a rock mass as measured by a Schmidt hammer. The rationale to incorporate these modifications was that intact rock strength alone could not fully describe hillslope formation, and thus other contributing parameters should be considered. My discussion above follows this rationale; however, the physical principles on which the Schmidt hammer is based suggest that the Schmidt hammer incorporates several of the modifying parameters into a single measurement, and a Rock Mass Strength Index classification may not be necessary in some cases.

Other studies have hinted at the relationship between structure and strength (Selby, 1980; Whipple et al., 2000). Kahraman (2001) investigated the relationship between P-wave velocity, number of joints, and Schmidt hammer rebound value and found that P-wave velocity is strongly negatively correlated to the number of joints in a sample and that Schmidt hammer rebound value is strongly positively correlated to P-wave velocity. This suggests indirectly that Schmidt hammer rebound value may be negatively correlated to the spacing of joints in a rock sample. In other words, fewer joints yield higher rock strength and higher Schmidt hammer rebound values. The

Schmidt hammer is used in this study to characterize rock strength in the valley walls by measuring the relative rebound of *in situ* bedrock.

I aim to address directly, with the use of the Schmidt hammer, the relationship between intact rock strength and joint spacing. In order to support the assumption that combined rock strength measurements made with the Schmidt hammer systematically incorporate joint spacing into intact rock strength, a Schmidt hammer test was performed on an outcrop from each lithologic group. I hypothesize that the presence of joints will reduce the intact rock strength measurements of bedrock, and that smaller joint spacing will reduce the measurements more than larger joint spacing. Confirmation of this hypothesis will demonstrate that both intact rock strength and joint spacing information can be combined by the Schmidt hammer into a single measure.

1.2.4 Spatial and Temporal Scales

Fluvial and hillslope processes operate at a wide range of spatial and temporal scales. An important spatial scale in fluvial erosion is the maximum joint block size that can be entrained and transported by the river. One meter diameter joint blocks are approximately the largest blocks that can be entrained and transported (Grant and Swanson, 1995). As joint block size decreases, plucking is facilitated and becomes the dominant erosional process. Joint blocks greater than one meter do not experience plucking; rather, abrasion is the dominant erosional process (Grant and Swanson, 1995; Hancock et al., 1998; Whipple et al., 2000).

The Schmidt hammer has a spatial resolution of a few centimeters, but the number and distribution of measurements can cover large areas. Sub-meter resolution makes the

Schmidt hammer an ideal tool for this study because it can determine strength at the scale that fluvial processes (i.e. bedrock and sediment being weathered, fractured, abraded, and transported) are operating.

1.3 Approach

The approach of this study was to measure the relative *in situ* rebound value of bedrock in the valley walls and compare it to four valley parameters: valley floor width, channel gradient, hillslope gradient, and hillslope hypsometry. Thirteen reaches were identified along Big Creek for detailed study. Rock strength was measured on both sides of the valley with a Schmidt hammer. Valley floor width was measured in the field with a laser rangefinder. Channel gradient and the hillslope gradient on both sides of the valley were calculated from data extracted from 10-m digital elevation models (DEMs). Hypsometric integrals were also calculated for the hillslopes from 10-m DEMs.

The data were analyzed with analysis of variance (ANOVA), t-test, and regression to determine 1) if there are significant differences between reaches, between lithologic types, and between north and south sides of the valley, and 2) if there are significant correlations between rock strength and each of the valley parameters. Finally, I explain the correlations or lack of correlations using principles of rock mechanics and fluvial and hillslope processes.

CHAPTER 2. STUDY AREA

2.1 Regional Setting

2.1.1 Topography and Tectonics

Big Creek is located in Valley and Idaho Counties in central Idaho (Figure 5). It is an east-flowing tributary to the north-flowing Middle Fork Salmon River and is ultimately part of the Columbia River Basin. Central Idaho is characterized by steep, high-relief mountains covering a broad area rather than arranged in linear ranges. The mountains surrounding Big Creek are called the Salmon River Mountains, whose northern boundary is roughly described by the Main Fork of the Salmon River. The Big Creek drainage basin lies entirely within the Payette National Forest and the Frank Church-River of No Return Wilderness Area. As a result there is little anthropogenic alteration, though the basin does have a history of small scale mining and backcountry hunting camps.

The Miocene – Recent uplift history of central Idaho is not well established. It is apparent that significant uplift has occurred to create the high elevation and deeply cut river valleys. Topographic maps and digital elevation models (DEMs) demonstrate that the Salmon River Mountains, especially north of Big Creek, have many high, apparently concordant, plateaus that may define an ancient low-relief topographic surface.
A few studies have estimated paleoelevations or uplift rates (Axelrod, 1968; Sweetkind and Blackwell, 1989; Wolfe et al., 1998; Meyer and Leidecker, 1999). Axelrod (1968) used paleobotanical evidence to reconstruct the pre-Snake River Plain topography of central Idaho. However, that study does not take climate change into account, only inferring elevation changes from changes in floral taxa present. He concludes that

Eocene elevations surrounding the present Snake River Plain ranged from 1200 to 1800 m.

Wolfe et al. (1998) also used paleobotanical evidence to estimate paleoelevations in central Idaho. Fossil leaf assemblages from near Salmon, Idaho indicate that Eocene and Oligocene elevations, "were comparable to or higher than present-day" elevations. Because of poor age constraint (K/Ar of ash partings), a wide range of elevations are suggested, from 1800 m to >2000 m to over 4000 m. Paleoelevations of 4000 m or more seem excessive considering modern mean elevation is closer to 1500 m and the highest peaks are approximately 3000 m. These paleoelevations are hard to relate to the Salmon River Mountains because the data were collected at the edge of the Basin and Range Province where tectonic history is significantly different.

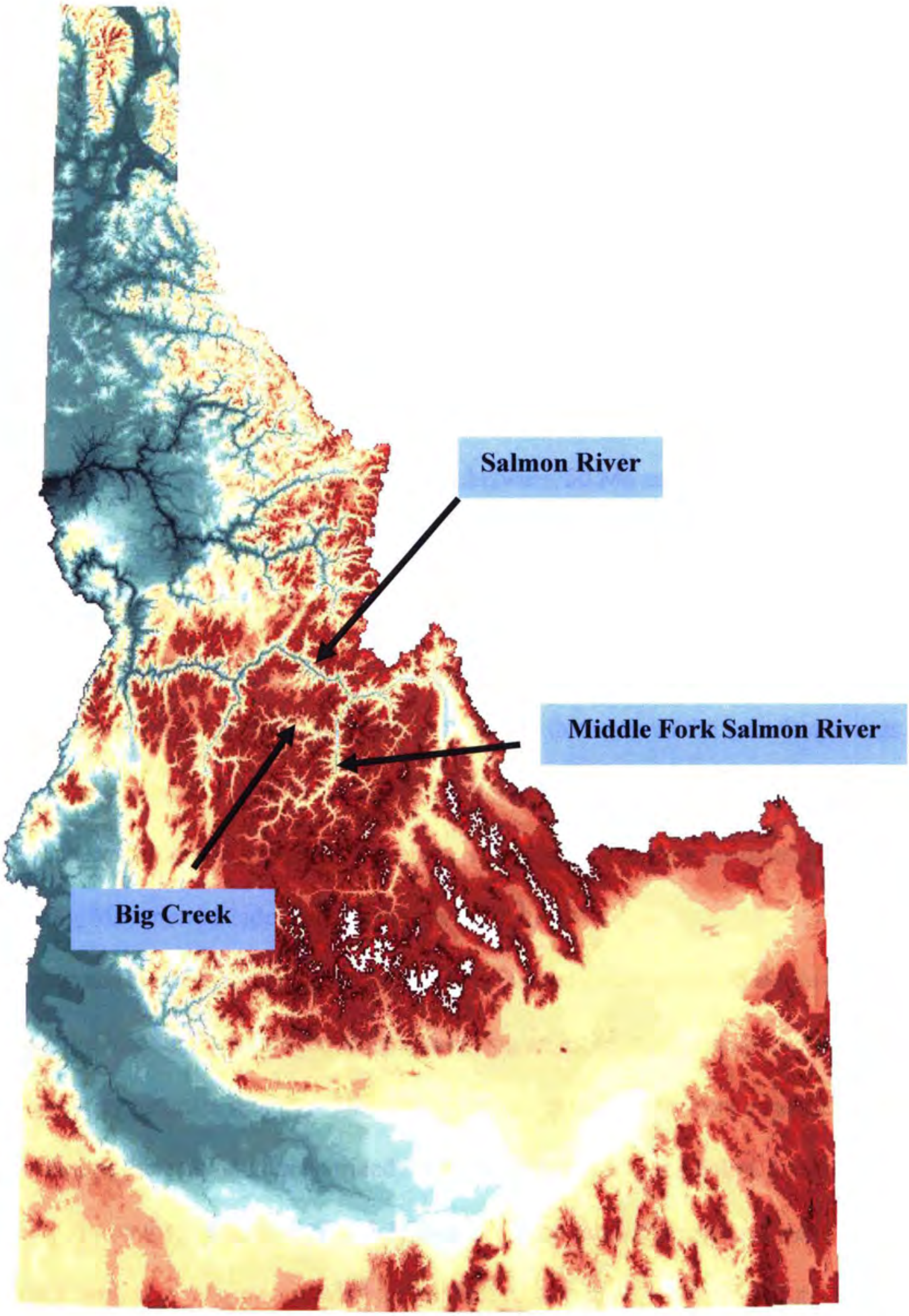

Figure 5. False color DEM of Idaho. Greens and cooler colors represent low elevations, red and warmer colors represent high elevations.

Sweetkind and Blackwell (1989) used apatite and zircon fission track thermochronology to determine the rate of exhumation of the Idaho batholith, a large (40000 km^2) composite mass of granitic plutons in central Idaho that was emplaced during the Cretaceous between 100 Ma and 70 Ma. They found that from 50 Ma to 10 Ma the batholith was shallowly buried (no deeper than 4 km) and was exhumed. This requires rapid uplift in Eocene time (60 – 50 Ma), and slow uplift from 50 – 10 Ma. Since 10 Ma they propose a second phase of rapid downcutting. Present topography supports this two-phase history: topography at high elevation is composed of subdued plateaus, which may represent slow downcutting between 50 Ma and 10 Ma, while the deeply incised river canyons are a result of recent rapid downcutting since 10 Ma (Sweetkind and Blackwell, 1989). Isostatic uplift caused by crustal thickening and emplacement of buoyant Idaho batholith rock initiated erosion of central Idaho (Lewis et al. 1987; Jordan, 1994). Jordan (1994) estimates crustal thickness in the Late Cretaceous within the Atlanta lobe of the Idaho batholith to be 64 – 52 km. Erosional denudation exhumed Idaho batholith rock, thinned the crust, and triggered further isostatic response (Jordan, 1994; Meyer and Leidecker, 1999).

Meyer and Leidecker (1999) also noticed the bimodal topography described above along the Middle Fork Salmon River, and using an estimated incision rate of 0.12 – 0.16 m/kyr, they estimate that the ~300 m deep inner gorge (i.e. the most recently incised portion of the canyon characterized by steep and narrow walls below a sharp break in slope) was formed since 2.63 – 1.85 Ma. Incision rates are based on weathering rind age estimates, so they are somewhat uncertain. An actual recent incision rate of 0.74

m/kyr was calculated for the 12 m above river level since 14.5 cal ka. This short term rate is not thought to represent long term average rates of incision.

Central Idaho does indeed have deep canyons, and they are likely related both to rock uplift and to a drop in base level. The subsidence of the Snake River Plain is coeval with the rapid downcutting since 10 Ma, but there is no evidence that the Salmon River ever drained directly to the Snake River Plain, as Sweetkind and Blackwell (1989) suggest on the premise that the Salmon River canyon could only have formed after initiation of Basin and Range faulting and eastward migration of the continental divide. Link et al. (1999) suggest that as recently as 3 Ma the Salmon River may have drained northeast into Montana through what is now Lost Trail Pass. The present Salmon River flows north, east, north, and then west, ultimately draining into the Snake River below Hell's Canyon well north of the Snake River Plain.

Capture of the upper Snake River by the lower Snake River, and infilling of Pliocene Lake Idaho at 2 – 4 Ma (Malde, 1991; Othberg, 1994; Repenning et al., 1994; Wood, 1994; Wood and Clemens, 2004) may have significantly increased the discharge of the Lower Snake River, thus increasing incision and lowering the base level for the entire Salmon River drainage basin (Meyer and Leidecker, 1999). While changes in base level due to stream capture may have caused rapid recent incision, the overall high topography in central Idaho must be attributed to surface uplift.

2.2 Big Creek Drainage Basin

2.2.1 Basin Parameters

The Big Creek drainage basin covers 1539 km^2. The main trunk of the river is 67.2 km long. Mean elevation of the basin is 2101 m. Basin relief is 1876 m, with a maximum elevation of 2906 m and a minimum elevation of 1030 m at its outlet (Figure 6).

2.2.2 Geology

The underlying geology of the Big Creek drainage basin is diverse, both temporally and compositionally (Figure 7). The most detailed geologic mapping has been performed by Stewart, et al. (unpublished maps, 1995-2004). Geologic maps of the Salmon and Payette National Forests have been compiled from a variety of sources but are generally at a small scale (1:100,000 or less) and Big Creek geology is extrapolated from surrounding areas (Lund et al., 1998; Tysdal et al., 2003).

Eocene east-central Idaho has undergone at least five distinct episodes of extension. The pre-Challis volcanic, main post-Challis volcanic, and Recent Basin and Range episodes extended the crust in a northeast-southwest direction, creating northwest-trending normal faults. Syn-Challis volcanic and early Miocene episodes extended the crust in a northwest-southeast direction, creating northeast-trending normal faults (Link and Janecke, 1999). The Trans-Challis fault system trends northeast and extended during Middle Eocene Challis volcanism. As Challis volcanism waned, a 100 km wide rift opened in what Link and Janecke (1999) and Janecke (1994) refer to as the "Paleogene basin-forming event." Several half grabens, including the Panther Creek half graben

(Janecke et al., 1997), formed during this event. Many northeast trending normal faults and Challis volcanic dikes have been mapped in the Big Creek region (Figure 7; Stewart et al., unpublished; Digital Atlas of Idaho, 2005).

Three geologic preconditions are important to the modern Big Creek drainage. First, the Eocene Cow Creek fault, a major northeast-trending, northwest-dipping normal fault, coincides with the downstream boundary of the Cabin Creek reach (Reach #8), with weak volcanic tuff in the headwall and stronger intruded diorite in the footwall. This fault is a major structural control on the longitudinal gradient of Big Creek because it has downdropped weak rock and left a resistant bedrock barrier. The stream gradient upstream of this point has graded to the local base level of the fault. Second, Miocene – Recent erosional denudation has caused exhumation of the crust and surface uplift in central Idaho. And third, Late Miocene – Pliocene lowering of the Salmon River base level has increased the rate of incision of the Middle Fork Salmon River and caused a knickpoint to migrate up Big Creek. The stream gradient below the Cow Creek fault is controlled by this knickpoint and has not yet equilibrated to the base level drop.

The rocks of the Big Creek drainage basin can be divided into four groups: 1) Mesoproterozoic quartzites and siltites, 2) Neoproterozoic mafic intrusions, 3) Tertiary (Eocene) intrusive granodiorites, and 4) Tertiary (Eocene) volcanic tuffs and porphyry dikes of the Challis Volcanic Group. The map units in the Big Creek drainage basin described by Stewart, et al. (unpublished maps) are adopted in this study. Also included are some additional notes regarding the weathering, fracturing, and erodability of the units as observed by Stewart and myself. Some of the same units have been described by Tysdal et al. (2003) at different locations.

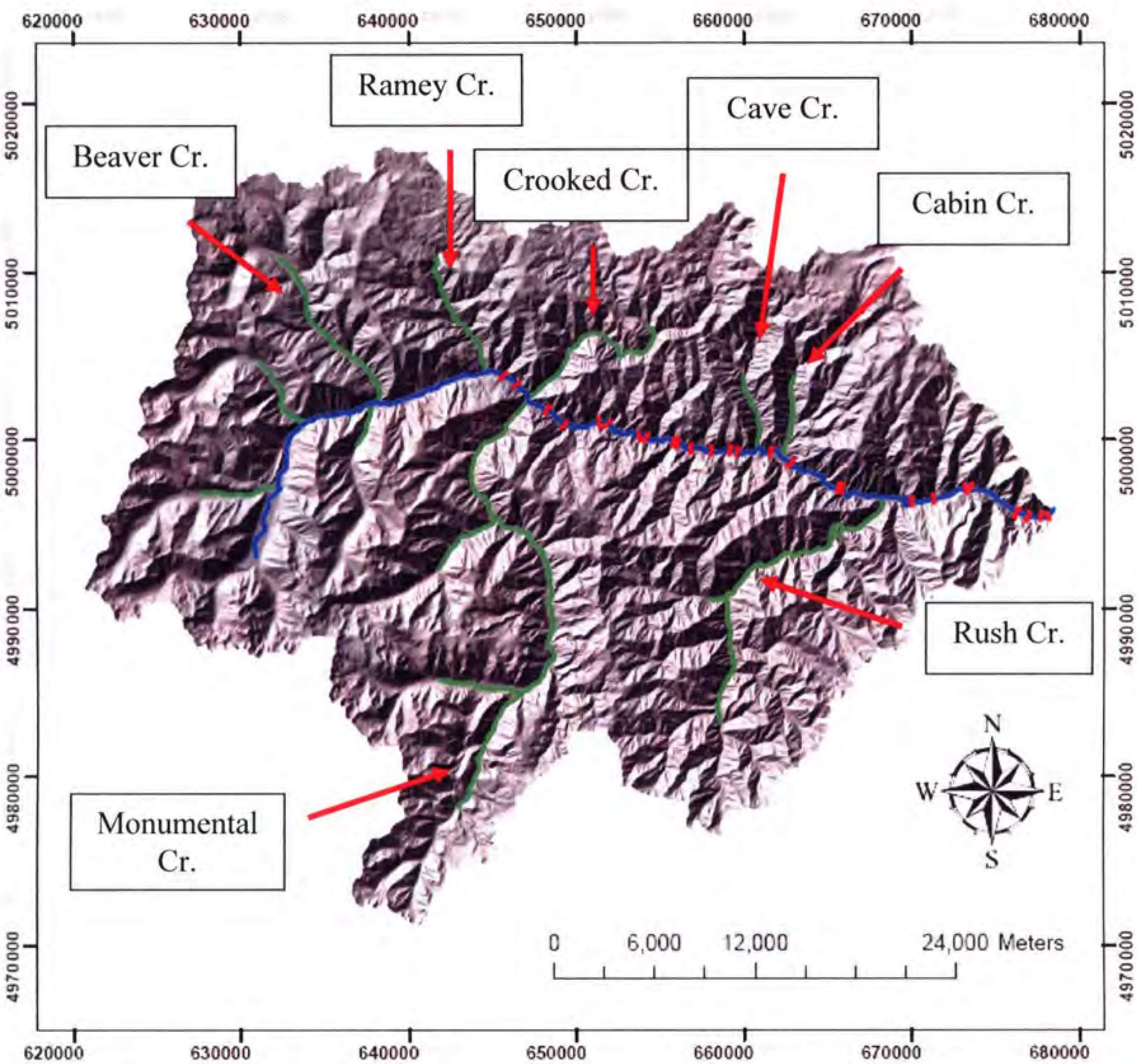

Figure 6. Hillshade DEM of Big Creek Drainage. Blue line is the main stem of Big Creek, green lines are tributaries, red brackets are reaches studied.

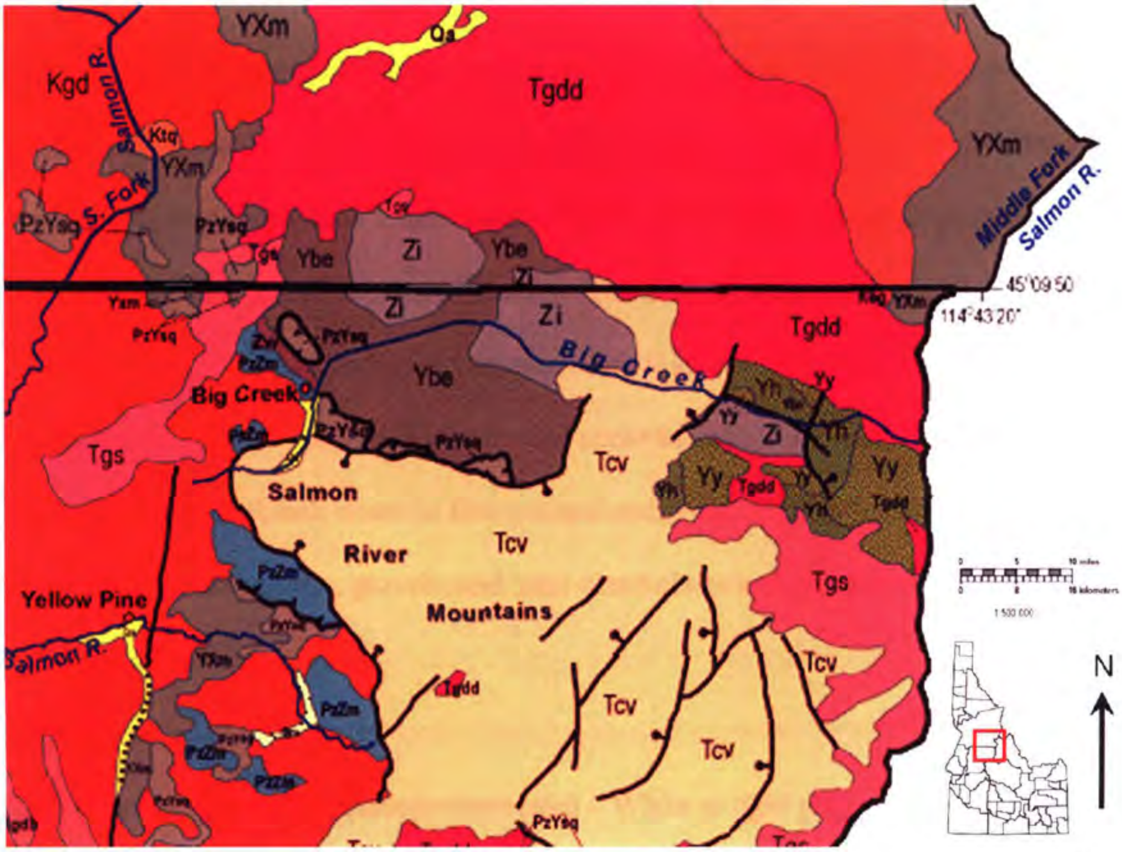

Figure 7. Geologic map of Idaho and Valley Counties, central Idaho. Qa = Quaternary alluvial deposits, Tcv = Eocene Challis Volcanic Group, Tgs = Eocene granite, Tgdd = Eocene granodiorite, Kgd = Cretaceous Idaho Batholith granite and granodiorite, Ktg = Cretaceous tonalite and quartz diorite, PzZm = Paleozoic/Neoproterozoic metasedimentary rocks, PzYsq = Paleozoic/Mesoproterozoic quartz and schist, Zi = Neoproterozoic intrusive rocks, Ybe = Mesoproterozoic Belt Supergroup, Yh = Mesoproterozoic Hoodoo Quartzite, Yy = Mesoproterozoic Yellowjacket formation. (From Digital Atlas of Idaho, 2005)

2.2.2.1 Description of Map Units

2.2.2.1.1 Mesoproterozoic quartzites and siltites

The Yellowjacket Formation and Hoodoo Quartzite are part of the Belt Supergroup; the Hoodoo Quartzite may be the southern extension of the Revett Formation and the Yellowjacket is correlative to the lower Ravalli Group (Link et al., 2002; Link et al., 2003).

(Yy) Yellowjacket Formation (Mesoproterozoic) – Light to dark gray, black, green to pale orange heterogeneous formation consisting of fine-grained thin- to medium-bedded feldspathic quartzites, thin bedded siltites, and dark thinly laminated argillites, all of which have been metamorphosed to varying grades of hornfels; and thin- to medium-bedded calc-silicates. Rare thin carbonate beds are also present. Locally phyllitic. Sedimentary structures such as pinch and swell laminates, graded bedding, ripple marks, and cross stratification are observed locally. The Yellowjacket Formation is composed of 70% quartz, 15% biotite, and 15% feldspar. Unit thickness is approximately 2250 m. Quartzites and siltites are quite resistant and occur as cobble and gravel in the stream channel. Argillites break down to fine-grained sediment. Calc-silicates occur in the stream channel as cobble-, gravel-, and sand-sized clasts and are more susceptible to chemical weathering.

(Yh) Hoodoo Quartzite (Mesoproterozoic) – White to light gray or light pink, fine- to coarse-grained, medium- to thick-bedded hornfelsed quartzite. Feldspathic in part. Sedimentary structures are rarely well preserved; ripple marks and cross stratification are locally present. Thin siltite interbeds make up a minor portion of the unit. Composed of about 80 – 90% well-rounded quartz; 5 – 10% feldspar; and 5 – 10% biotite, chlorite, sericite, and iron oxide. Total thickness is approximately 1100 m. Grades downward to Yellowjacket Formation (Yy) over a 200 m transition zone. Large boulders of this unit are not common in the stream channel because it has been densely fractured due to emplacement of intrusives. Cobble and gravel sized clasts are quite persistent in the stream channel.

(Yaq) Argillacerous quartzite (Mesoproterozoic) – Thinly bedded argillaceous quartzite, siltite, and argillite that are stratigraphically above the Hoodoo Quartzite. Bedding is tilted to nearly vertical and is deformed. Only a small segment of this unit is exposed along Big Creek; this unit does not contribute much sediment to the channel.

2.2.2.1.2 Neoproterozoic mafic intrusions

(Zdi) Dioritic Complex (Neoproterozoic) – A distinct but variable mafic intrusive unit. Predominantly medium-grained diorite composed of white plagioclase and up to 60% black euhedral to subhedral hornblende. Quartz and biotite occur only as minor constituents. This unit also includes a fine-grained variety (microdiorite). Weathers to fine, dark soil and contributes sand-sized and smaller clasts to the stream channel. Forms ribs, buttresses, and protrusions in the channel.

(Zsy) Syenite (Neoproterozoic) – White to light gray, medium-grained. Potassium feldspar is the dominant mineral, with up to 25% hornblende. Quartz and biotite are minor constituents. Locally exhibits a weak foliation. Forms sills and dikes that range in thickness from 1 to 30 m. Usually occurs with diorite (Zdi). Slightly more resistant to weathering than diorite (Zdi), but also weathers to sand- and fine gravel-sized sediment in the stream channel.

2.2.2.1.3 Tertiary intrusive granodiorites

(Tgd) Granodiorite (Eocene) – Light to dark gray, fine- to medium-grained equigranular hornblende biotite granodiorite (Figure 8). Plagioclase is the most abundant constituent, followed by quartz and potassium feldspar. Biotite is commonly euhedral, and hornblende is a conspicuous constituent. Mafic xenoliths are found locally within the granodiorite. Dacite dikes (Td) and dacite porphyry dikes (Tdp) are textural variants of the granodiorite and commonly occur along its margins. Breaks down to coarse sand- to fine gravel-sized grus of its constituent minerals: plagioclase, quartz, K feldspar, biotite, and hornblende. Fresh surfaces tend to be very smooth and hard, but weathered surfaces tend to be very grusified and broken apart with fingers (Figure 9).

Figure 8. Photograph of Tertiary granodiorite (Tgd) in the Breeching Creek reach.

Figure 9. Grusified variation of Tertiary granodiorite (Tgd) caused by surface weathering.

2.2.2.1.4 Tertiary Challis Volcanic Group tuffs and porphyry dikes

(Tss) Sunnyside tuff (Eocene) – White to pink moderately to densely welded rhyolitic lapilli to ash flow tuff with multiple cooling units. Weathers to coarse light-colored sand or to plates in densely welded zones. Pumice, white to pale green, comprises 0 – 30% of the rock. Pumice is 0.3 – 3 cm in size, moderately to highly flattened. Crystals make up 20 – 60% of the rock and consist of up to 60% feldspar and up to 55% quartz; crystal sizes are 0.5 – 2 mm. Biotite is a minor constituent (less than 5%). Lithic fragments, primarily of volcanics but with some quartzite and siltite, are present in variable amounts. Unit is locally intensely altered. The unit locally does not support vegetation, and is easily eroded to form white scars on hillsides. Vitrophyres occur locally. This unit is rarely cut by dikes. The Sunnyside tuff is associated with the nearby Thunder Mountain Caldera and has been K-Ar dated between 45 and 49 Ma (Leonard and Marvin, 1982). Unit can be as much as 1000 m thick.

(Tdq) Dime and Quarter tuff (Eocene) – Light gray to light green locally purple lithic lapilli to ash flow tuff with multiple cooling units. Densely welded. Light to dark gray green, moderately to highly flattened pumice between 0.5 and 4 cm in size comprises 0 – 25% of tuff. Pumice clasts contain plagioclase, with lesser quartz, biotite up to 5%, and minor hornblende. Hornblende is more common north of Big Creek and locally occurs as acicular crystals up to 2 mm in length. Lithics, generally less than 3 cm in size, consist of volcanic fragments, quartzite, siltitie/argillite, and rarely of two-mica blocks. The unit is extensively cut by dacite dikes (Td), rhyolite dikes (Tr), and rhyolite porphyry dikes (Trp). Alteration, predominantly propylitic, is moderate to intensive south of Big Creek, and slight to moderate north of Big Creek. The wide range in the degree of welding of this tuff has significant morphological implications. Densely welded regions are very resistant to weathering and form high cliffs. Hydrothermally altered or poorly welded regions have almost no cohesion and will erode very rapidly. Transitions between very different states of induration and weathering occur over very short distances. In terms of weathering and erodability, this unit is by far the most variable, from very densely welded cliff-forming regions to barely cohesive rock that crumbles in ones hand.

(Tdp) Dacite porphyry dikes (Eocene) – Dark gray to dark green aphanitic groundmass with conspicuous white phenocrysts of plagioclase up to 10 mm in size. Phenocrysts comprise up to 50% of the rock. Also contains lesser amounts of K feldspar, hornblende, biotite, and quartz phenocrysts. Generally more resistant to weathering and erosion than the tuffs that it cuts. Can form protrusions in hillsides and ribs, cascades, or falls in the stream channel. Occurs as persistent cobble and gravel sized clasts in the stream channel.

2.3 Reach Descriptions

Thirteen reaches were studied along the lower two-thirds of the main stem of Big Creek (Figure 10). The reach names were derived from nearby tributary streams or unique features; they also numbered 1 – 13 from upstream to downstream. The reaches are not continuous in their coverage, and their lengths range from 288 meters to 1716 meters. Figure 11 is the longitudinal profile for the main stem of Big Creek, with reaches labeled. Below are descriptions of each reach, numbered sequentially from upstream to downstream. Descriptions include bedrock type, noticeable joint spacing and orientation, presence of terraces or floodplains, presence of alluvial fans, hillslope characteristics, presence of bedrock buttresses, channel morphology (using the Montgomery and

Buffington [1997] classification), presence of exposed bedrock in the channel, and grain size and sorting of channel-bed sediment.

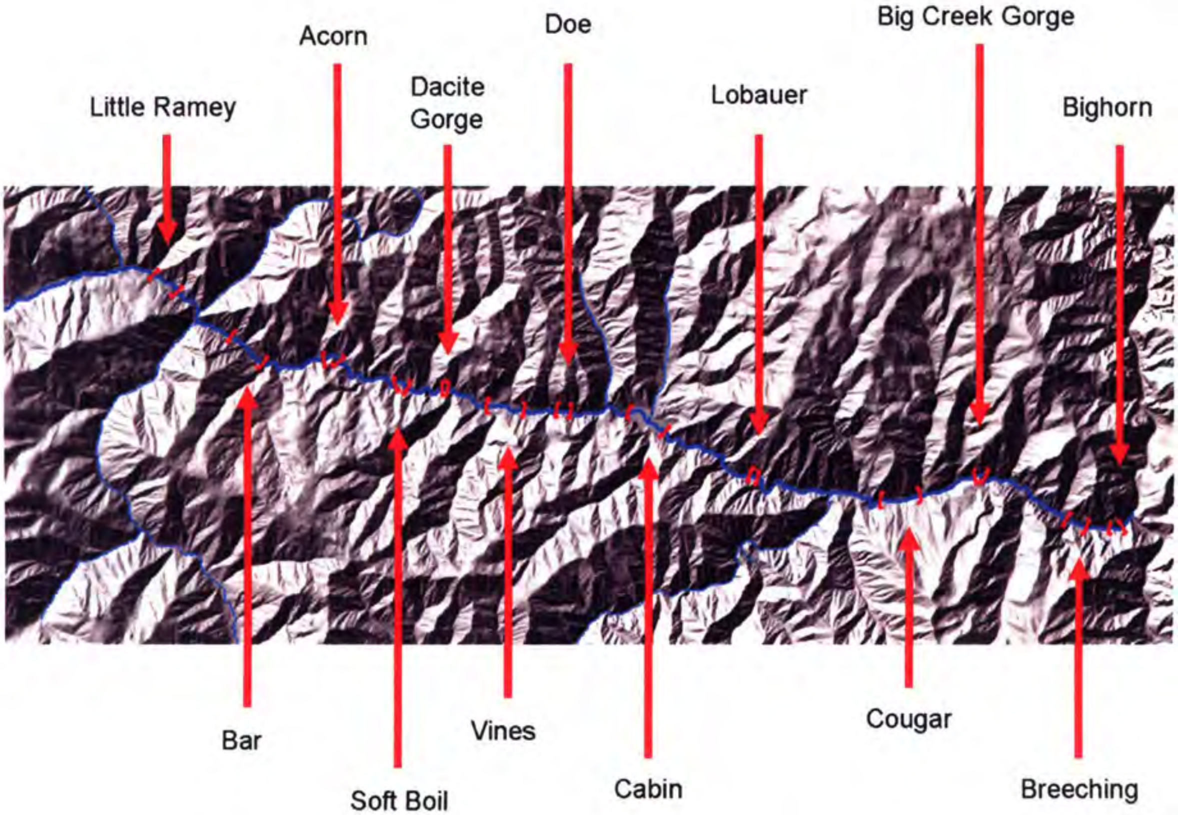

Figure 10. Hillshade DEM of the lower two-thirds of Big Creek, from Ramey Creek to the Middle Fork Salmon River. Reaches are bounded by red brackets and labelled with arrows.

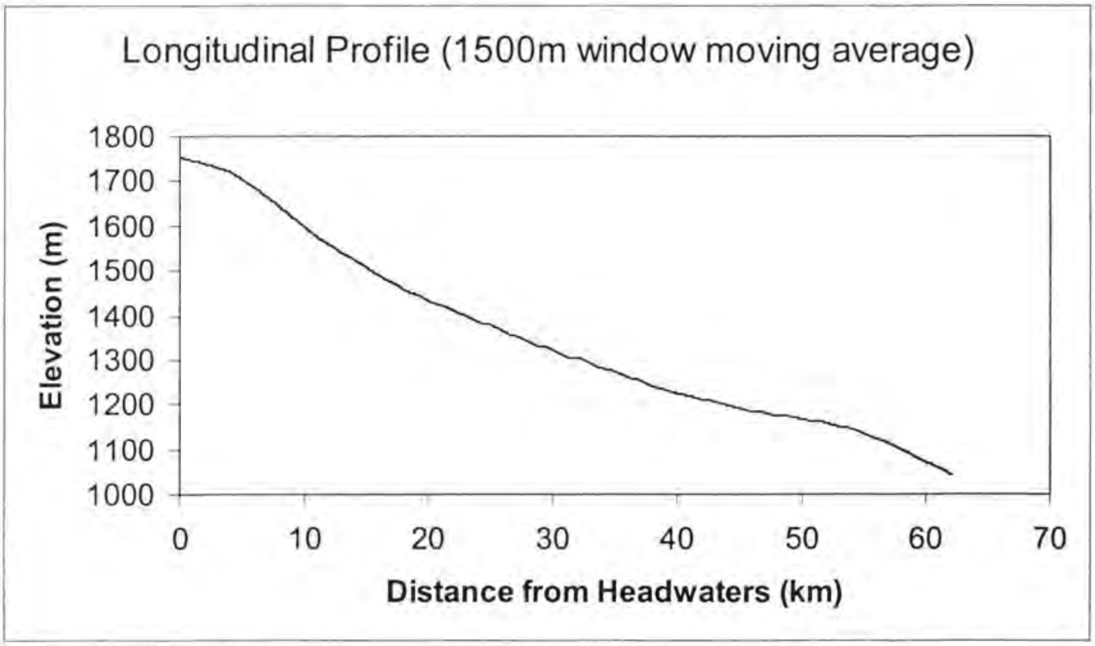

Figure 11. Longitudinal profile of the main stem of Big Creek. Elevation points were measured every 45 m along the stream channel and averaged with a 1500m moving window. Vertical exaggeration is approximately 87X.

2.3.1 Little Ramey Creek Reach (Reach #1)

Bedrock type is diorite. The valley floor is moderately wide (~90 m) and thickly vegetated. The upstream end of the reach is just below the Little Ramey Creek alluvial fan. Hillslopes are vegetated, the south side (north-facing) more than the north side. Hillslopes above the lower end of the reach are talus covered. Outcrops of bedrock are exposed on both sides of the valley and a bedrock buttress extends into the channel at mid-reach. Aside from this buttress, the channel-bed is alluvial. Channel morphology is pool and riffle, bed material is cobble – boulder. Several large woody debris jams are present in the channel. No terraces are present in this reach.

2.3.2 Bar Creek Reach (Reach #2)

Bedrock type is diorite. This reach has steep hillslopes and a straight channel with a steep gradient. No floodplain or terraces are present; the channel is the valley floor. The south side hillslope alternates between exposed bedrock and large talus fans. The north side hillslope is covered with talus and colluvium. Bedrock is exposed in the channel in the upstream end of the reach; however, gradient is controlled by abundant alluvium supplied by the hillslopes. Talus fans constrict the channel, increasing the stream power and thus increasing the stream gradient. Channel morphology is pool and riffle and plane bed. The channel bed is relatively flat, but the center is deeper. Bed material is cobble – boulder with sand filling interstices. Many large (1-2 m) boulders are in the channel.

2.3.3 Acorn Creek Reach (Reach #3)

Bedrock type is diorite. The river makes a sweeping right-hand turn. Valley floor is relatively wide (~100 m); terraces and floodplain are developed on both sides of the valley. This reach begins just downstream of the large Acorn Creek alluvial fan that has a steeply cut toe. No bedrock is exposed in the channel; the stream gradient is controlled by alluvium. A bedrock buttress extends to the valley floor from the south side at mid-reach. Hillslopes are mostly covered with talus and colluvium. Channel morphology is pool and riffle; the channel bed has distinct topography. Bed material is cobble – boulder, with some large (1m) boulders. A small longitudinal cobble bar is present.

2.3.4 Soft Boil Bar Reach (Reach #4)

Bedrock type is diorite, with a small exposure of tuff in a bedrock buttress on the south side of the valley. This reach is moderately long (~500 m) and wide (~60 m). Floodplain and terraces are present. The north side hillslope is oversteepened by cut-bank erosion on the outside of the bend. North side hillslope has a few small outcrops of bedrock exposed near the valley floor, but is mostly covered with colluvium. Several large, stable, vegetated islands are formed in the channel. Many gravel and cobble bars exist in the channel, with secondary channels cutting across them. Channel morphology is pool and riffle. A few large woody debris jams are present in the channel. The stream gradient is controlled by alluvium. Bed material is cobble – boulder, with sand filling interstices.

2.3.5 Dacite Gorge (Reach #5)

Bedrock type is very densely welded dacite – andesite crystal lithic tuff. This reach is short (~300 m) and narrow (~25 m), with a steep and bouldery channel. No floodplain or terraces exist; valley floor width is channel width. Vertical bedrock cliffs are exposed on both sides of the valley. A pile of large (1-2 m) boulder debris is at the base of the cliff and in the channel. Bed material is primarily large (1 m) boulders and sand, with some boulders up to 3 – 5 meters in diameter. Channel morphology is step pool. Several large woody debris jams are present. This reach has a lot of exposed bedrock and a limited amount of alluvial fill; the gradient is controlled by bedrock.

2.3.6 Vines Reach (Reach #6)

Bedrock type is tuff. This reach is very long (~1500 m) and wide (~200 m). The river meanders through well-developed terraces (3-4 m high) and floodplain. Bedrock is exposed in upper hillslopes and in a bedrock buttress at mid-reach that extends to the valley floor from both sides and was presumably connected before the river breeched it. The north side of the valley has several alluvial fans reaching the valley floor. The south side of the valley has at least seven terrace levels preserved. The channel is wide and has low topographic relief on the bed. Channel morphology is plane bed and pool and riffle. Bed material is large cobble – boulder and very little sand. A few large (1 m) boulders are in the channel. Stream gradient is controlled by alluvium. A small landslide extends down to the valley floor from Garden Creek on the north side of the valley and is no longer active.

2.3.7 Doe Creek Reach (Reach #7)

Bedrock type is welded tuff. This reach is narrow (~20 m) and straight. The south side of the valley is a vertical bedrock cliff that extends down into the channel. The north side of the valley is a bedrock cliff with an apron of boulder talus at its base. Foliation joints are sub-horizontal and dip slightly upstream. There are many very large boulders (up to 10 m) in the channel that were derived from the cliffs above the river. No floodplain or terraces are present. Stream gradient is controlled by bedrock. Channel morphology is plane bed, with very large obstructions.

2.3.8 Cabin Creek Reach (Reach #8)

Bedrock type is tuff; the south side of the valley is densely welded and forms vertical cliffs, whereas the north side is weakly welded and forms gentle slopes with little exposed bedrock. Major foliation joints are vertical and spaced approximately 1 m apart. An apron of talus lies at the base of the bedrock cliff on the south side of the valley. The upstream and downstream ends of the reach are bounded by bedrock buttresses. This reach is long (~1700 m) and is the widest (~400 m) reach studied. The river meanders through a well developed floodplain. At least seven terrace levels are preserved. Stream gradient is low and controlled by alluvium. Channel width is approximately 35 m. The channel morphology is pool and riffle; bars, secondary channels, and transient islands are present in this reach. Bed material is well-sorted cobbles with some patches of boulders. The downstream end of the reach corresponds to the fault contact between Challis volcanic tuffs (Tdq) and Neoproterozoic diorite intrusions (Zdi); diorite bedrock creates buttresses, and the valley floor narrows significantly below this reach boundary.

Figure 12. Photograph of Big Creek in the Cabin Creek Reach, the widest valley floor on the river.

2.3.9 Lobauer Reach (Reach #9)

Bedrock type is diorite. This reach is short and moderately wide (~100 m). Reach is bounded on the upstream end by a bedrock buttress extending from the north side of the valley, and on the downstream end by a bedrock buttress extending from the south side of the valley. The south side hillslope is steeper than the north side but has few bedrock outcrops exposed in the lower slope. The north side hillslope is covered with talus and several alluvial fans; some soil has developed, and the slope is covered with grass. The channel is straight and approximately 30 m wide. A small longitudinal bar and a dry secondary channel are present. Low (1-2 m) terraces exist on both sides of the valley and are heavily vegetated. Channel morphology is plane bed, and the bed material is well-sorted cobbles with some large (1 m) boulders. Stream gradient is low and controlled by alluvium.

2.3.10 Cougar Creek Reach (Reach #10)

Bedrock type is quartzite with sub-horizontal joints dipping slightly northwest. This reach is long (~1500 m) and moderately wide (~110 m). The upstream end of the reach is bounded by a bedrock buttress. The north side hillslope has a bedrock cliff in the upper slope and a large apron of talus covering the lower slope. The south side hillslope is generally steeper and has more exposed bedrock than the north side. Floodplain and terraces (3-4 m above the river) are present in this reach. Two large, stable, heavily vegetated islands are present in mid-channel. No bedrock is exposed in the channel. Stream gradient is gentle, but steepens around the stable islands, and is controlled by alluvium. Channel morphology is plane bed, with riffles above and below the stable islands. Bed material is cobble – boulder. The downstream boundary of this reach is approximately the present position of a knickpoint that has migrated up from the Middle Fork Salmon River.

2.3.11 Big Creek Gorge Reach (Reach #11)

Bedrock type is granodiorite. This reach is short (~375 m) and very narrow (<20 m). The river is constricted to a narrow bedrock gorge with vertical walls. No floodplain or terraces are present; the valley floor width is the channel width. Bedrock is foliated but has no trend in direction. Channel morphology is bedrock, with some large (2-3 m) boulders in the channel. River flows directly against bedrock walls. Gradient is steep and controlled by bedrock.

Figure 13. Photograph of Big Creek Gorge. No floodplain is developed here; river channel is in direct contact with bedrock walls.

2.3.12 Breeching Creek Reach (Reach #12)

Bedrock type is granodiorite with horizontal foliation joints that are spaced 1-2 m apart. Valley floor width is narrow (~20 m). Hillslopes are steep and mostly exposed bedrock. Bedrock is exposed in the channel; the stream gradient is controlled by bedrock. Channel morphology is step pool; large (1-4 m) boulders create steps, and pools are 3 m deep and bottomed with sand and gravel. Large, immobile boulders exhibit flutes, potholes, and other evidence of abrasion.

2.3.13 Bighorn Bridge Reach (Reach #13)

Bedrock type is granodiorite with horizontal foliation joints spaced 1-2 m apart. This reach has a steep stream gradient and is moderately long (~500 m). Valley floor width is narrow (~20 m). Hillslopes are steep and mostly exposed bedrock. Bedrock is exposed in the channel in many places. No floodplain or terraces are present in this reach. The channel is bedrock covered with a thin layer of alluvium composed of large (1-4 m) boulders and some sand and gravel. Stream gradient is steep and controlled by bedrock. Channel morphology is step pool, with 2-3 m pool spacing.

CHAPTER 3: METHODS

3.1 Introduction

Four types of data were collected in this study. First, rock strength data for both sides of the valley were obtained with the Schmidt hammer. Second, valley floor widths were measured in the field with a laser rangefinder. Third, the stream gradient of each reach was calculated by measuring stream length and stream elevation on digital elevation models. Fourth, hillslope gradient and hypsometric integral for both sides of the valley were calculated from digital elevation models. Additional data extracted from digital elevation models included relief, main trunk channel length, mean basin elevation, basin area, hypsometric curves, and hypsometric integrals.

3.2 Reach Delineation

Reaches were chosen on the basis of valley floor width, as measured on USGS 7.5' topographic maps. Valleys of uniform width bounded by marked changes in width at both ends were identified. This criterion follows the general criteria outlined by Grant and Swanson (1995). A range of widths were chosen to represent the variety of morphometry in Big Creek valley. Reaches that encompass major tributary junctions were not used because of the confounding effects of a point source sediment supply. The Cabin Creek reach (Figure 12) is an exception to this criterion because the Big Creek valley is exceptionally wide in this reach, and Cabin Creek is a minor tributary that does not contribute enough sediment to alter the morphometry of the valley floor or stream channel. Most reaches are bounded by bedrock outcroppings that are referred to herein as "bedrock buttresses." In some cases reach boundaries (i.e. distinct changes in valley floor width) correspond to lithologic boundaries (e.g. the downstream boundary of Reach #8 is a northeast-trending normal fault putting tuff on diorite).

Because valley floor widths are not normally distributed, they are displayed on a log scale when graphing. Field measurements of the stream reaches were made in June and July 2004.

3.3 Rock Strength

3.3.1 In situ measurement using the Schmidt hammer

The Schmidt hammer was used to measure the *in situ* rebound values of bedrock outcrops exposed in the valley walls (Figure 14). Rebound values were used as a relative measure of rock strength. Measurements were made in June and July 2004 and August 2005. Rebound measurements were taken on both the north and south valley walls for discrete analyses. The number of measurements collected varied by reach, based on reach lengths and amount of exposed bedrock but ranged between 60 and 150 measurements per valley side (see Appendix B). Measurements were spaced by at least 10 cm. The Schmidt hammer was always oriented normal to the surface being measured (Figure 14). The lowest elevation outcrops were measured, ranging from river level to 100 m above the valley floor. Because a purely objective grid method of taking measurements was impractical in the field, where bedrock exposure is sporadic, measurements were obtained to best represent the variability of rock characteristics in each reach. For example, outcrops with a uniform distribution of joints or fractures and weathering were sampled uniformly with measurements taken on weathered surfaces, fresh surfaces, between fractures, and directly on or near fractures. This provides an overall rebound measure that incorporates not only intact rock strength, but also irregularities such as weathering and fracture density. Another example includes an outcrop free from weathering and fractures, but with a zone of intense fracturing cut through it. The fracture zone does not account for a large proportion of the total exposed area of the outcrop, but it influences the overall strength of that outcrop. To measure the rebound values of this outcrop the majority of the measurements were concentrated on the fresh and unfractured surfaces. A number of measurements of the fracture zone, proportional to the area of the outcrop covered by the fracture zone, were also obtained. In other words, if the fracture zone covers 10% of the area of the outcrop, then 10% of the total rebound measurements of that outcrop would be from the fracture zone. This method is somewhat subjective, but considering the alternative (i.e. measuring intact rock strength and fracture density separately and trying to combine them) it is an effective way to obtain representative rebound measurements from an outcrop.

Figure 14. Photograph of the Schmidt hammer being used to measure bedrock rebound. Measurements were taken with the hammer positioned normal the surface being measured.

Four Schmidt hammer tests (one on each lithologic type) were performed in order to determine what effect joint spacing has on intact rock strength. Thirty measurements of unweathered, intact bedrock with joint spacing of one meter or greater were made. In regions of the outcrop with joint spacing of 0.5 m, 0.25 m, 0.125 m, and 0.06 m, 15 measurements were made on the center of the joint blocks and 15 measurements were made on the edges of joint blocks. Finally, 30 measurements were made on the interior and edges of joint blocks in a random manner to create a combined rock strength measurement. Rebound values from each category were averaged and compared. The combined rock strength measurement is the primary method for characterizing rock strength in this study, so this test is used to check the validity of that method.

Several methods for using the Schmidt hammer in the field have been suggested, but there is no universal procedure used in geomorphology (Day, 1980; Selby, 1980; ISRM, 1981). There is some debate as to what the Schmidt hammer measures and whether it is applicable to hillslope engineering or geomorphology. Engineers typically want to determine mechanical properties of a rock mass such as uniaxial compressive strength or Young's modulus of elasticity. Geomorphologists, on the other hand, are usually more interested in the surface properties of rock such as surface hardness, as well as fracturing. Because of surface irregularities such as weathering and roughness, Aoki and Matsukura (2004) suggest that repeated impacts be performed on the same point to determine the intact rock strength, whereas a single impact should be used to determine surface hardness. Day (1980) claims that, "surface hardness, as measured by the hammer, may be a better measure of resistance to erosion than the bulk compressive strength."

As previously discussed, rebound values can vary depending on the orientation of the Schmidt hammer. Most measurements were taken with the Schmidt hammer in the horizontal position. Some vertical measurements were taken, and in those cases an equal number were taken downward as were taken upward in order to eliminate any variability caused by gravity. Because the rebound values are used in this study as a relative measure, and because each reach is measured consistently, the positional variability is not as important as if absolute compressive strength values were being determined.

Measuring only exposed bedrock outcrops may bias the sampling toward stronger rock. On one hand exposed bedrock may be inherently stronger than unexposed or previously eroded bedrock. On the other hand strong bedrock at the base of the hillslope may be covered with talus derived from weak, weathered, or fractured bedrock further up the hillslope. In the latter case, exposures of bedrock do not reflect the strength of the bedrock and are simply a consequence of other processes. This is a possible source of error in the representation of overall rock strength by rebound values. Since exposed bedrock was the only bedrock that was possible to measure, those were the measurements that were made for this study.

3.4 Valley Morphometry

3.4.1 Valley Floor Width

Valley floor width is defined as the width of the flat valley bottom between valley walls. This includes the stream channel, floodplain, and any fluvial terraces up to 4 m above the floodplain. In Big Creek canyon, the valley floor is typically easy to delineate and is marked by a very distinct break in slope between the valley walls and valley floor. The width of the valley floor in Big Creek varies from just the width of the channel to a broad alluvial floodplain (Figures 12 and 13).

The valley floor width was measured with a Laser Technology Inc. Impulse LR infrared laser rangefinder. Six to ten transects were measured across the valley floor perpendicular to the valley axis at each reach. The transect distances for each reach were averaged together to obtain an average valley floor width for each reach. Most reaches had clear lines of sight across the valley floor, facilitating the use of the rangefinder. In cases where thick vegetation blocked a clear laser shot, many short distances were shot from landmark to landmark and a cumulative distance was calculated. Because live vegetation strongly reflects infrared radiation, the rangefinder is especially sensitive to foliage. This can be advantageous in cases where direct shots are obscured by undergrowth but large trees stand above shorter vegetation; the tree can be used as a landmark and the distance to the top can be shot and a horizontal distance calculated.

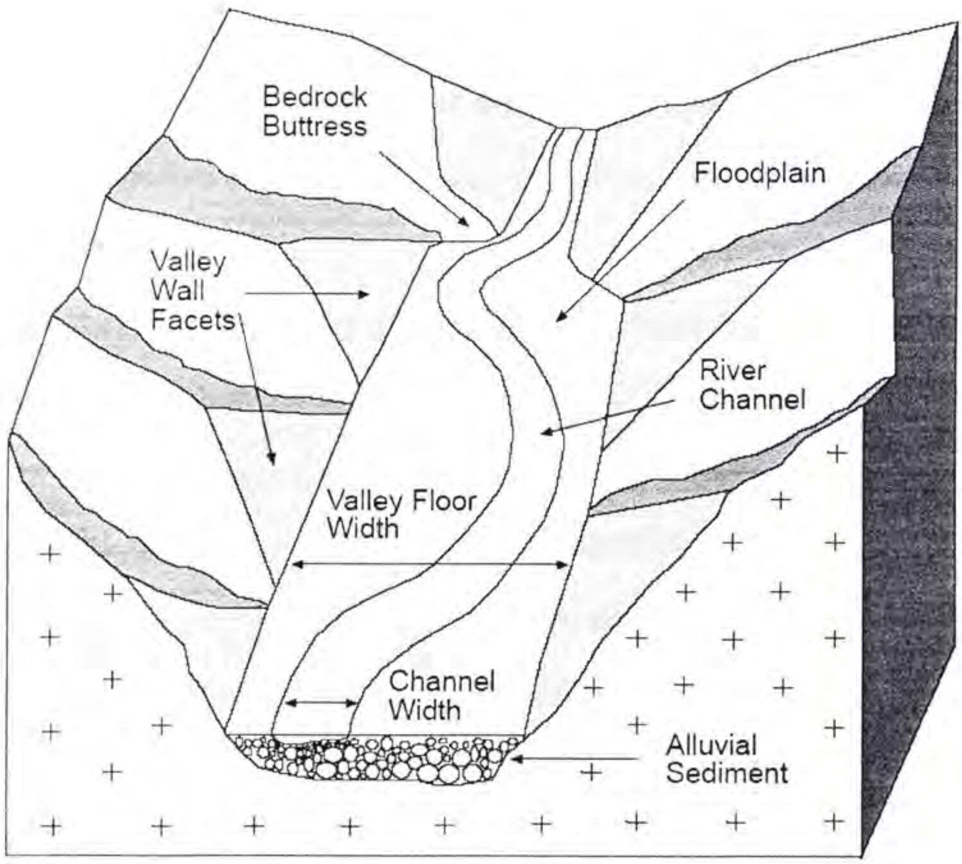

Figure 15. Schematic diagram of a river valley showing valley floor, river channel, floodplain, hillslope facets, bedrock buttresses, and a thin veneer of alluvial sediment. Plus symbols indicate bedrock.

3.4.2 Stream Gradient

Stream gradient is the ratio of the change in elevation to change in horizontal distance of the stream bed. Stream gradients for each reach were calculated using ArcMap 9.0 (Environmental Systems Research Institute, Inc., 2004). The stream channel was extracted from 7.5' USGS SDTS digital elevation models (DEMs) with 10 m resolution using the Soil and Water Assessment Tool (SWAT) (Grassland, Soil and Water Research Lab, 2002). The gradient was calculated in four different ways: 1) a gross change from the upstream end of the reach to the downstream end. 2) a gradient calculated over a longer distance in order to smooth out small scale variability. 3) a moving average gradient calculated with a 400 m window, and 4) a gradient measured directly from hard copy 7.5' topographic maps with contour intervals of 40 and 80 feet. For the second method, a buffer was created 100% of the reach length upstream and downstream of the reach so that the gradient was calculated over a distance three times the length of the actual reach. The stream gradients were compared to the average bedrock rebound value at each reach to determine the relationship between the two. I consider the 4th method to be the most representative, and the results from that method are presented in the results section.

3.4.3 Hillslope Gradient

Hillslope gradient is the gradient of the valley walls bounding the valley. Only valley walls (i.e. facets) whose strike parallels the valley axis are used (Figure 15). Valley walls of tributaries and gullies were not included in the measurement. The slopes of the valley-parallel facets were measured up to approximately 250 – 300 m above the valley floor. This elevation roughly corresponds to the tops of most facets and is a break in slope representing the initiation of recent rapid incision (Meyer and Leidecker, 1999). Slopes higher than this threshold elevation are vertically and horizontally distant from the rock strength measurements.

Hillslope gradient was measured separately for the north and south side of each reach. Measurements were made from 7.5' USGS SDTS DEMs with a resolution of 10 m in ArcMap 9.0 software (Environmental Systems Research Institute, Inc., 2004). Slope was calculated using the Slope tool over the area of each hillslope facet. The Slope tool returns mean, minimum, and maximum slope values for each facet. Average hillslope gradient was compared to average bedrock rebound value at each reach to determine the relationship between the two.

3.4.4 Hypsometric Analysis

In addition to hillslope gradient, a hypsometric curve and hypsometric integral were calculated for the north and south side hillslope facets adjacent to the river (the same hillslopes used to calculate hillslope gradient). Hypsometric analysis (also referred to as area-altitude analysis) is used to reveal the convexity of a hillslope (Strahler, 1952). A hypsometric curve is made by plotting the proportion of elevation versus the proportion of area. Hypsometric analysis can be performed on entire drainage basins (e.g. Figure 28), sub-basins, or single hillslopes. The curve produced is essentially a frequency distribution of elevations in a given area. In the case of a raster grid, such as a digital elevation model, each pixel has a known area and a known elevation. It is simple to compute the proportion of the pixels with an elevation above a given datum. The datum in the case of a drainage basin is the lowest point, the outlet. The hypsometric curve is not a topographic profile, but its shape does provide information about the slope. A convex up curve means that most of the area has a relatively high elevation. A concave up curve means that most of the area has a relatively low elevation. A convex or concave hypsometric curve reflects a convex or concave slope, respectively. The hypsometric integral is the area under the hypsometric curve. It is a dimensionless number between 0 and 1 that is calculated by integrating the hypsometric curve. A hypsometric integral of 0.50 is a perfectly straight line and means that the area is uniformly distributed among all elevations, and the slope is a straight line. Hypsometric integrals >0.50 describe slopes with more area at higher elevations than at lower elevations, and the slope would be convex up. Conversely, hypsometric integrals <0.50 describe slopes with more area at lower elevations than at higher elevations, and the slope would be concave up.

The same DEM-derived hillslope facets that were used in the hillslope gradient analysis were used in the hypsometric analysis. RiverTools software (Rivix, 2004) was used to calculate hypsometric data for each facet. Hypsometric integral was compared to average bedrock rebound value to determine the relationship between the two.

3.5 Data Analysis

The data collected were used to determine if correlations exist between: 1) rebound value and valley floor width, 2) rebound value and stream gradient, 3) rebound value and hillslope gradient, and 4) rebound value and hypsometric integral. T-tests and analysis of variance were performed to determine if the data from each reach, each lithologic group, and each aspect were significantly distinct. Regression analyses were performed to determine how robust the correlations are.

CHAPTER 4: RESULTS AND INTERPRETATION

4.1 Schmidt hammer rebound data

Bedrock rebound data collected with the Schmidt hammer were separated by reach, lithology, and aspect. The valley sides are designated as north and south. Twenty-six groups of data are possible from the 13 reaches; however the south banks of the Big Creek Gorge and Breeching Creek reaches were inaccessible and no bedrock rebound data were collected at these two sites (Figures 6 and 10). An average rebound value was calculated for each data group (Table 1). The logarithms of all rebound data were calculated before statistical analyses were performed. An analysis of variance (ANOVA) was performed on the data to determine if the variance between each reach was greater than the variance within each reach. If the variance within a reach is greater than between reaches, it would be impossible to statistically differentiate one reach from another.

ANOVA for the north side of the reaches and the south side of the reaches shows that in both cases the variance between reaches is greater than within reaches and that each reach has a significantly different bedrock rebound value. The P-values for the rebound values on the north and south sides of each reach are 4.17×10^{-63} and 1.32×10^{-26}, respectively; both P-values are well below the 0.05 value for testing significance.

Rebound data were also organized into lithologic groups. The four lithologic groups are: 1) Hoodoo Quartzite (Yh) and Yellowjacket Formation (Yy), 2) Diorite and Syenite intrusions (Zdi and Zsy), 3) Sunnyside tuff (Tss) and Dime and Quarter tuff (Tdq), and 4) Granodiorite (Tgd). Reaches (both north and south sides of the valley) are grouped by the underlying bedrock type. ANOVA was performed on the data with regard to lithology, and demonstrates that the different lithologies have distinct rebound values and the variance between the lithologic types is greater than the variance within the lithologic types ($P = 6.16 \times 10^{-07}$).

			Schmidt Rebound		Hypsometric Integral		Hillslope Gradient	
#	Reach	Average Valley Floor Width (m)	North (R)	South (R)	North Side Hillslope	South Side Hillslope	North (degrees)	South (degrees)
1	Little Ramey Cr.	89.83	38	47	0.3715	0.4332	33.85	26.36
2	Bar Cr.	21.15	50	51	0.3685	0.4302	38.17	34.21
3	Acorn Cr.	95.86	42	41	0.4024	0.3896	36.17	29.87
4	Soft Boil Bar	63.56	40	42	0.3743	0.3543	34.94	30.41
5	Dacite Gorge	25.84	53	56	0.3768	0.3678	31.95	33.64
6	Vines	208.53	35	44	0.3512	0.3348	33.33	32.69
7	Doe Cr.	22.30	48	44	0.4356	0.3993	38.70	32.43
8	Cabin Cr.	412.45	30	49	0.3615	0.3478	26.79	33.90
9	Lobauer	103.24	45	43	0.4917	0.3466	31.04	38.91
10	Cougar Cr.	109.08	43	46	0.3833	0.4712	33.86	29.14
11	Big Creek Gorge	18.06	54	N/A	0.4610	0.4904	45.66	37.65
12	Breeching Cr.	22.24	50	N/A	0.3396	0.3594	40.18	40.04
13	Bighorn Bridge	20.12	48	53	0.3892	0.4359	40.79	34.46

Table 1. Summary of rock strength and valley morphometric data collected at Big Creek. N/A indicates that data were not collected.

In addition to ANOVA, t-tests (two sample, assuming unequal variances) were performed on the data to determine if any significant differences exist between the north and south side rebound values (Table 2). The north and south side data were compared to each other in three ways: 1) with data organized by reach, 2) with data organized by lithology, and 3) with all north side data compared to all south side data. Five reaches have significant differences between north and south side rebound values: Little Ramey Creek, Vines, Doe Creek, Cabin Creek, and Bighorn Bridge. Six reaches do not have significant differences between north and south side rebound values: Bar Creek, Acorn

Creek, Soft Boil Bar, Dacite Gorge, Lobauer, and Cougar Creek. Overall, though, there is a significant difference between the rebound values for the north side data and the south side data, combined among all reaches ($P = 1.24 \times 10^{-07}$). Some reaches have such large differences between the north and south sides of the valley that they strongly influence the t-test for the combined north and south side data. The Cabin Creek reach, in particular, has highly variable rebound values and a very high P-value ($P = 7.00 \times 10^{-26}$). The Vines reach also has a highly significant difference ($P = 9.73 \times 10^{-08}$) in rebound values on the north and south sides of the valley that contributes to the overall significant difference in the combined north and south side data.

When organized by lithology, the north/south variability in rebound is significantly different for Diorite and Syenite (Zdi and Zsy), Sunnyside tuff (Tss) and Dime and Quarter tuff (Tdq), and granodiorite (Tgd), but not for Hoodoo Quartzite (Yh) and Yellowjacket Formation (Yy). From field observation, the tuffs are by far the most variable unit and a significant difference between north and south rebound values is not surprising. The diorite/syenite and granodiorite units are also visibly weathered, and have variable rebound values. The diorite/syenite weathers easily along mineral grain boundaries, and the granodiorite commonly weathers to grus.

The quartzite units, on the other hand, tend to be less resistant to weathering and are generally more consistent in the way they weather, alter, and fracture than the other lithologic types. Thus, no significant difference exists between north and south side rebound values in the quartzite units.

The significant difference in rebound between the north side of the valley and the south side of the valley is an interesting and unexpected result. The north valley wall (which is south-facing) has a lower average rebound than the south valley wall (which is north-facing). I propose that lower rebound values on south-facing slopes may be caused by the higher frequency of freeze-thaw cycles that occur where solar radiation during the day can melt ice that formed at night. By contrast, north-facing slopes remain in shadow throughout the day and are continuously frozen or covered with snow, preventing high frequency freeze-thaw cycles. See Chapter 5 for a more detailed discussion.

#		P-Value (two-tail)	Significant Difference between N & S?
1	Little Ramey Cr.	0.0009	Yes
2	Bar Cr.	0.6636	No
3	Acorn Cr.	0.3432	No
4	Soft Boil Bar	0.1127	No
5	Dacite Gorge	0.1142	No
6	Vines	9.73×10^{-08}	Yes
7	Doe Cr.	0.0428	Yes
8	Cabin Cr.	7.00×10^{-26}	Yes
9	Lobauer	0.4792	No
10	Cougar Cr.	0.0895	No
11	Big Creek Gorge	N/A	N/A
12	Breeching Cr.	N/A	N/A
13	Bighorn Bridge	0.0039	Yes
	Yh/Yy	0.0895	No
	Zdi/Zsy	0.0110	Yes
	Tss/Tdq	4.23×10^{-15}	Yes
	Tgd	0.0039	Yes
	All North vs. All South	1.24×10^{-07}	Yes

Table 2. Summary of results from t-test comparing north and south side rebound data. N/A indicates that data from only one side of the valley were collected and a t-test was not possible. Tests in which the P-value is less than 0.05 are considered statistically significant.

Table 3 summarizes the results from the four Schmidt hammer joint spacing tests that were performed (one on each lithologic group). These data show several important trends. First, Schmidt hammer rebound values decrease as joint spacing decreases because joint blocks are smaller and can vibrate or move when impacted, thus attenuating some of the energy that can be rebounded.

	Average Schmidt Hammer Rebound Value (R)			
Joint Spacing	**Granodiorite**	**Quartzite**	**Densely Welded Tuff**	**Diorite**
Intact	63.6	69.6	67.4	52.3
0.5 m (center)	65.2	66.3	59.9	53.9
0.5 m (edge)	42.1	61.7	55.6	46.2
0.5 m (comb.)	50.1	63.0	56.4	51.6
0.25 m (center)	49.1	68.0	52.4	47.4
0.25 m (edge)	41.5	56.6	47.6	33.4
0.25 m (comb.)	46.7	62.6	48.4	43.5
0.12 m (center)	43.2	61.6	51.3	38.6
0.12 m (edge)	32.2	56.3	44.2	32.5
0.12 m (comb.)	33.4	59.9	49.5	34.1
0.06 m (center)	33.4	56.4	47.4	27.0
0.06 m (edge)	31.1	50.9	46.6	19.7
0.06 m (comb.)	32.0	50.1	45.1	24.1

Table 3. Summary of Schmidt hammer joint spacing tests on outcrops of each lithologic group. "Center" represents measurements made on the center of joint blocks, "edge" represents measurements made on the edge of joint blocks, and "comb." represents measurements using the combined rock strength method.

Second, measurements made on the edges of joint blocks are lower than measurements made on the center of joint blocks, again because of the ability of joints to attenuate energy. Third, the average combined rock strength measurement almost always lies between the average joint block center and average joint block edge measurements. Finally, all the lithologic groups follow the above trends, but each group has a characteristic behavior. For example, diorite rebound measurements vary widely from wide to narrow joint spacing, and the difference between joint block center and edge values is large. Quartzite rebound measurements are high even at small joint spacing, and the difference between joint block center and edge values is smaller compared to other lithologic groups. These tests demonstrate that joints decrease intact rock strength and that the combined rock strength method of measuring with the Schmidt hammer systematically incorporates joint spacing into intact rock strength. Thus, the combined rock strength method used in this study is a valid way of estimating rock strength with a Schmidt hammer without necessarily knowing the joint spacing of each outcrop measured.

4.2 Valley Floor Width

The valley floor width transects measured in each reach were averaged together (Table 1). In order to test possible relationships between rock strength and geomorphic processes, average valley floor width was compared to five categories of bedrock rebound value: 1) average rebound of the north side of the valley (Figure 16), 2) average rebound of the south side of the valley (Figure 17), 3) average rebound of both sides together (Figure 18), 4) average rebound of the strongest valley side in each reach (Figure 19), and 5) average rebound of the weakest valley side in each reach (Figure 20). A regression analysis was also performed for each comparison to determine how significant each correlation was. Because rebound data were not collected for the south sides of Breeching Creek reach and Big Creek Gorge reach, those data points do not appear on the graphs.

Strong negative correlations exist between valley floor width and rebound on the north sides ($r^2 = 0.8530$, $P = 6.61x10^{-6}$), valley floor width and rebound on both sides together ($r^2 = 0.7712$, $P = 7.86X10^{-5}$), and valley floor width and rebound of the weakest sides ($r^2 = 0.8394$, $P = 1.08x10^{-5}$). Negative correlations are weaker between valley floor width and rebound on the south sides ($r^2 = 0.2957$, $P = 0.0547$), and between valley floor width and rebound on the strongest sides ($r^2 = 0.3959$, $P = 0.0212$). It is immediately apparent that the graphs of the north sides and south sides are quite different, as would be expected from the t-tests that showed a significant difference between the two. Furthermore, the graph of the strongest valley sides (Figure 19) corresponds very closely to the graph of the south sides (Figure 17), and the graph of the weakest valley sides (Figure 20) corresponds very closely to the graph of the north sides (Figure 16).

Figure 18 shows the valley floor width versus the rebound value of both sides of the valley averaged together. The negative correlation is fairly strong ($r^2 = 0.7712$), but is probably not the best representation of the relationship between valley floor width and rebound. The t-test shows that there is a significant difference between the rebound values of the north and south sides of the valley, so combining the values together simply yields a single averaged value that does not represent the rebound value of the valley walls in that reach. If there was no discernible difference between the rebound of the north and south valley walls (i.e. the t-test returned a P-value of >0.05), then combining the rebound values of the two valley walls would be more practical.

The weakest side graph (Figure 20) is probably the best representation of the relationship between bedrock rebound value and valley floor width. In cases where one side of the valley has a higher strength, the energy of the river will do more erosive work on the weaker side than on the stronger side. The weaker side, therefore, has a greater influence on the morphometry of the valley floor. The stronger side reflects or diverts much of the energy of the river. The Cabin Creek reach is an excellent example of this. The north side of the valley has a much lower average rebound value than the south side of the valley. As a consequence, the south side of the valley is straight, parallel, and close to the valley axis, while the north side of the valley is a large, rounded embayment with the valley wall displaced approximately 300 m from the valley axis. Most of the valley floor width in this reach is the result of erosion of the weaker (north) side of the valley. The graphs of the strongest sides (Figure 19) and the weakest sides (Figure 20) support this explanation and show that valley floor width is most strongly controlled by rock strength on the weaker side.

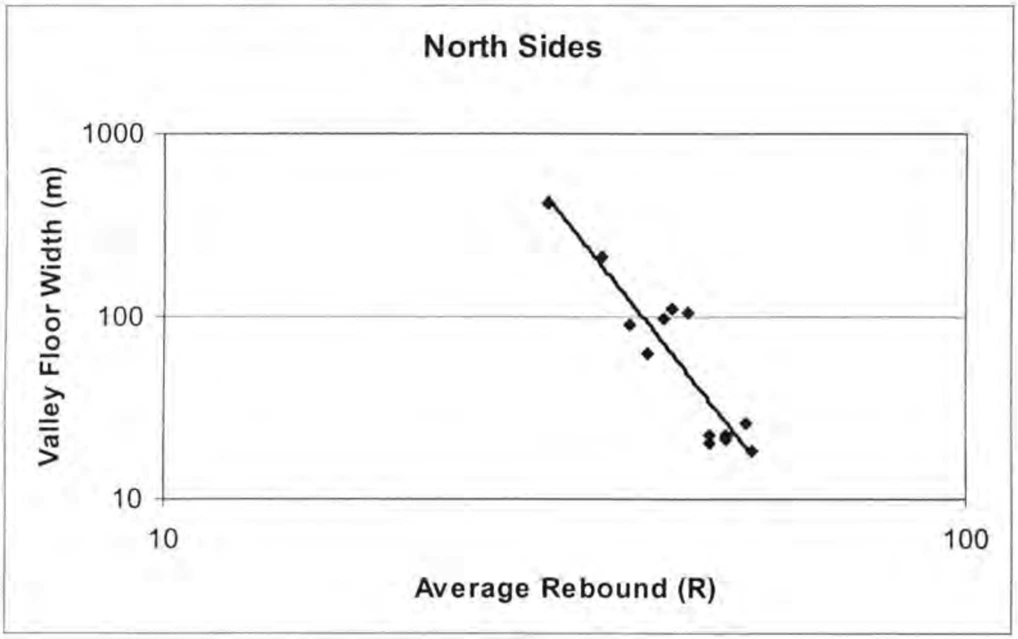

Figure 16. Log-log graph of north side bedrock rebound versus valley floor width. Each point represents a reach ($r^2 = 0.8530$, $P = 6.61x10^{-06}$).

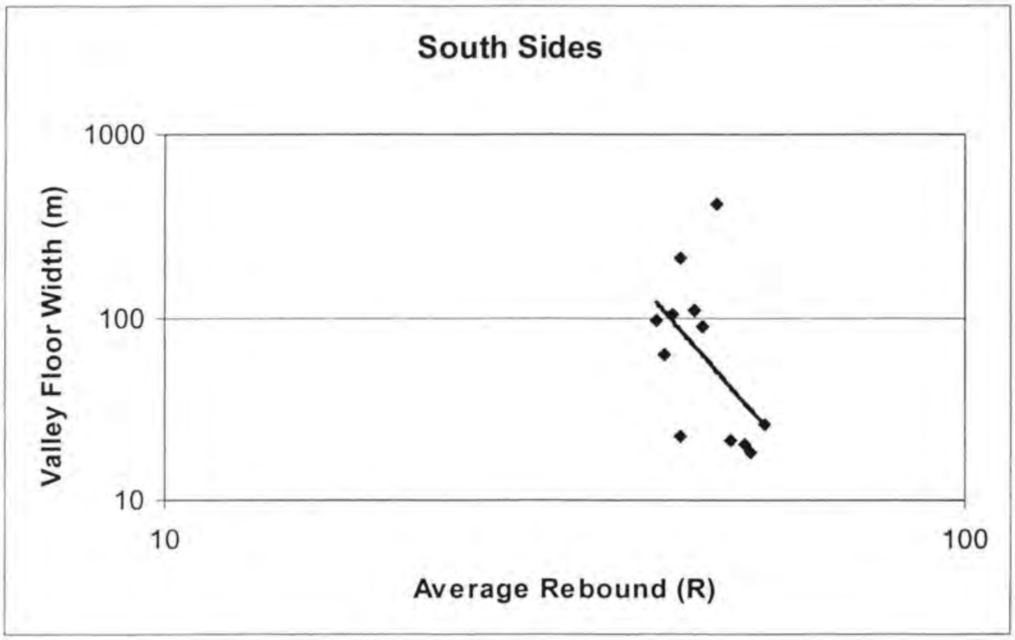

Figure 17. Log-log graph of south side bedrock rebound versus valley floor width. Each point represents a reach ($r^2 = 0.2957$, $P = 0.0547$).

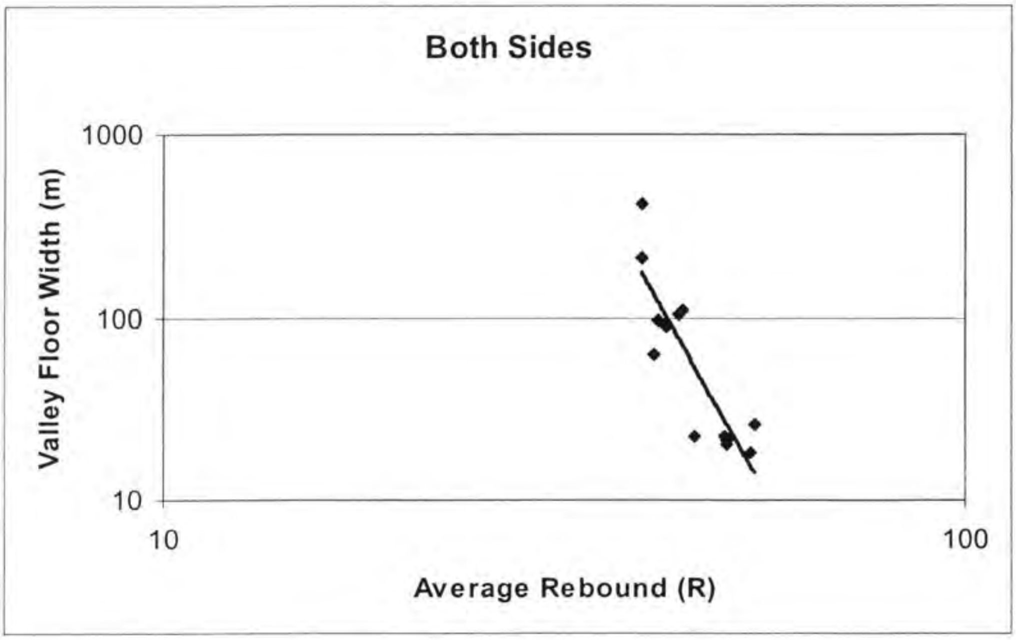

Figure 18. Log-log graph of bedrock rebound on both side of the valley versus valley floor width. Each point represents a reach ($r^2 = 0.7712$, $P = 7.86 \times 10^{-05}$).

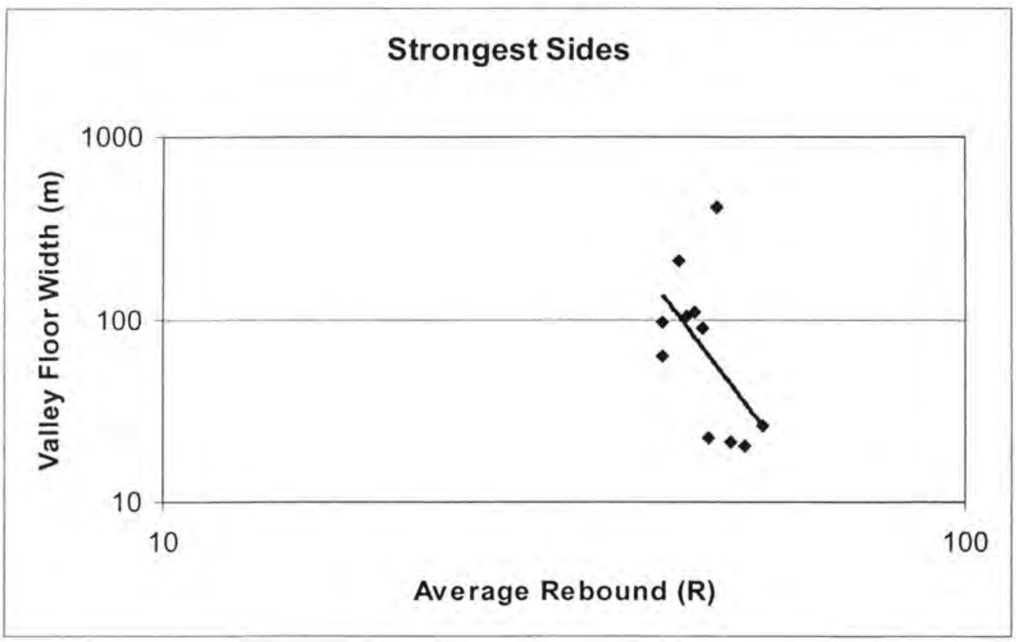

Figure 19. Log-log graph of bedrock rebound from the strongest side of the valley versus valley floor width. Each point represents a reach ($r^2 = 0.2801$, $P = 0.0941$).

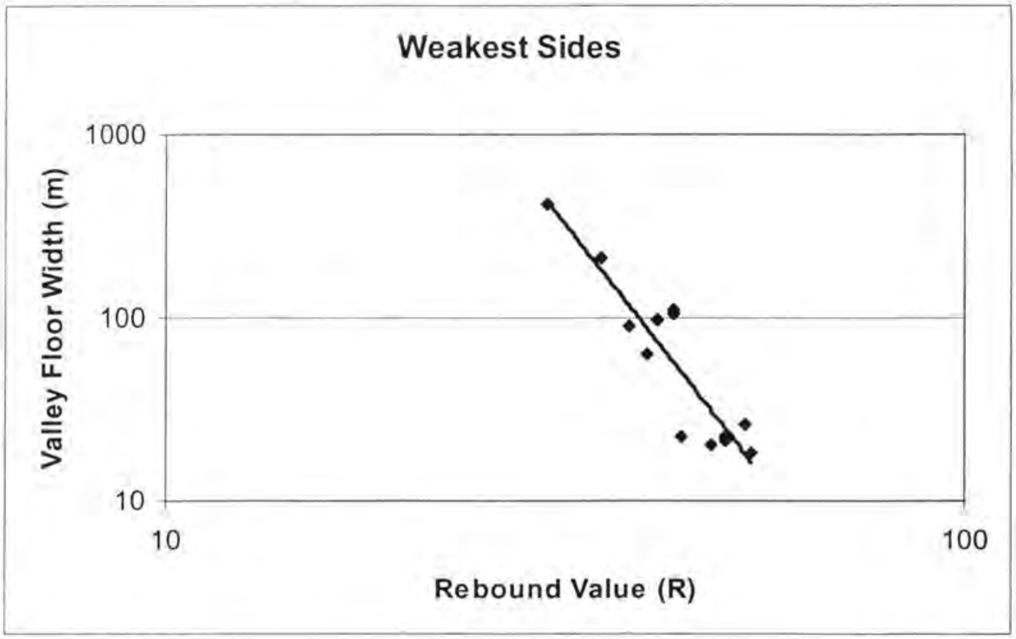

Figure 20. Log-log graph of bedrock rebound from the weakest side of the valley versus valley floor width. Each point represents a reach ($r^2 = 0.8394$, $P = 1.08 \times 10^{-05}$).

4.3 Stream Gradient

Stream gradient was calculated in four ways, as described in section 3.4.2. Only the stream gradients derived from the hard-copy topographic maps is presented here because it fits the overall longitudinal profile of Big Creek the best of all four methods. DEM-derived stream gradient data is presented in full in Appendix C, and in Table 5 for comparison. Tables 4 and 5 and Figures 21 and 22 summarize the stream gradient data. Gradient varies from 0.5% to 2.0%. The reach gradients, which are ordered sequentially from upstream to downstream in Table 5, do not decrease systematically downstream as one would expect in a graded stream. The longitudinal profile of the entire main stem of Big Creek reveals that it is not an ideal graded stream (Figure 28).This can be accounted for by a structural base level control at the down stream of the Cabin Creek Reach (Reach

#8) and a prominent knickpoint at the upper end of Big Creek Gorge (Reach #11) which likely originated from recent incision of the Middle Fork Salmon River (Meyer and Leidecker, 1999).

#	Reach	Reach Length (m)	Channel Width (m)	Reach Length (channel widths)	Δ Elevation (m)
1	Little Ramey Cr.	1139.6	26.9	42	7.2
2	Bar Cr.	1516.8	21.2	71	10.4
3	Acorn Cr.	755.6	41.6	18	18.3
4	Soft Boil Bar	568.5	37.0	15	3.0
5	Dacite Gorge	287.8	25.8	11	3.4
6	Vines	1531.8	34.3	45	20.3
7	Doe Cr.	531.3	21.1	25	13.6
8	Cabin Cr.	1715.8	36.0	48	12.7
9	Lobauer	322.8	30.0	11	0.3
10	Cougar Cr.	1480.2	33.8	44	9.9
11	Big Creek Gorge	372.9	18.0	21	4.9
12	Breeching Cr.	781.7	22.2	35	5.9
13	Bighorn Bridge	513.6	20.1	26	11.5

Table 4. Data for 13 reaches at Big Creek.

#	Reach	Gross Gradient (%)	Gradient with buffer (%)	Moving Average Gradient (%)	Topo Derived Gradient (%)	Channel Type
1	Little Ramey Cr.	0.63	1.26	0.69	1.2	Alluvial
2	Bar Cr.	0.68	1.14	0.63	1.1	Alluvial
3	Acorn Cr.	2.42	1.10	2.24	0.9	Alluvial
4	Soft Boil Bar	0.53	1.41	0.64	0.9	Alluvial
5	Dacite Gorge	1.18	1.67	1.79	0.9	Bedrock
6	Vines	1.32	1.15	1.27	0.7	Alluvial
7	Doe Cr.	2.56	0.86	1.68	1.1	Bedrock
8	Cabin Cr.	0.74	0.70	0.71	0.5	Alluvial
9	Lobauer	0.09	0.48	0.24	0.5	Alluvial
10	Cougar Cr.	0.67	0.85	0.65	0.7	Alluvial
11	Big Creek Gorge	1.31	1.09	1.39	1.4	Bedrock
12	Breeching Cr.	0.75	1.03	0.98	1.3	Bedrock
13	Bighorn Bridge	2.24	1.49	1.94	2.0	Bedrock

Table 5. Stream gradient data for 13 reaches at Big Creek. "Topo Derived Gradient" was calculated from 7.5' topographic maps.

Average rebound value on the strongest side of the valley is not related to reach gradient derived from topographic maps (Figure 21, $r^2 = 0.1855$, $P = 0.1859$). A weak, but statistically significant, relationship exists between the average rebound value on the weakest side of the valley and the reach gradient (Figure 22, $r^2 = 0.3158$, $P = 0.0456$).

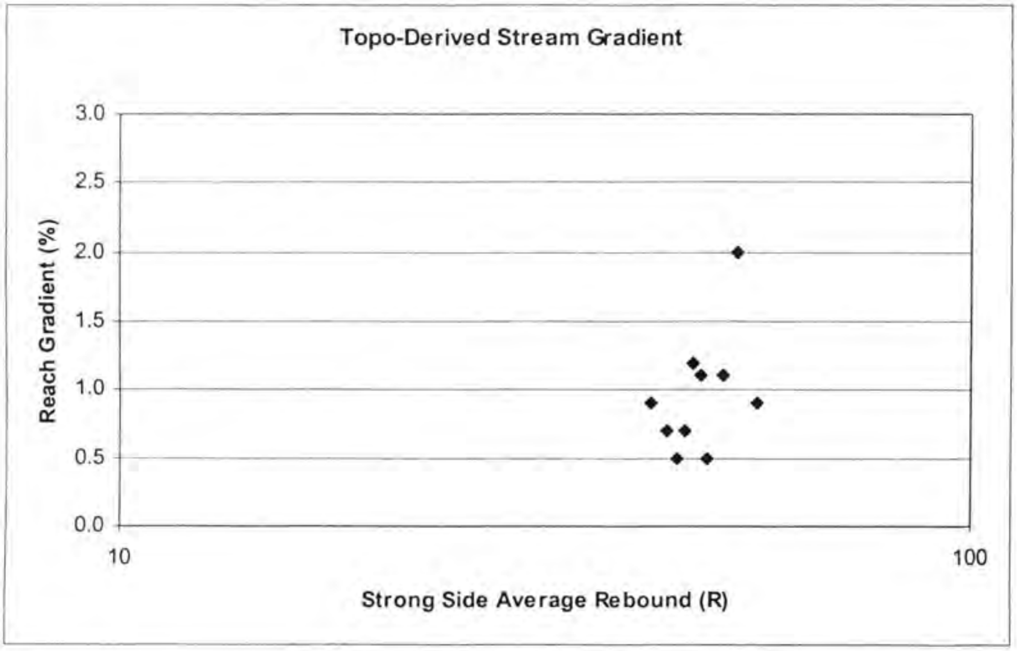

Figure 21. Semi-log graph of average rebound on the strong side of the valley vs. reach gradient measured from 7.5' topographic maps ($r^2 = 0.1856$, $P = 0.1859$).

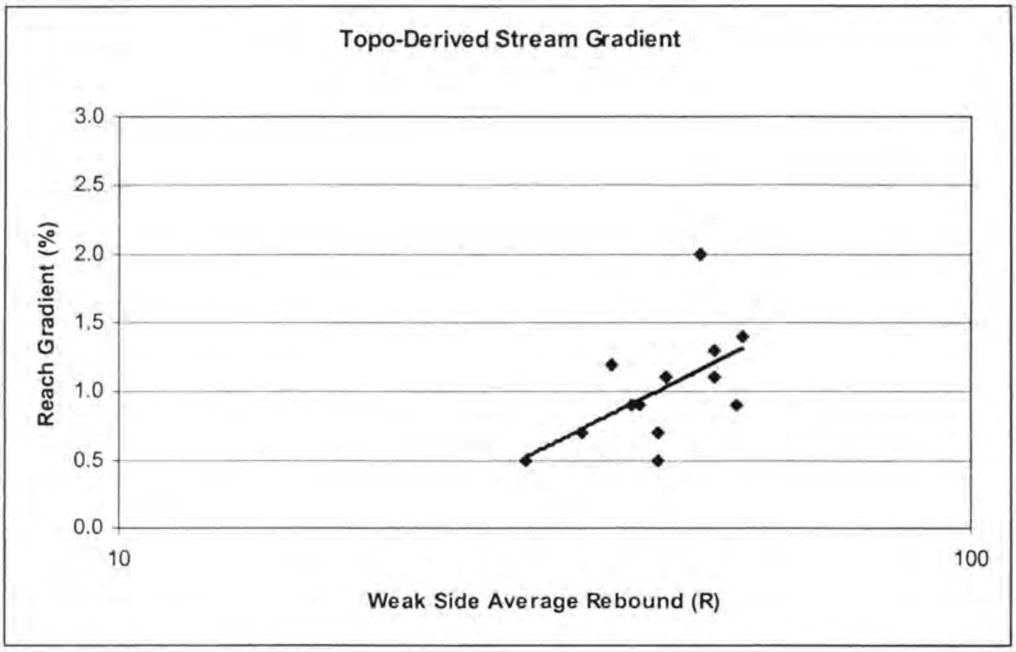

Figure 22. Semi-log graph of average rebound on the weak side of the valley vs. reach gradient measured from 7.5' topographic maps ($r^2 = 0.3158$, P = 0.0456).

Reaches are classified as either alluvial or bedrock according to the previously described definition (Table 5). Since alluvial reaches have depositional channel morphologies, the channel gradient may not reflect the gradient of the bedrock of the valley floor. To test if the channel bed type (e.g. alluvial or bedrock) has an influence on the relationship between bedrock rebound and stream gradient, reaches were separated by bed type and only bedrock channel reaches were used to determine if a correlation exists. Five reaches were identified as having a bedrock channel: Reaches #5, #7, #11, #12, and #13. When only these five points are plotted on a graph of average rebound on the weakest side of the valley versus topographic map-derived stream gradient (Figure 23), no correlation exists ($r^2 = 0.0205$, P = 0.8181).

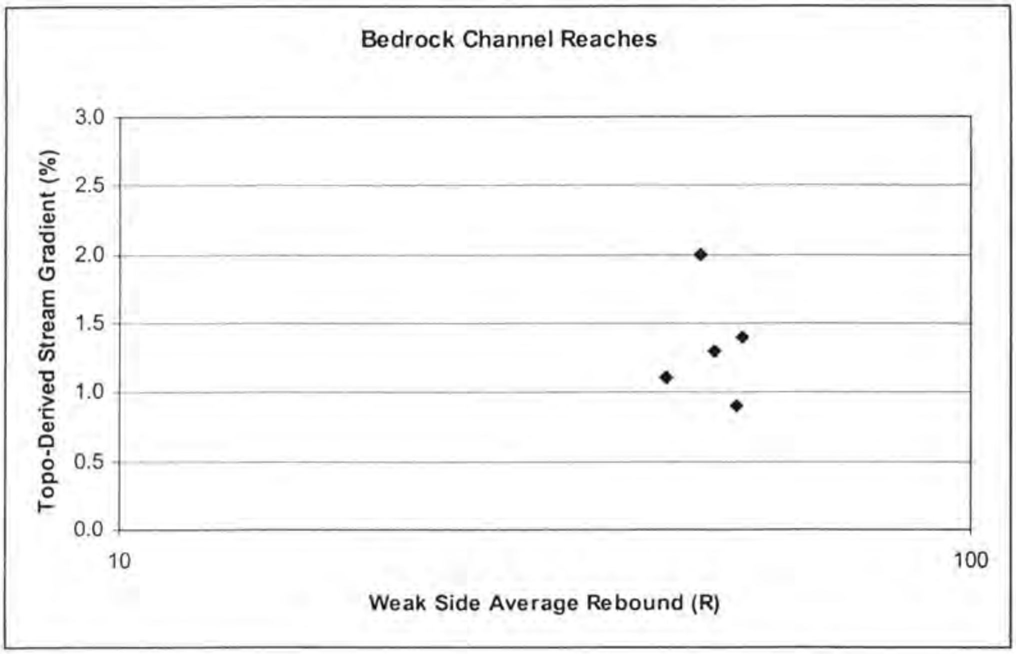

Figure 23. Semi-log graph of weakest side average rebound vs. topo-derived stream gradient for only bedrock-channel reaches.

4.4 Hillslope Gradient

Hillslope data are presented in Table 1 and Figures 24-27. Data in the graphs are presented in four ways. Figure 24 shows north side rebound data versus average hillslope gradient on the north side of the valley. Figure 25 shows south side rebound data versus average hillslope gradient on the south side of the valley. Figure 26 shows rebound data for both sides combined versus the average of the north and south side average hillslope gradient. Finally, Figure 27 compares hillslope gradients of the north side and south side with valley floor width. Correlations between most of these variables are weak, as demonstrated by the low r^2 values and high P-values. Average north side hillslope gradient versus north side rebound also exhibits a moderate, but statistically significant, correlation (Figure 24, $r^2 = 0.4906$, $P = 0.0071$). Average hillslope gradient of both valley sides combined versus bedrock rebound (Figure 26) has an r^2 value of 0.5113 and a P-value of 0.0057. Hillslope gradient and bedrock rebound at Big Creek are only moderately related. There is also a moderate correlation between the average north side hillslope gradient and the logarithm of valley floor width (Figure 27, $r^2 = 0.6591$, P = 0.0009).

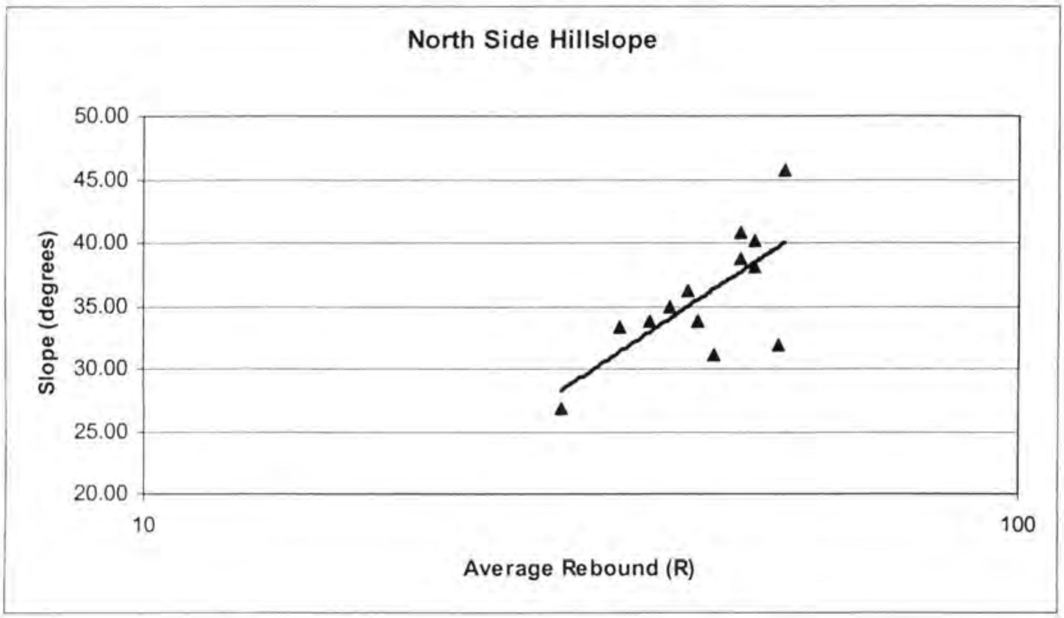

Figure 24. Semi-log graph of average rebound value versus average hillslope gradient on the north side of the valley ($r^2 = 0.4976$, P = 0.0071).

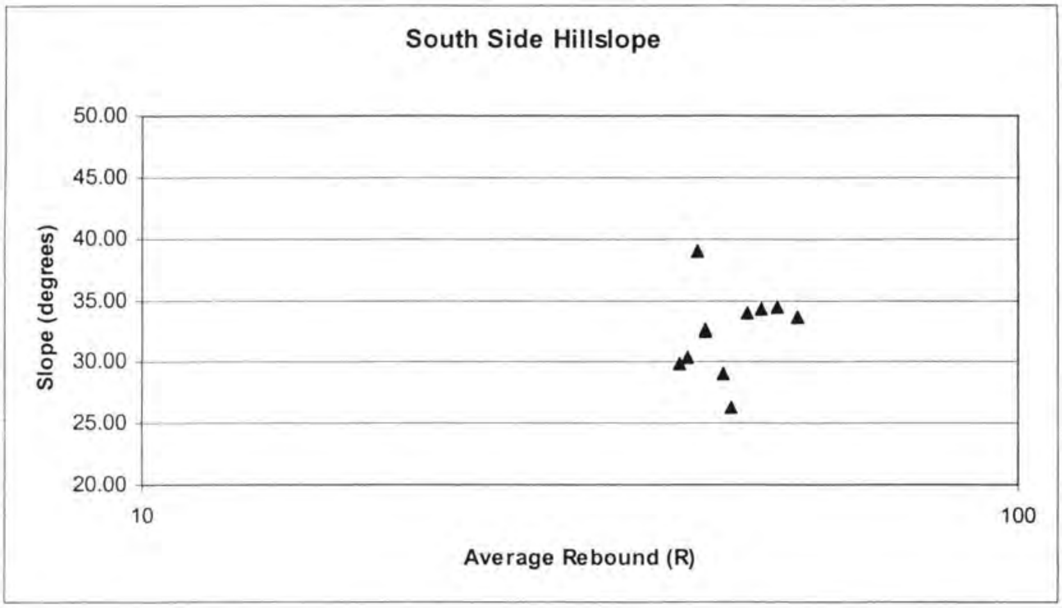

Figure 25. Semi-log graph of average rebound value versus average hillslope gradient on the south side of the valley ($r^2 = 0.0449$, $P = 0.5316$).

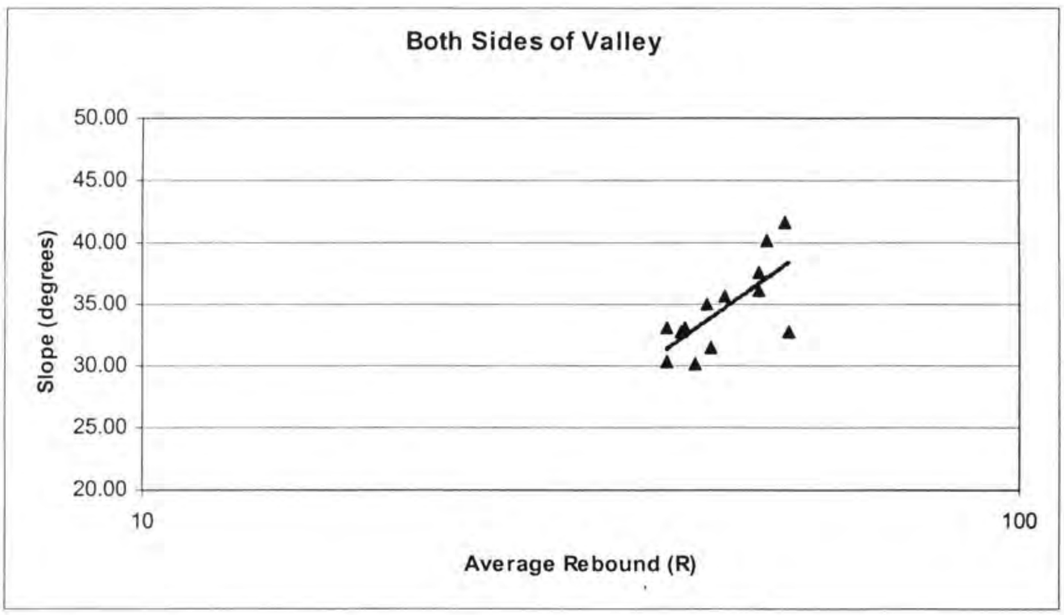

Figure 26. Semi-log graph of average rebound value versus average hillslope gradient on the both sides of the valley ($r^2 = 0.5153$, $P = 0.0057$).

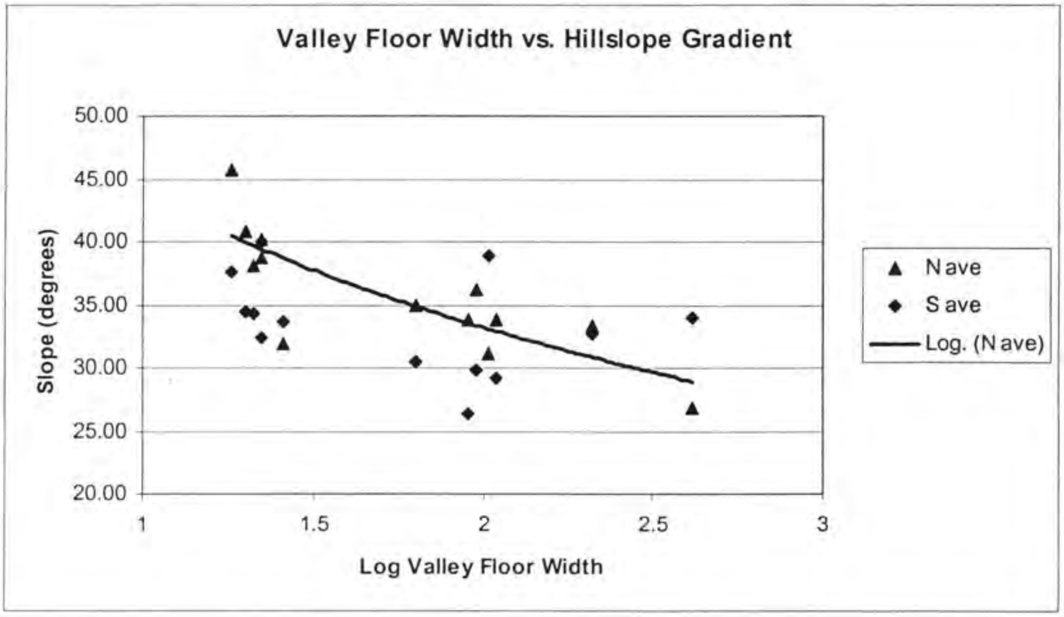

Figure 27. Graph of the logarithm of valley floor width versus hillslope gradient of north ($r^2 = 0.6591$, $P = 0.0009$) and south sides of the valley ($r^2 = 0.0147$, $P = 0.7226$).

4.5 Hypsometric Analysis

Figure 28 is an example of a hypsometric curve, in this case for the entire Big Creek drainage basin. Relative elevation (h/H) is calculated by dividing the elevation of a given pixel (h) by the total relief of the area of interest (H). Relative area (a/A) is calculated by dividing the area of a pixel or group of pixels with the same relative elevation (a) by the total area of interest (A). Figure 28 shows that 70% of the area (i.e. 70% of the pixels in the DEM) occurs in the upper 50% of the elevation of the basin. About 50% of the area occurs in the upper 40% of the elevation of the basin.

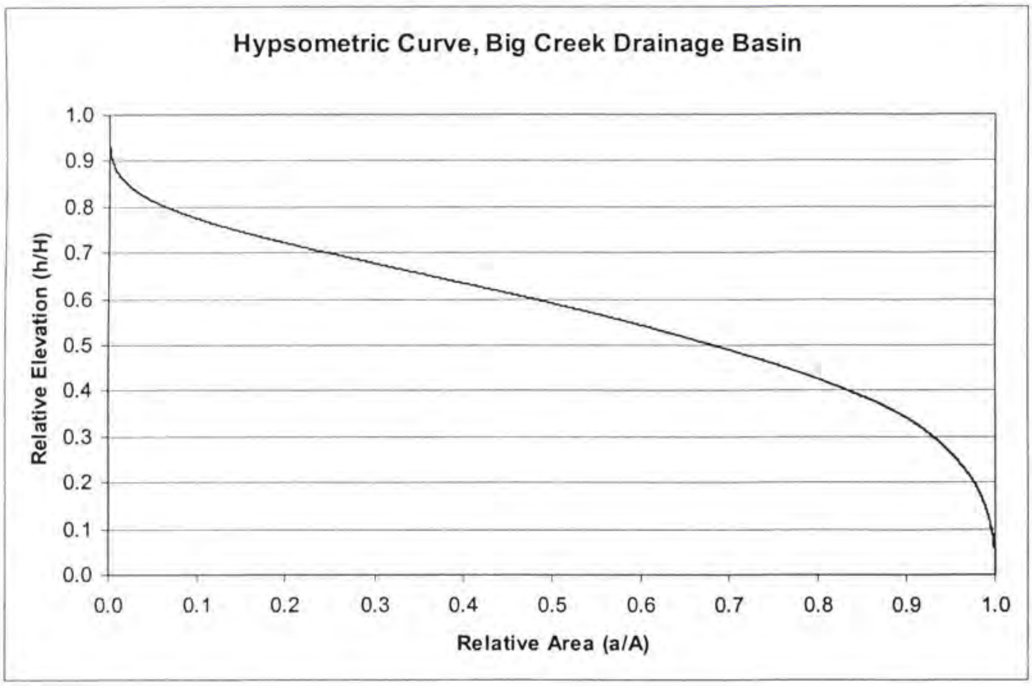

Figure 28. Hypsometric curve of the entire Big Creek drainage basin, calculated using RiverTools. Almost 70% of the basin area lies in the upper 50% of the elevation.

Hypsometric data are presented in Table 1 and Figures 29 and 30. No relationship exists between hypsometric integral and bedrock rebound data. Figure 29 is a graph of the hypsometric integral on the north side hillslope versus the logarithm of the north side bedrock rebound ($r^2 = 0.1282$, $P = 0.2297$). Similarly, the graph of the hypsometric integral on the south side hillslope versus the logarithm of the south side bedrock rebound (Figure 30) does not reveal a significant correlation: $r^2 = 0.0743$, $P = 0.4172$.

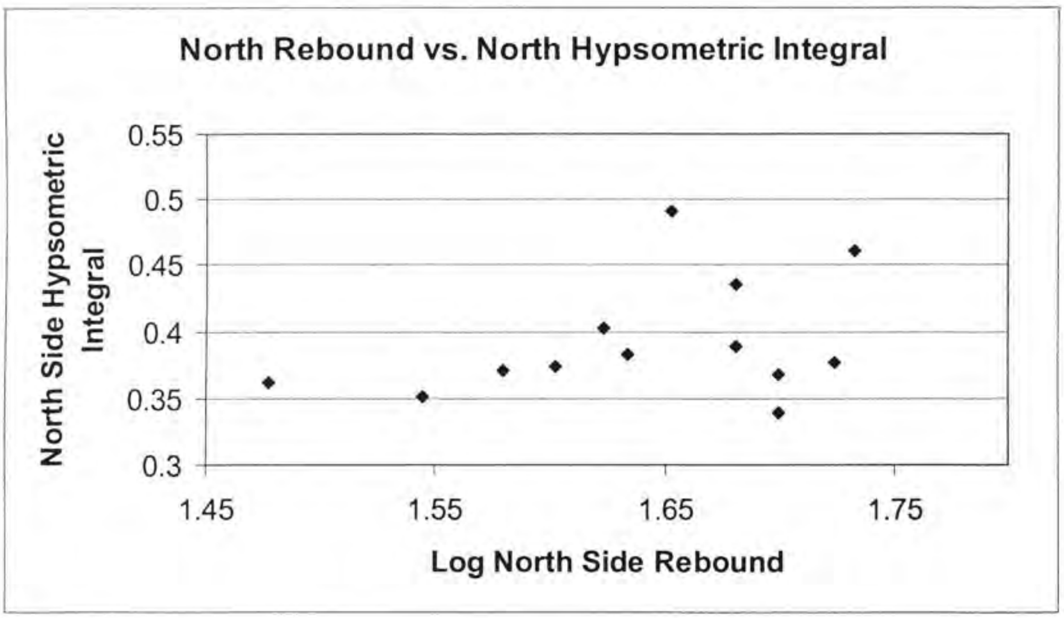

Figure 29. Graph of the logarithm of the north side rebound vs. the north side hypsometric integral. $r^2 = 0.1282$, P = 0.2297.

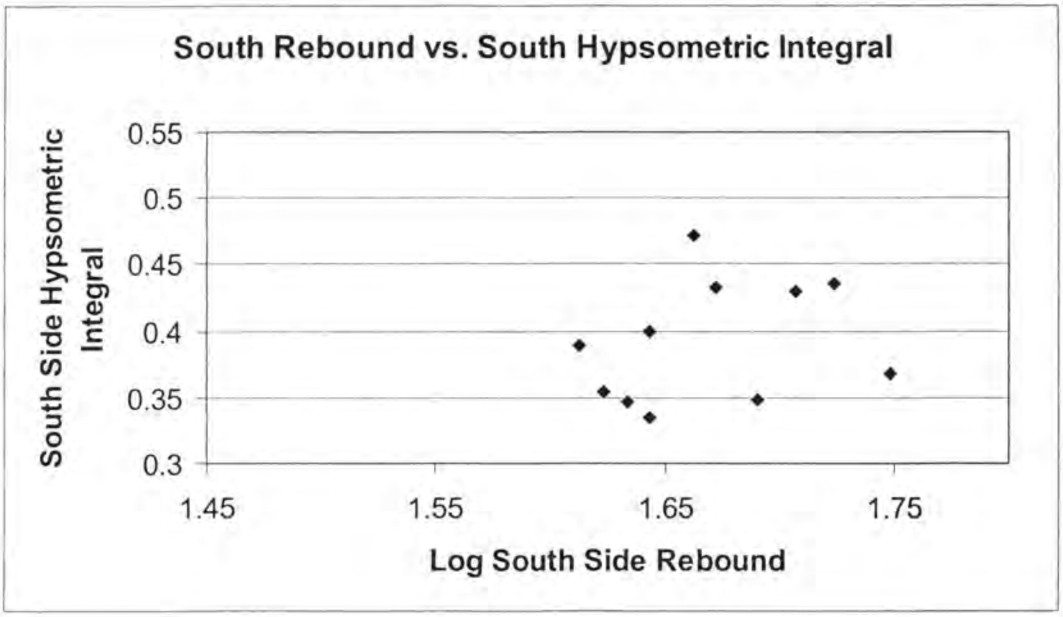

Figure 30. Graph of the logarithm of the south side rebound vs. the south side hypsometric integral. $r^2 = 0.0743$, $P = 0.4172$.

4.6 Summary of Results

Analyses of Schmidt hammer rebound data demonstrate that average rebound values for each reach are statistically distinct from one another, that rebound measurements from the north side are statistically lower than from the south side, and that the four lithologic groups have statistically distinct rebound measurements. The average rebound value of the weakest side of the valley is strongly negatively correlated to the valley floor width, but the average rebound value of the strongest side is not. Of the four different ways stream gradient was calculated, those derived from hard-copy topographic maps were the most reliable because they fit the overall longitudinal profile of the river They demonstrate the strongest relationship to bedrock rebound. On the north side of the valley, hillslope gradient is moderately correlated to bedrock rebound.

There is no correlation between these two variables on the south side of the valley.

Finally, hypsometric integral is not statistically related to bedrock rebound.

CHAPTER 5: DISCUSSION

5.1 Introduction

The following discussion is divided into six sections. The first section addresses only the rebound data, and the subsequent three sections discuss how they are related to Valley Floor Width, Stream Gradient, Hillslope Gradient, and Hypsometric Integral. Finally, I discuss the implications of this study for the use of the Schmidt hammer in geomorphology, and make suggestions for future work.

5.2 Bedrock strength

5.2.1 Aspect variability

Statistical analysis of the Schmidt hammer rebound values demonstrates that there is a significant difference between the rebound values of the north and south sides of Big Creek. The north side of the valley, which is south-facing, has lower Schmidt hammer rebound values than those on the south side of the valley, which is north-facing. There are two possible explanations for this phenomenon: 1) during the summer, diurnal heating and cooling of rocks on south-facing slopes by solar radiation creates strong thermal gradients and enough stress to cause fracturing (McFadden et al., 2005), and 2) during the winter the south-facing slopes receive more solar radiation and therefore experience more freeze-thaw cycles than the shaded north-facing slopes. In fact, both processes are likely working. Thermal cracking is plausible, but it has only been tested in an arid desert environment, so it is unknown if it could apply to a location in central Idaho, which is somewhat cooler and wetter, and at a higher latitude. North-facing slopes typically have more vegetative cover than south-facing slopes in the Big Creek valley, thus providing protective shade. The second explanation is very plausible in central Idaho, where seven months out of the year have average minimum temperatures below freezing (Taylor Ranch weather station; Western Regional Climate Center, 2005).

Burnett et al. (2002) observed an opposite rock strength phenomenon in the Colorado Plateau region. Their Schmidt hammer data showed that bedrock rebound values on the south side of the valley (north-facing slopes) were lower than those on the north side of the valley. They suggest that increased soil moisture on north-facing slopes (caused by greater vegetative cover) has increased the rate of weathering through clay hydration and expansion. Biologically enhanced water retention and increased weathering of bedrock is certainly plausible at Big Creek, but McFadden et al. (2005) conclusions suggest that south-facing slopes should have lower rock strength because of more exposure to solar radiation, not north-facing slopes as is the case with the Burnett et al. (2002) study. At Big Creek, the high frequency of freeze-thaw cycles is the most likely explanation for the decreased rock strength on the north side of the valley.

5.2.2 Lithology

Statistical analysis of Schmidt hammer rebound data also demonstrates that the lithologic groups have significantly distinct rebound values. It is not surprising that bedrock of the same lithology would have similar intact rock strength since it is genetically related and has similar mineralogic composition and structure. If bedrock of a given lithology weathers in similar ways and to similar degrees, then generalizations can be made about possible lithologic controls on morphometry of river valleys. For example, if each lithology has a distinct strength and strength is correlated to valley floor width, then each lithology should produce a distinct range of valley floor widths. Some lithologies, however, have highly variable intact rock strength or weathering characteristics. In Big Creek, the Tertiary tuffs (Tdp and Tss) display by far the most variable rebound values. This variability is caused by the wide range of welding intensity. Other factors can influence rock strength independent of lithology, such as local metamorphism, tectonic strain, and variable microclimate (e.g. aspect-controlled freeze-thaw). These independent factors make lithology alone an unreliable method of predicting river valley morphometry. This is at the heart of the rationale for this study.

5.3 Valley Floor Width

The clearest statistical relationship between rock strength and valley morphometry links Schmidt hammer rebound and valley floor width. The side of the valley with the weaker average Schmidt hammer rebound value is strongly negatively correlated to the width of the valley floor. There is no relationship between rebound value on the strongest side of the valley and valley floor width. Thus, it appears that the weak side of the valley controls the width of the valley floor of Big Creek.

In order to explain the strong relationship between valley floor width and Schmidt hammer rebound, I propose a conceptual model that describes how valley floor width is created in a river bounded by bedrock valley walls (Figure 31). Both vertical and lateral erosion occur in a channel and in both cases rock is removed (by abrasion and/or plucking) at the base of the adjacent hillslopes. Removal of rock oversteepens these lower slopes and reduces their stability. Rock masses with no joints or weathering typically fail along shear planes when the force of gravity acting on a rock mass overcomes the strength of that rock mass. The maximum height of a vertical cliff of un-jointed rock is approximately equal to the uniaxial compressive strength divided by the unit weight of rock (Terzaghi, 1962). At high compressive strengths this vertical height limit is approximately 1500 m (Selby, 1980). Joints, fractures, or faults occur in almost all rock masses and act as planes of weakness or failure, so the expected maximum cliff height is rarely achieved. Oversteepened slopes are susceptible to erosion, and hillslope processes will move material on and above the oversteepened slope into the channel through shear failures, topples, falls, or slides. Assuming that the river has enough transport capacity, it will remove the material and leave the valley floor wider.

My conceptual model of valley floor widening (Figure 31) was created to explain the relationship between rock strength and valley floor width. Data collected in this study demonstrate that the valley floor width depends strongly on the rock strength of the weaker side of the valley. These data suggest that bedrock with high strength is resistant to lateral fluvial erosion and can hold an oversteepened slope, preventing further widening, when lateral fluvial erosion does occur. When widening of the valley floor is prevented, stream power is maintained or focused, thus promoting vertical erosion rather than lateral erosion. Conversely, bedrock with low strength is less resistant to lateral fluvial erosion and easily fails when oversteepened, thus facilitating valley floor widening. Furthermore, widening of the valley floor reduces stream power, which initiates lateral migration of the channel and may be a feedback for continued widening.

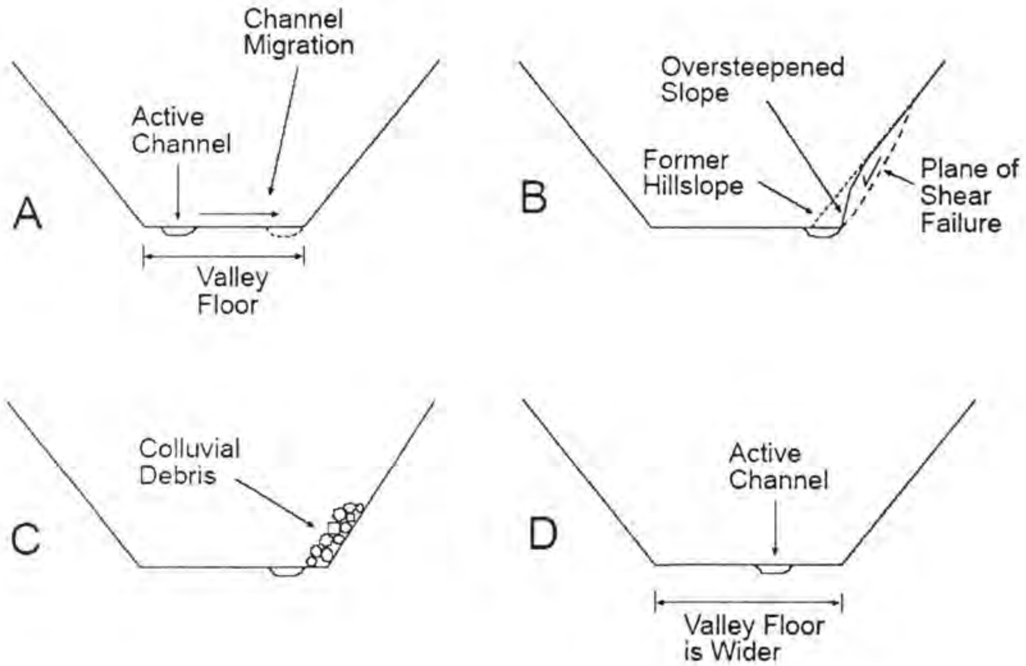

Figure 31. Schematic diagrams of process of valley floor widening. A) Lateral migration of the channel applies erosive force to the valley wall. B) Erosion by plucking and abrasion oversteepens the valley wall. Shear failure and mass wasting moves material to valley floor. C) Colluvial debris on the valley floor is transported by the river. D) The channel across the floodplain again, leaving the valley floor wider.

5.4 Stream gradient

Reach-scale stream gradient has only a weak statistical relationship to rock strength in Big Creek. However, Mackley and Pederson (2004) found a strong correlation between these two parameters on the Colorado River in Grand and Glen Canyons. Pederson (pers. comm., 2005) has also observed a relationship between bedrock strength and stream gradient on other rivers within the Colorado Plateau. As a generalization, one would expect higher bedrock strength to correspond to steeper stream gradients in equilibrated streams (Gilbert, 1877; Powell, 1895). Therefore, it is somewhat surprising that no such relationship exists at Big Creek. Stream gradient at each reach was calculated using four different methods in order to reduce possible inconsistencies in DEM data, so it is unlikely that the lack of correlation is due to data error. There are several geologic explanations for the weak correlation.

1) A strong relationship between bedrock rebound and stream gradient may be contingent upon the channel being dominated by bedrock. The relationship seen by Mackley and Pederson (2004) and Pederson (pers. comm., 2005) occurred in rivers with bedrock channels. The channel types of the reaches studied in Big Creek are variable. Vines Reach and Cabin Creek Reach have wide, well-developed floodplains, low stream gradients, and are obviously alluvial. Dacite Gorge Reach and Big Creek Gorge Reach are narrow, contain only large boulders, and have steep stream gradients so are easily classified as bedrock channels. The channel types of the other reaches are more ambiguous. Most of these reaches have some alluvial sediment on the valley floor, but it is unclear how much; therefore, it is impossible to know if it is simply a thin veneer that can be mobilized during a flood or if it is thick layer that is shielding the bedrock below from erosion.

The definitions of a bedrock channel presented in the introduction are all suitable descriptions of what a bedrock channel is conceptually. However, it seems that a more practical definition is needed that is based on field observations and can be easily applied to a given reach. Wohl (1998) offers part of such a definition; she suggests that a bedrock channel is one in which the morphology is dominated by erosional processes. Potholes, longitudinal grooves, ripples, flutes, and knickpoints are examples of typical erosion-dominated morphology (Wohl, 1998; Whipple et al., 2000). This definition implies that alluvial channels are those in which the morphology is dominated by depositional processes. Examples of deposition-dominated morphology includes pools and riffles, meanders, bars, cut banks, floodplains, and alluvial terraces. The primary advantage of using this definition is that most of these morphologic features can be quickly and easily identified in the field. One drawback, however, is the fact that this definition does not explicitly take time into account. For example, a thin veneer of sediment that can be mobilized during flood events may be present. By previous definitions, this would be considered a bedrock channel, which is conceptually correct. However, deposition-dominated morphology can occur in an alluvial veneer even as thin as 3 m, so this new definition would classify the channel as alluvial. When observed during average flows, the channel is essentially acting like an alluvial channel; however during infrequent flood events the alluvial veneer would be mobilized and the channel would be acting like a bedrock channel. Obviously, time scale is an important consideration when classifying a channel. Over short time scales the above example would be considered an alluvial channel, but over longer time scales it would be considered a bedrock channel. With respect to Big Creek, the period of observation is very short, so reach-by-reach classifications must be made based on present conditions.

2) Spatial and temporal scales at Big Creek may be too small for rock strength to dominate gradient. Mackley and Pederson (2004) found a strong relationship between stream gradient and rock strength along the Colorado River in Glen and Grand Canyons. There are some important differences between their study and this study. First, their reaches were much longer (775 channel widths long) than the reaches I used at Big Creek (10 – 70 channels widths long), and small scale gradient variability is not an issue at such

a large scale. Second, lithologic units along the Colorado River have very uniform intact strength and joint spacing, whereas the lithologic units (as well as the intact strength, joint spacing, and weathering) along Big Creek change over comparatively much shorter distances. Pazzaglia and Brandon (2001) conclude that the rate of bedrock incision varies at time scales less than 100 k.y., but is relatively steady when averaged over longer time scales. Thus, Big Creek might not have equilibrated with recent rapid incision due to rock uplift or base-level lowering.

3) A combination of a short observational time perspective and an abundance of Pleistocene post-glacial sediment may temporarily mask the bedrock channel gradient. An episode of increased sediment production (especially coarse sediment) occurred during the late Pleistocene in southern and eastern Idaho (Pierce and Scott, 1982) and probably in central Idaho as well. Evidence for deposition of abundant late Pleistocene gravel, followed by deposition of finer, less abundant Holocene sediment, is found in glaciated and unglaciated basins throughout the Rocky Mountains. Big Creek basin was not glaciated, but an accumulation of coarse sediment left over from the late Pleistocene may still be moving through the fluvial system. If this is the case, then Big Creek is currently not in transport/supply equilibrium and sediment is slowly being transported out of the basin. Given enough time, the sediment fill may be flushed out of the basin and the system might return to interglacial conditions that are closer to transport/supply equilibrium. When the excess sediment is removed, more of the channel may be a true bedrock channel and its gradient may reflect bedrock strength.

4) Big Creek is not in equilibrium with recent tectonic and base-level changes; namely, movement on a branch of the Cow Creek normal fault has down-dropped the

upstream headwall block and incision of the Middle Fork Salmon River has caused a knickpoint to propagate up Big Creek.

The Cow Creek fault is the downstream boundary of the Cabin Creek reach (Reach #8) and puts weak tuffs in the headwall against diorite in the footwall. The fault, which is not active, downdropped weak Eocene Challis tuff exposing a more resistant bedrock type that acts as a barrier to incision of the stream. The longitudinal profile of Big Creek (Figure 28) illustrates the influence of the Cow Creek fault on the gradient. The fault crosses Big Creek at river kilometer 47, exactly the inflection point separating the concave-up upstream portion of the river and the convex-up downstream portion of the river. The fault acts as a local base-level control for the gradient upstream of it; the river above the fault grades to it, the river below it steepens. The stream gradients of each reach derived from hard-copy topographic maps fit this pattern well. From upstream down, the gradient of each reach decreases until the fault at reach #8. Below the fault, the reach gradients increase all the way to the mouth. The stream gradient below the fault is not graded to the Middle Fork Salmon River because the Middle Fork is actively incising and lowering base-level for Big Creek. Meyer and Leidecker (1999) calculated the incision rate on the Middle Fork to be 0.74 m/k.y. in the last 14.5 k.y. (2-3 times greater than the estimated 1 m.y. average rate of incision), so the Middle Fork is rapidly incising and causing a knickpoint to propagate up its tributaries, including Big Creek. Both the fault and the knickpoint have altered the longitudinal profile of the river and thus stream gradient is not being controlled exclusively by rock strength.

5.5 Hillslope gradient

Data from this study show that hillslope gradient is moderately dependent on bedrock rebound values. Other studies have found strong correlations between these parameters (Selby, 1980; Püspöki et al., in press). Püspöki et al. (in press) compared the frequency distribution of slope gradients to the unconfined compressive strength (UCS) of bedrock. UCS is very strongly correlated to Schmidt hammer rebound (Day, 1980; Katz et al., 2000; Yaşar and Erdoğan, 2003), and in fact the Schmidt hammer manufacturer's curves for converting rebound value to MPa or psi are based on this relationship. Selby (1980) created the rock mass strength (RMS) index to incorporate Schmidt hammer rebound values with other parameters (such as weathering, joint spacing, and joint orientation) as a way of characterizing hillslope morphometry. The classification assigns weights to each parameter; the weighting system was calibrated so that RMS index values were highly correlated to hillslope examples in New Zealand and Antarctica (Selby, 1980). Intact rock strength as measured by the Schmidt hammer and joint spacing are the most influential parameters in the RMS index.

The lack of a stronger correlation may reflect late Pleistocene gravel and cobbles that may remain on the hillslopes of the Big Creek drainage basin, as discussed above. While steep slopes and exposed bedrock indicate that Big Creek is an actively incising river, many slopes at Big Creek are partially covered with talus and colluvium, likely from the late Pleistocene or more recently. Talus tends to form straight slopes that cover bedrock and can mask the bedrock gradient of the hillslope. Given enough time to transport the accumulated late Pleistocene sediment, the basin would return to interglacial conditions, more bedrock would be exposed, and the true hillslope gradient would be apparent.

Hypsometric analysis of the hillslopes at each reach reveals that the hypsometric integral, which essentially describes the concavity or convexity of a slope, is not related to the average Schmidt hammer rebound value. Since the hypsometric integral is thought to represent basin "maturity" and the balance between fluvial and hillslope processes (Strahler, 1952), the lack of correlation is probably due to the current disequilibrium of the river with regard to uplift and incision. The lower portion of Big Creek (below the Middle Fork knickpoint) is rapidly incising and the hillslope processes are not responding as rapidly, thus the hillslopes are convex up. The upper portion of Big Creek (above the Cow Creek fault) has graded to that base-level and is stable. The hypsometric integral of a hillslope is not dependent on the rock strength, but on time. Rock is moved from high elevations to low elevations, thus changing the hypsometric integral of a slope. Rock strength has some influence on the rates of hillslope processes, but other factors are probably more dominant.

5.6 Implications for the use of the Schmidt hammer in a geomorphic context

The Schmidt hammer has been shown to be a useful tool in the study of valley morphometry. If used properly, it can produce robust data sets that characterize bedrock strength at the spatial scale appropriate for the study of fluvial processes in bedrock channels. The Schmidt hammer, combined with observational data and additional data such as fracture density, can accurately characterize integrated bedrock strength. Understanding the processes and mechanisms of fluvial erosion is essential to effective use of the Schmidt hammer. In particular, one must know which properties of bedrock strength are being measured and how those properties influence the processes and mechanism (and therefore the resulting morphometry) of erosion. The Schmidt hammer seems to be particularly well suited to studies of bedrock rivers, where erosive processes directly control morphometry.

5.7 Conclusions

This study related bedrock strength, as measured by the Schmidt hammer, to four parameters of valley morphometry: valley floor width, stream gradient, hillslope gradient, and hypsometric integral. The conclusions of this study are: 1) valley floor width is strongly dependent on the bedrock strength of the weaker side of the valley, 2) a moderate correlation exists between bedrock strength and hillslope gradient, 3) a weak correlation exists between bedrock strength and stream gradient, 4) no correlation exists between bedrock strength and hypsometric integral, 5) a statistically significant difference was found between north and south side rebound values, with the north side being lower.

Analysis of the longitudinal profile reveals two major controls on the large-scale gradient: 1) a northeast-trending normal fault, and 2) rapid incision of the Middle Fork Salmon River and the resulting knickpoint. Stream and hillslope gradient may be further masked by late Pleistocene sediment load. An explicit model for valley floor width formation has been proposed. Lateral erosion of the river (through abrasion and/or plucking) oversteepens the lower hillslopes, which respond by mass wasting at a rate determined by rock strength. When the resulting rock debris is removed, the valley floor is wider.

The Schmidt hammer is shown to be a useful tool for comparing the relative bedrock strength of diverse lithologies. This study demonstrates that the Schmidt hammer can incorporate intact rock strength and modifying factors such as joint spacing into a single, combined measurement that is representative of an entire outcrop.

Rivers are complex systems in which many factors work to control the morphometry. This study has isolated one such factor, bedrock strength as measured by Schmidt hammer rebound, which has a strong control on valley floor width. In mountain drainage basins with diverse lithology, Schmidt hammer rebound is a useful parameter for describing variations in valley floor width.

5.8 Future work

Future work at Big Creek should include dating of the numerous, well-preserved fluvial terraces to constrain the uplift and incision rates in the region. At least two exposures of fine-grained lake bed deposits (Figure 32) underlying terrace treads offer the possibility of optically stimulated luminescence (OSL) dating to find the age of both the terrace surface and the damming of the river that created the temporary lake. Large boulders sitting on terrace treads may be dated using cosmogenic radionuclide techniques to constrain a minimum age of that surface. Further work needs to be done on a large landslide complex at Big Creek Gorge. The landslide appears to record the damming of the river and its subsequent incision through the nearly intact bedrock. Several paired strath terraces are cut into the bedrock of the landslide complex (Figure 33).

Similar studies of valley morphometry using the Schmidt hammer in both similar and different rock types and climates would useful for comparison. This would help test the relationships and conclusions found in this study. Future studies of this type should use the highest resolution DEMs possible, such as LiDAR DEMs, for calculating stream gradient. Manual surveying of reaches would be the most reliable method for calculating stream gradient. Schmidt hammer rebound measurements should also be distributed all the way up hillslopes that are being studied. When comparing hillslope gradient to bedrock strength, using the rock mass strength (RMS) index (Selby, 1980) may be preferable to using Schmidt hammer rebound values alone, although this study has demonstrated that the Schmidt hammer data reflect joint spacing and other components of RMS.

Figure 32. Photograph of fine-grained lake bed deposits near Cave Creek.

Figure 33. Series of terraces cut into the bedrock of a large landslide complex above Big Creek Gorge.

APPENDIX A: GIS METHODS

Stream Gradient

Twenty-six 7.5' USGS SDTS DEMs with 10 m resolution were mosaicked together to completely cover the Big Creek drainage basin. The following DEMs were downloaded from GIS Data Depot (http://data.geocom.com):

Acorn Butte, Idaho

Aggipah Mountain, Idaho

Bear Creek Point, Idaho

Big Creek, Idaho

Bismark Mountain, Idaho

Center Mountain, Idaho

Chicken Peak, Idaho

Cold Meadows, Idaho

Cottonwood Butte, Idaho

Dave Lewis Peak, Idaho

Edwardsburg, Idaho

Lodgepole Creek, Idaho

Monument, Idaho

Mormon Mountain, Idaho

Mosquito Peak, Idaho

Papoose Peak, Idaho

Parks Peak, Idaho

Profile Gap, Idaho

Puddin Mountain, Idaho

Rainbow Peak, Idaho

Safety Creek, Idaho

Shellrock Peak, Idaho

Stibnite, Idaho

Vinegar Hill, Idaho

Wapiti Creek, Idaho

Wolf Fang Peak, Idaho

DEMs were mosaicked using the DEM to Raster tool in ArcToolbox. The new full coverage DEM was opened in AVSWAT-2000 (Di Luzio et al., 2002), which is an ArcView extension of the Soil and Water Assessment Tool (SWAT; Arnold et al., 1998). SWAT is a watershed scale model designed to study the effects of land management practices on river basins. Bad data values in the DEM (known as sinks or depressions) are filled and the software delineates the boundaries of the watershed based on flow paths from pixel to pixel. From the same depressionless DEM, the stream channels are delineated (Figure 34). The threshold size of the basin contributing to a stream can be varied, effectively changing the sensitivity of the channel delineation. For example, if the threshold basin area is small, then many small channels will be identified. A larger threshold basin area restricts the delineation to larger channels.

Watershed delineation produces a shape file of the drainage basin. In ArcInfo, the shape file was converted to a coverage which was then used as a mask and is clipped out of the mosaicked DEM using the LATTICECLIP function. This produces a DEM of only the drainage basin. In ArcCatalog, basin statistics (such as area and minimum, maximum, and mean elevation) can be viewed in the Preferences of the DEM.

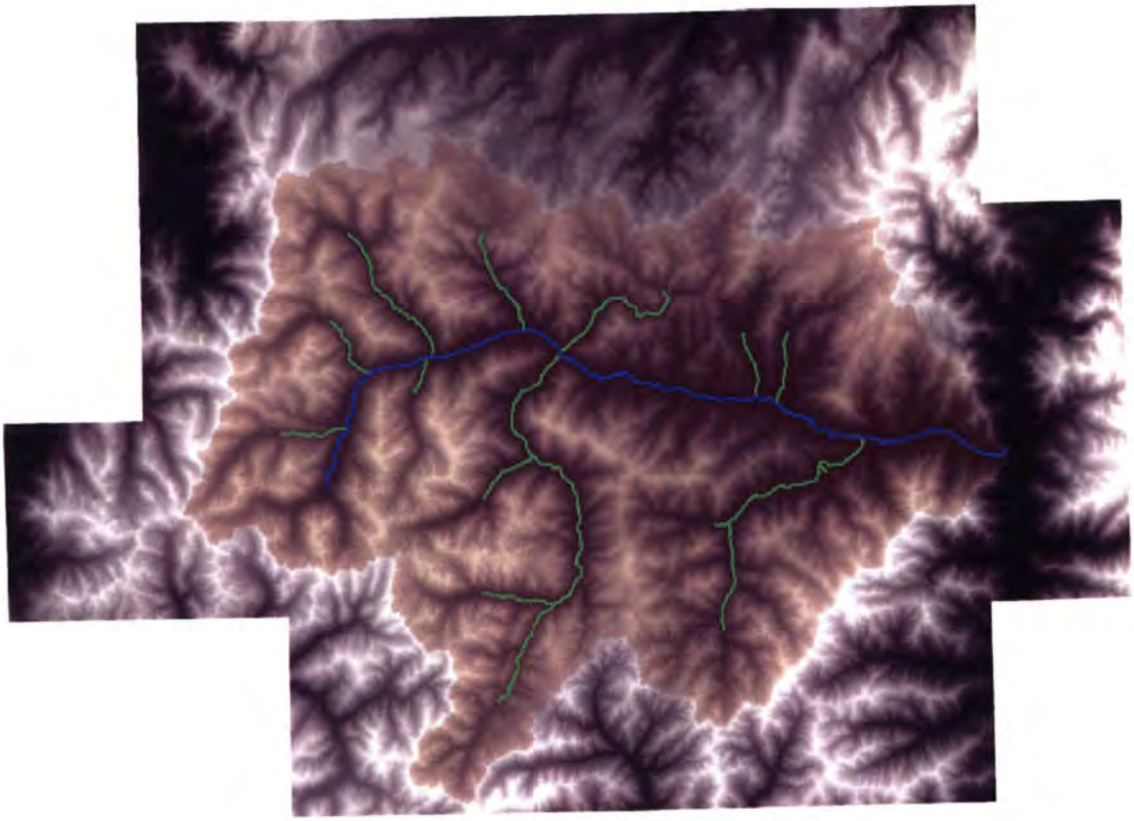

Figure 34. Image from ArcMap showing the mosaicked 7.5' DEMs (dark is lower elevation, light is higher elevation) and the watershed and stream channels delineated by SWAT. Watershed is transparent brown, main trunk of Big Creek is blue, and tributary channels are green.

Stream channel delineation produces a set of shape files. Each segment of channel is a separate file; the intersection of any two channel sections (which in reality is a confluence) is a node that separates channel segments. The segments composing the main trunk channel of Big Creek were grouped and converted from shape files to coverages and from coverages to routes. Distances along routes from one of the end points can be easily measured using the Identify Route Locations command in the Linear Referencing category of custom tools. The Identify Tool in the toolbar was used to find elevations on the DEM layer of pixels that lie along the stream channel. Knowing stream channel length and the change in elevation from an upstream endpoint to a downstream endpoint allowed me to calculated stream gradient at each reach. An alternative stream gradient was calculated for each reach using the same method, but over a distance of three times the reach length.

Hillslope Gradient

The watershed DEM was converted to a hillshade model. Hillslope facets with strikes parallel to the river valley were identified on both sides of the river at each reach. Selected facets were traced over with polygons and saved as shape files (Figure 35). Each shape file was converted to a coverage and the coverages of the individual hillslope facets were used as masks to clip out of the DEM using the LATTICECLIP function in ArcInfo. A slope map was created of each facet DEM using the Slope tool in ArcMap. Statistics (such as minimum, maximum, and mean slope) of each slope map can be viewed in the Preferences of the DEM in ArcCatalog.

Hypsometric Analysis

The clipped DEMs of each hillslope facet were used in the hypsometric analysis. Each DEM was opened in ENVI as an ESRI Grid file, then saved as an Arc Binary Raster file with .bil and .hdr files, and then imported in RiverTools (Rivix, 2004). RiverTools creates a hypsometric curve and calculates the hypsometric integral for each DEM. The no-data threshold value was set to one meter below the minimum pixel value in order to exclude no-data pixels and to perform the hypsometric analysis between the minimum and maximum elevations of the facet.

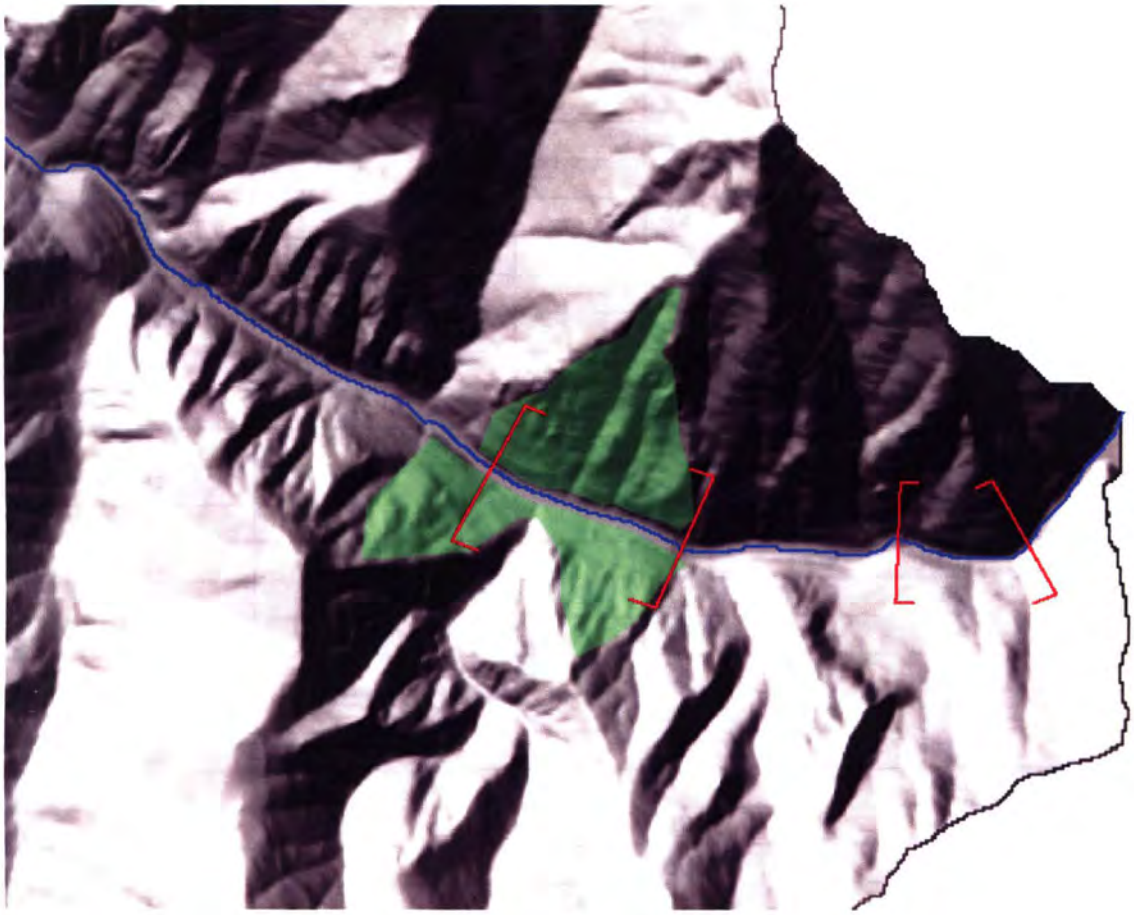

Figure 35. Image from ArcMap showing a hillshade DEM, Big Creek in blue, red brackets are the boundaries of Breeching Creek Reach. Transparent green polygons are hillslope facets selected for calculating gradient.

APPENDIX B:

SCHMIDT HAMMER REBOUND DATA

Little Ramey Creek Reach

North Rebound					South Rebound			
60	53	45			52	35	26	67
29	67	50			45	63	52	44
57	44	38			43	32	62	40
68	45				42	43	41	61
66	30				31	46	51	69
34	50				35	18	45	31
42	46				53	51	64	
49	27				51	31	10	
36	27				56	66	51	
52	37				46	57	59	
40	48				40	67	56	
42	41				41	43	38	
54	62				55	49	30	
26	52				52	49	42	
43	16				33	44	64	
44	10				28	54	32	
45	10				55	54	50	
10	10				44	49	42	
10	18				51	51	44	
16	33				49	34	64	
13	34				60	38	49	
17	36				41	58	62	
47	27				27	29	67	
34	57				60	38	35	
24	66				56	35	44	
10	45				45	35	60	

Bar Creek Reach

North Rebound					South Rebound			
58	58				51	56	47	
67	65				50	46	64	
37	60				52	56	60	
52	63				31	46	46	
58	62				56	53	31	
55	66				59	44	47	
40	49				60	65	67	
54	38				44	58	52	
56	42				47	34	64	
60	42				36	47	58	
25					40	52	54	
35					45	50	52	
32					54	63	46	
54					27	46	35	
60					47	50	49	
63					40	42	59	
54					64	53	54	
54					63	35	50	
40					42	54	26	
34					46	55	47	
39					34	37	63	
45					62	62	57	
53					64	58	50	
40					41	42	64	
44					68	50	54	
62					66	50	54	
38					66	52		
46					63	38		
51					46	50		
56					49	52		
52					52	41		
41					30	50		
44					57	65		
34					57	35		
57					59	49		
52					61	51		
62					59	68		
60					57	41		
50					49	64		
60					59	50		

Acorn Creek Reach

North Rebound					South Rebound			
53	37				17	10		
35	39				42	50		
46	39				37	33		
49	48				15	45		
34	57				20	54		
50	50				36	53		
56	30				51	17		
35	22				57	49		
46	53				57	52		
41	59				62	40		
42	42				62	46		
40	43				59	34		
20	35				42	50		
24	58				28	49		
50	44				42	30		
50	54				41	33		
22	50				43	46		
39	56				43	33		
51	47				21	13		
42	33				21	49		
58					50	37		
42					38	33		
54					15	22		
54					50	30		
28					52	56		
38					40	42		
37					51	50		
46					44	48		
46					60	56		
37					55	52		
32					50	59		
37					38	58		
35					28	57		
54					38	44		
58					44	49		
52					24	52		
21					21	48		
21					51	60		
22					21			
31					10			

Soft Boil Bar Reach

North Rebound					South Rebound			
19	48				30	47		
44	21				42	38		
33	34				34	41		
22	56				39	40		
29	52				44	44		
30	18				36	35		
59	48				51	29		
37	23				40	39		
15	33				45	53		
27	60				44	62		
45	38				42	36		
36	16				43	54		
56	16				52	52		
27	46				29	40		
37	45				44	30		
48					40			
57					30			
42					62			
54					19			
41					37			
44					48			
33					45			
63					36			
50					28			
47					40			
28					53			
57					47			
45					52			
43					49			
67					50			
28					34			
44					44			
48					47			
26					41			
14					38			
62					21			
54					50			
40					39			
45					53			
27					39			

Dacite Gorge Reach

North Rebound					South Rebound			
62	57	63			64	61	58	
60	44	59			52	58	65	
58	38	40			56	41	45	
67	57	43			52	65		
47	59	43			67	68		
63	54	40			60	45		
56	41	53			42	63		
58	68	41			55	54		
58	56	44			55	62		
58	68				64	47		
59	54				56	69		
60	55				51	70		
41	36				54	58		
59	50				57	34		
40	45				60	36		
60	48				42	59		
65	64				44	57		
46	66				59	65		
63	37				58	66		
61	50				58	61		
64	66				59	45		
41	56				52	64		
40	52				59	68		
54	62				55	55		
14	62				60	66		
45	66				59	56		
42	54				67	56		
43	52				69	63		
48	58				57	50		
41	55				68	66		
58	54				65	44		
28	55				68	66		
44	65				64	42		
54	56				67	62		
48	58				22	63		
54	50				56	60		
65	40				59	37		
48	60				59	26		
59	51				41	26		
56	62				47	46		

Vines Reach

North Rebound				South Rebound				
57	23	23		28	59	54	41	51
42	22	14		58	48	53	35	55
50	24	22		48	44	34	49	36
20	30	45		61	45	40	35	49
29	50			50	33	43	25	44
29	55			36	58	47	43	27
38	42			35	52	39	44	33
41	26			38	26	41	38	37
22	32			46	41	51	46	45
34	25			58	48	44	53	20
24	28			56	31	44	42	43
36	43			39	51	54	46	42
52	39			39	52	35	45	31
41	41			40	36	48	45	53
41	48			44	52	48	53	45
13	38			53	50	34	44	38
12	33			68	40	54	46	45
13	53			16	34	42	33	44
34	41			45	47	42	43	30
18	39			50	49	45	45	
32	32			63	49	43	38	
28	40			55	47	43	45	
43	47			37	58	36	43	
47	45			46	42	31	37	
32	38			39	44	49	40	
44	34			47	42	41	29	
13	30			49	26	50	45	
44	15			58	48	44	45	
35	44			52	39	49	44	
23	54			69	28	50	48	
59	19			67	38	40	34	
56	31			44	50	32	41	
40	65			67	59	32	34	
37	50			58	48	48	44	
38	10			67	39	33	58	
27	29			64	31	35	39	
36	28			41	40	58	14	
55	10			32	54	41	46	
20	54			56	36	42	38	
31	10			33	36	38	48	

Doe Creek Reach

North Rebound					South Rebound			
58	41	31	54		48	52	41	
42	34	54	60		35	52	44	
54	58	58	58		45	38	48	
50	59	38	49		34	38	41	
48	43	32	36		39	54		
51	57	44	54		49	45		
55	49	43	54		40	57		
64	55	39	48		38	40		
46	71	38	56		44	40		
54	62	59	50		41	42		
31	46	36	55		41	33		
28	58	50	57		35	44		
47	53	59	65		39	35		
34	55	39	34		27	39		
16	46	44	19		46	47		
38	58	54			49	46		
54	54	34			40	40		
36	64	43			43	55		
50	49	36			31	33		
61	50	42			30	34		
40	54	31			52	38		
51	60	50			52	34		
48	31	51			41	50		
58	53	20			35	51		
61	35	58			32	50		
58	41	53			32	42		
30	61	32			25	55		
66	39	40			39	49		
63	43	33			37	57		
58	61	28			54	64		
34	50	44			35	37		
42	48	41			50	48		
65	35	36			53	45		
54	45	38			45	59		
51	31	38			59	56		
30	56	57			40	44		
45	59	64			50	54		
55	68	51			60	62		
40	58	61			55	40		
43	27	58			48	40		

Cabin Creek Reach

North Rebound				South Rebound				
26	46	29		55	45	56	39	35
62	10	13		48	35	62	59	36
48	14	34		54	30	53	61	52
12	28	24		62	62	58	27	35
32	24	22		51	51	43	29	53
36	24	43		45	54	51	50	32
39	23	35		62	55	57	33	46
53	17	24		58	55	54	46	41
15	26	47		55	51	47	56	31
22	60	17		57	47	54	53	44
40	39	23		51	40	49	59	39
29	34	50		49	38	47	58	
42	15	12		59	48	49	48	
22	26	37		52	51	54	67	
29	38	19		50	48	37	41	
47	34	17		56	55	56	48	
36	59	19		50	45	49	57	
29	29	22		41	45	48	54	
24	23	21		38	41	62	45	
29	56	18		54	39	48	44	
53	32	19		49	59	57	43	
16	25	24		50	42	59	49	
40	24	10		45	37	50	40	
42	30	40		31	43	67	33	
22	18	43		35	52	53	39	
35	28	56		44	43	62	51	
39	43	20		36	59	61	54	
30	26	23		56	36	55	50	
24	29	24		50	59	40	52	
30	27	42		55	63	55	49	
45	29			42	48	48	57	
55	16			42	44	52	58	
30	24			47	48	60	50	
21	30			58	54	55	37	
27	18			61	39	50	36	
34	20			60	53	50	42	
17	27			52	44	30	40	
10	28			50	57	31	51	
20	21			40	42	54	22	
16	50			53	60	41	42	

Lobauer Reach

North Rebound					South Rebound			
53	59				49	60	39	50
50	58				45	44	53	40
24	53				42	62	30	51
63	54				43	39	33	36
61	58				38	61	10	39
45	55				59	40	46	44
54	67				45	39	42	43
50	47				56	37	39	43
32	50				48	23	33	49
25	45				48	24	20	
28					35	28	59	
45					70	54	40	
32					70	38	34	
44					52	42	55	
38					47	50	29	
30					57	41	47	
20					54	44	32	
49					56	60	25	
19					43	46	42	
30					54	58	31	
61					34	30	46	
58					45	34	30	
51					51	51	39	
20					50	53	48	
27					40	54	38	
26					44	47	38	
57					53	39	48	
28					51	48	52	
50					50	33	11	
38					43	22	50	
52					34	30	42	
29					54	56	29	
56					54	45	31	
56					40	31	36	
50					43	41	20	
44					39	37	10	
54					57	25	40	
39					49	18	50	
48					51	43	37	
51					59	60	44	

Cougar Creek Reach

North Rebound				South Rebound				
60	21			65	45	32	32	46
62	28			71	52	54	50	53
54	45			44	59	50	31	42
48	53			31	52	29	56	43
34	12			55	55	24	44	30
60	42			21	61	48	54	32
39	57			55	54	42	34	38
44	33			62	27	29	55	55
55	19			29	67	25	56	39
32	18			32	55	21	57	37
56	10			55	61	27	45	36
35	48			34	61	44	20	38
54	40			48	61	48	47	32
62	50			37	62	67	46	42
56	48			55	39	63	53	39
45	55			38	59	59	35	26
45	45			50	62	47	64	45
40	25			46	63	45	45	
65	46			40	33	27	56	
56	56			50	50	41	44	
33	46			47	40	58	57	
25	34			43	42	50	34	
18	24			58	51	59	43	
36	46			60	46	53	33	
32	40			43	59	36	47	
64	33			63	64	52	61	
56	41			51	56	63	34	
54	56			26	36	48	37	
40	60			42	53	44	58	
58				60	40	55	48	
33				44	55	60	35	
34				38	43	51	39	
27				25	49	43	42	
42				15	40	27	49	
34				44	56	39	59	
47				66	35	34	20	
52				51	63	28	36	
63				50	56	55	45	
44				51	66	39	42	
64				65	49	48	44	

Big Creek Gorge Reach

North Rebound					South Rebound			
50	62	60						
54	47	49						
60	62	53						
60	58	44						
55	64	51						
59	44	52						
60	49	55						
55	40	56						
69	45	48						
58	42	59						
58	71	60						
54	48	39						
69	54	65						
62	46	60						
47	35	62						
40	47	62						
62	51	62						
40	58	47						
55	48	37						
53	49	62						
57	36	68						
58	53	56						
60	56	54						
74	41	52						
60	60	68						
42	45	62						
46	55	72						
62	52	62						
54	46	46						
35	12	46						
49	53	45						
48	23	55						
65	61	64						
56	44	55						
52	60	65						
53	37	71						
28	61	66						
44	64	56						
65	58	66						
45	49	58						

Breeching Creek Reach

North Rebound					South Rebound			
47	47	60						
44	56	65						
49	27	68						
42	26	65						
50	27	59						
40	60	44						
40	58	54						
64	65	43						
61	45	41						
39	64	41						
50	49	40						
42	67	45						
30	49	47						
46	58	26						
55	38	30						
58	55	31						
31	55	29						
48	41	41						
64	56	33						
33	52	23						
37	56	72						
21	66	68						
23	61	62						
39	43	63						
39	67	70						
32	64	65						
18	66	65						
20	64	67						
21	58	59						
64	57	52						
40	57	55						
62	36	58						
56	50	53						
58	47	66						
39	69	61						
45	52	62						
48	64							
30	61							
31	63							
56	62							

Bighorn Bridge Reach

North Rebound					South Rebound			
52	52	37			58	42	59	
46	47	53			52	27	52	
43	58	54			54	45	61	
36	32	74			58	49	61	
42	29	49			59	42	53	
61	44				64	40		
45	54				49	41		
51	18				52	39		
50	55				57	39		
41	24				49	47		
50	15				64	22		
53	42				50	58		
55	33				56	71		
69	52				62	56		
68	41				74	61		
42	36				47	68		
62	40				65	64		
48	42				56	70		
48	45				57	65		
42	65				49	54		
40	51				55	66		
42	67				59	64		
42	72				58	43		
25	71				51	49		
34	66				46	52		
26	51				52	49		
30	55				52	48		
42	59				52	52		
51	37				33	41		
62	70				38	43		
47	47				36	45		
43	51				53	64		
56	50				45	54		
43	67				51	70		
48	41				42	68		
55	53				47	58		
66	56				53	68		
52	47				54	57		
59	40				53	68		
40	51				47	60		

T-TESTS (Two Sample Assuming Unequal Variances)

North vs. South by Reach

Little Ramey Creek Reach

	Ramey N	*Ramey S*
Mean	1.523231	1.650052
Variance	0.061269	0.018398
Observations	55	84
Hypothesized Mean Difference	0	
df	75	
t Stat	-3.47356	
P(T<=t) one-tail	0.000428	
t Critical one-tail	1.665426	
P(T<=t) two-tail	0.000856	
t Critical two-tail	1.992103	

Bar Creek Reach

	Bar N	*Bar S*
Mean	1.692079	1.699248
Variance	0.009581	0.008302
Observations	50	106
Hypothesized Mean Difference	0	
df	90	
t Stat	-0.43635	
P(T<=t) one-tail	0.331813	
t Critical one-tail	1.661961	
P(T<=t) two-tail	0.663626	
t Critical two-tail	1.986673	

Acorn Creek Reach

	Acorn N	*Acorn S*
Mean	1.606918	1.58106
Variance	0.016433	0.036271
Observations	60	78
Hypothesized Mean Difference	0	
df	134	
t Stat	0.95124	
P(T<=t) one-tail	0.171598	
t Critical one-tail	1.656304	
P(T<=t) two-tail	0.343195	
t Critical two-tail	1.977824	

Soft Boil Bar Reach

	SoftBoil N	*SoftBoil S*
Mean	1.565865	1.609873
Variance	0.031122	0.010358
Observations	55	55
Hypothesized Mean Difference	0	
df	86	
t Stat	-1.60251	
P(T<=t) one-tail	0.056355	
t Critical one-tail	1.662765	
P(T<=t) two-tail	0.11271	
t Critical two-tail	1.987933	

Dacite Gorge Reach

	Dacite N	*Dacite S*
Mean	1.712561	1.736522
Variance	0.009847	0.009719
Observations	89	83
Hypothesized Mean Difference	0	
df	169	
t Stat	-1.58774	
P(T<=t) one-tail	0.057107	
t Critical one-tail	1.653921	
P(T<=t) two-tail	0.114214	
t Critical two-tail	1.974099	

Vines Reach

	Vines N	*Vines S*
Mean	1.501619	1.630967
Variance	0.037784	0.01086
Observations	84	179
Hypothesized Mean Difference	0	
df	106	
t Stat	-5.72489	
P(T<=t) one-tail	4.87E-08	
t Critical one-tail	1.659355	
P(T<=t) two-tail	9.73E-08	
t Critical two-tail	1.982598	

Doe Creek Reach

	Doe N	*Doe S*
Mean	1.663818	1.635813
Variance	0.013661	0.007363
Observations	135	84
Hypothesized Mean Difference	0	
df	211	
t Stat	2.037915	
P(T<=t) one-tail	0.021403	
t Critical one-tail	1.652106	
P(T<=t) two-tail	0.042806	
t Critical two-tail	1.971271	

Cabin Creek Reach

	Cabin N	*Cabin S*
Mean	1.437422	1.677972
Variance	0.032938	0.007383
Observations	110	171
Hypothesized Mean Difference	0	
df	141	
t Stat	-12.9959	
P(T<=t) one-tail	3.5E-26	
t Critical one-tail	1.655733	
P(T<=t) two-tail	7E-26	
t Critical two-tail	1.976932	

Lobauer Reach

	Lobauer N	*Lobauer S*
Mean	1.627776	1.610348
Variance	0.021795	0.021348
Observations	50	129
Hypothesized Mean Difference	0	
df	88	
t Stat	0.710695	
P(T<=t) one-tail	0.239576	
t Critical one-tail	1.662354	
P(T<=t) two-tail	0.479152	
t Critical two-tail	1.987291	

Cougar Creek Reach

	Cougar N	*Cougar S*
Mean	1.608519	1.647423
Variance	0.029418	0.015572
Observations	69	177
Hypothesized Mean Difference	0	
df	97	
t Stat	-1.7154	
P(T<=t) one-tail	0.044732	
t Critical one-tail	1.660715	
P(T<=t) two-tail	0.089465	
t Critical two-tail	1.984722	

Bighorn Bridge Reach

	Bighorn N	*Bighorn S*
Mean	1.667195	1.716501
Variance	0.01588	0.008218
Observations	85	85
Hypothesized Mean Difference	0	
df	153	
t Stat	-2.92833	
P(T<=t) one-tail	0.001965	
t Critical one-tail	1.654873	
P(T<=t) two-tail	0.003929	
t Critical two-tail	1.975591	

All North Data vs. All South Data

	All North	*All South*
Mean	1.620513	1.654133
Variance	0.029982	0.015141
Observations	1078	1231
Hypothesized Mean Difference	0	
df	1913	
t Stat	-5.30824	
P(T<=t) one-tail	6.18E-08	
t Critical one-tail	1.645651	
P(T<=t) two-tail	1.24E-07	
t Critical two-tail	1.961207	

North vs. South by Lithology

Mesoproterozoic Quartzites (Yh/Yy)

	Yh North	*Yh South*
Mean	1.608519	1.647423
Variance	0.029418	0.015572
Observations	69	177
Hypothesized Mean Difference	0	
df	97	
t Stat	-1.7154	
P(T<=t) one-tail	0.044732	
t Critical one-tail	1.660715	
P(T<=t) two-tail	0.089465	
t Critical two-tail	1.984722	

Neoproterozoic Diorite and Syenite Intrusions (Zdi/Zsy)

	Zdi North	*Zdi South*
Mean	1.601141	1.633463
Variance	0.031039	0.020575
Observations	270	452
Hypothesized Mean Difference	0	
df	479	
t Stat	-2.55148	
P(T<=t) one-tail	0.005518	
t Critical one-tail	1.648041	
P(T<=t) two-tail	0.011036	
t Critical two-tail	1.964927	

Tertiary Tuffs (Tdq/Tss)

	Tdq North	*Tdq South*
Mean	1.582024	1.664247
Variance	0.035219	0.010326
Observations	418	517
Hypothesized Mean Difference	0	
df	610	
t Stat	-8.05384	
P(T<=t) one-tail	2.11E-15	
t Critical one-tail	1.647354	
P(T<=t) two-tail	4.23E-15	
t Critical two-tail	1.963863	

Tertiary Granodiorite (Tgd)

	Tgd North	*Tgd South*
Mean	1.667195	1.716501
Variance	0.01588	0.008218
Observations	85	85
Hypothesized Mean Difference	0	
df	153	
t Stat	-2.92833	
P(T<=t) one-tail	0.001965	
t Critical one-tail	1.654873	
P(T<=t) two-tail	0.003929	
t Critical two-tail	1.975591	

ANOVA (Single Factor)

North Side Reaches

SUMMARY						
Groups	*Count*	*Sum*	*Average*	*Variance*		
Cabin	110	158.1164	1.437422	0.032938		
Gorge	120	206.2663	1.718886	0.010487		
Lobauer	50	81.38882	1.627776	0.021795		
Cougar	69	110.9878	1.608519	0.029418		
Lt. Ramey	55	83.77768	1.523231	0.061269		
Bar	50	84.60393	1.692079	0.009581		
Acorn	60	96.41505	1.606918	0.016433		
Soft Boil	55	86.12255	1.565865	0.031122		
Dacite	89	152.418	1.712561	0.009847		
Doe	135	224.6155	1.663818	0.013661		
Vines	84	126.136	1.501619	0.037784		
Bighorn	85	141.7116	1.667195	0.01588		
Breeching	116	194.3539	1.675464	0.019527		
ANOVA						
Source of Variation	*SS*	*df*	*MS*	*F*	*P-value*	*F crit*
Between Groups	8.543391	12	0.711949	31.92876	4.17E-63	1.761254
Within Groups	23.74743	1065	0.022298			
Total	32.29082	1077				

South Side Reaches

SUMMARY						
Groups	*Count*	*Sum*	*Average*	*Variance*		
Cabin	171	286.9332	1.677972	0.007383		
Lobauer	129	207.7349	1.610348	0.021348		
Cougar	177	291.5938	1.647423	0.015572		
Lt. Ramey	84	138.6044	1.650052	0.018398		
Bar	106	180.1203	1.699248	0.008302		
Acorn	78	123.3227	1.58106	0.036271		
Soft Boil	55	88.54303	1.609873	0.010358		
Dacite	83	144.1313	1.736522	0.009719		
Doe	84	137.4083	1.635813	0.007363		
Vines	179	291.9431	1.630967	0.01086		
Bighorn	85	145.9026	1.716501	0.008218		
ANOVA						
Source of Variation	*SS*	*df*	*MS*	*F*	*P-value*	*F crit*
Between Groups	2.112121	10	0.211212	15.60659	1.32E-26	1.838448
Within Groups	16.5109	1220	0.013534			
Total	18.62302	1230				

Lithologic Groups

SUMMARY						
Groups	*Count*	*Sum*	*Average*	*Variance*		
Yh/Yaq	246	402.5816	1.636511	0.019658		
Zdi-sy	722	1170.633	1.621376	0.024695		
Tdq/Tss	935	1521.702	1.627488	0.023102		
Tgd/Tgdf	170	287.6142	1.691848	0.012589		
ANOVA						
Source of Variation	*SS*	*df*	*MS*	*F*	*P-value*	*F crit*
Between Groups	0.714262	3	0.238087	10.63337	6.16E-07	2.609205
Within Groups	46.3261	2069	0.022391			
Total	47.04036	2072				

APPENDIX C: DEM-DERIVED STREAM GRADIENTS

Gross Stream Gradient

Comparisons of bedrock rebound from the strongest side of the valley versus gross stream gradient (Figure 36; $r^2 = 0.0103$, $P = 0.7669$) and the weakest side rebound versus stream gradient (Figure 37; $r^2 = 0.0198$, $P = 0.6468$) reveal no correlation between these variables at Big Creek.

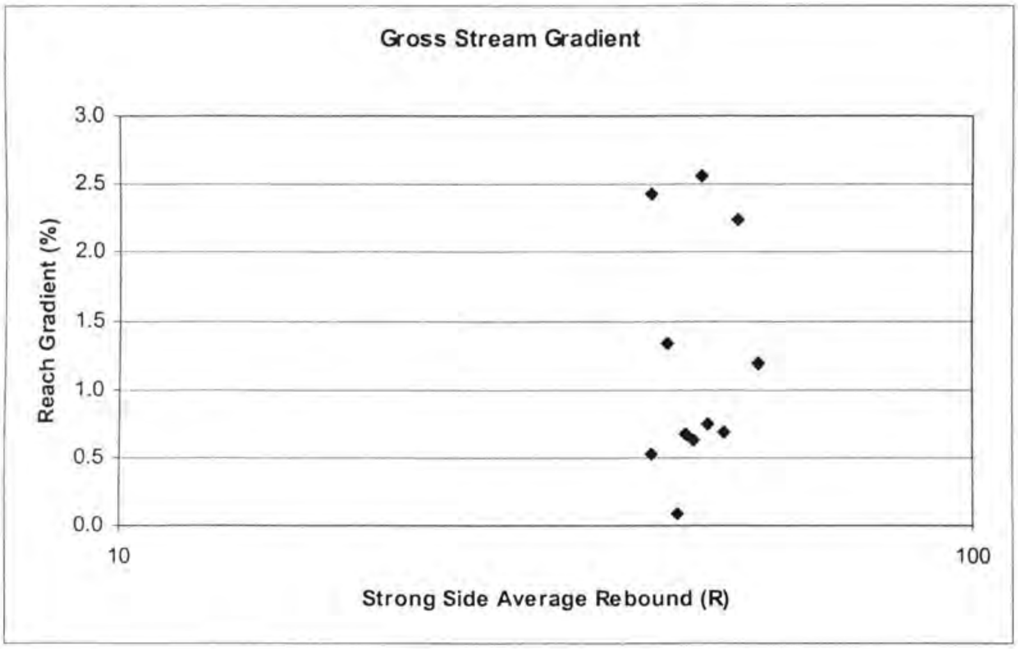

Figure 36. Semi-log graph of average rebound on the strong side of the valley vs. gross reach stream gradient ($r^2 = 0.0102$, $P = 0.7669$).

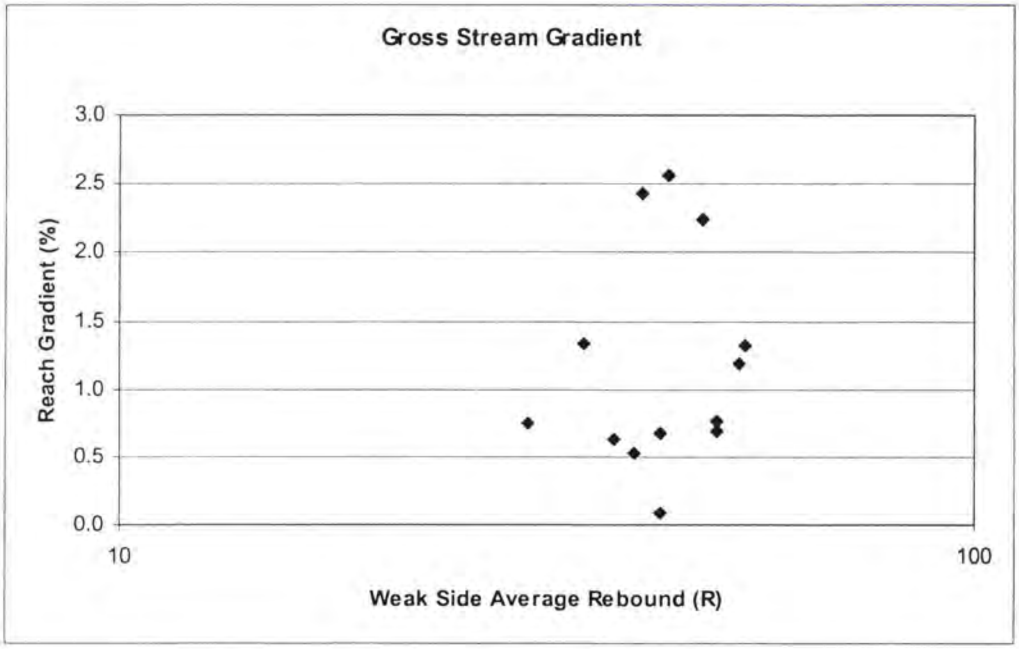

Figure 37. Semi-log graph of average rebound on the weak side of the valley vs. gross reach stream gradient (r^2 = 0.0198, P = 0.6468).

It is generally assumed that bedrock with high strength will yield steep stream gradients (Gilbert, 1877). A strong correlation exists between gradient and rebound on bedrock rivers in the Colorado Plateau (Mackley and Pederson, 2004; Pederson, pers. comm., 2005). However, the initial DEM-derived, gross stream gradients do not demonstrate this trend at Big Creek. To address the possibility that the data were inaccurate, reach gradients were calculated from DEMs in two different ways. First, each reach was centered in a window that extends 100% of the reach length upstream and downstream. A stream gradient was calculated over this longer distance (three times longer than the reach) to smooth out irregularities due to data inconsistencies or small scale variation in gradient. These stream gradients were then compared to bedrock rebound for each reach (Table 5; Figures 38 and 39). Second, gradient was calculated over each reach using a moving average with a 400m window (Table 5; Figures 40 and 41).

Buffered Stream Gradient

The stream gradients calculated with a buffer are more moderate than the original gradients calculated over the length of the reach only; values for the maximum (Dacite Gorge Reach, 1.6666%) and minimum (Lobauer Reach, 0.4762%) are less extreme. The recalculated gradients also fit into the overall pattern of the longitudinal profile better than the original reach gradients because small scale irregularities have been smoothed. The relationship between bedrock rebound and the recalculated gradients, however, is only slightly better than with the original gradients, and there is still no statistically significant relationship. The graphs of these relationships still show considerable scatter in the data. No relationship exists between these reach gradients and the strongest side of the valley (Figure 38, $r^2 = 0.1867$, $P = 0.1845$) or weakest side of the valley (Figure 39, $r^2 = 0.1261$, $P = 0.2338$).

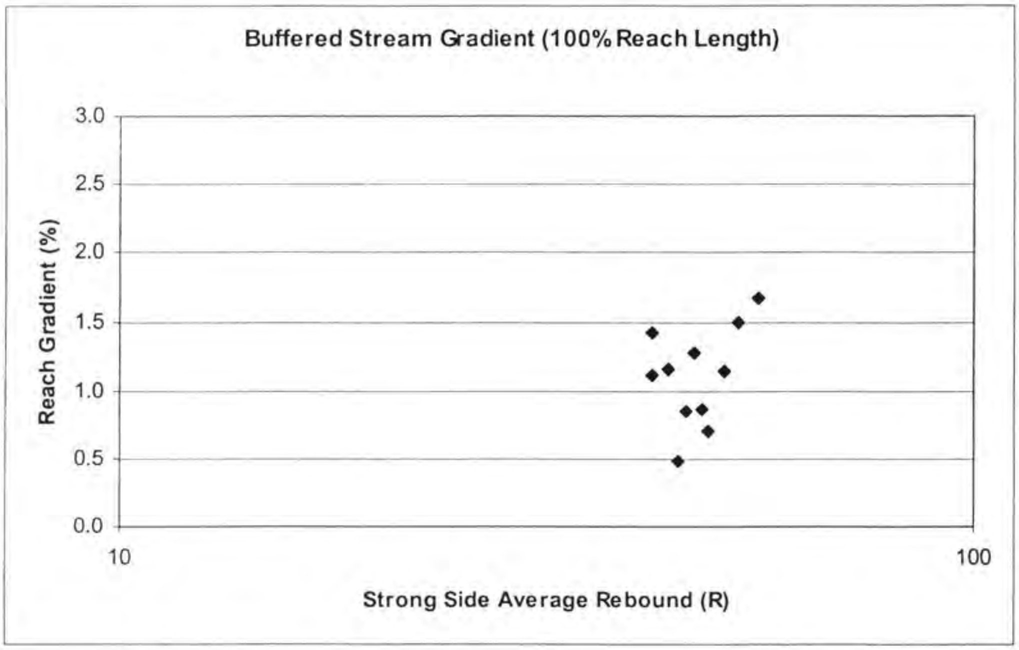

Figure 38. Semi-log graph of average rebound on the strong side of the valley vs. buffered stream gradient at each reach ($r^2 = 0.1348$, $P = 0.2667$).

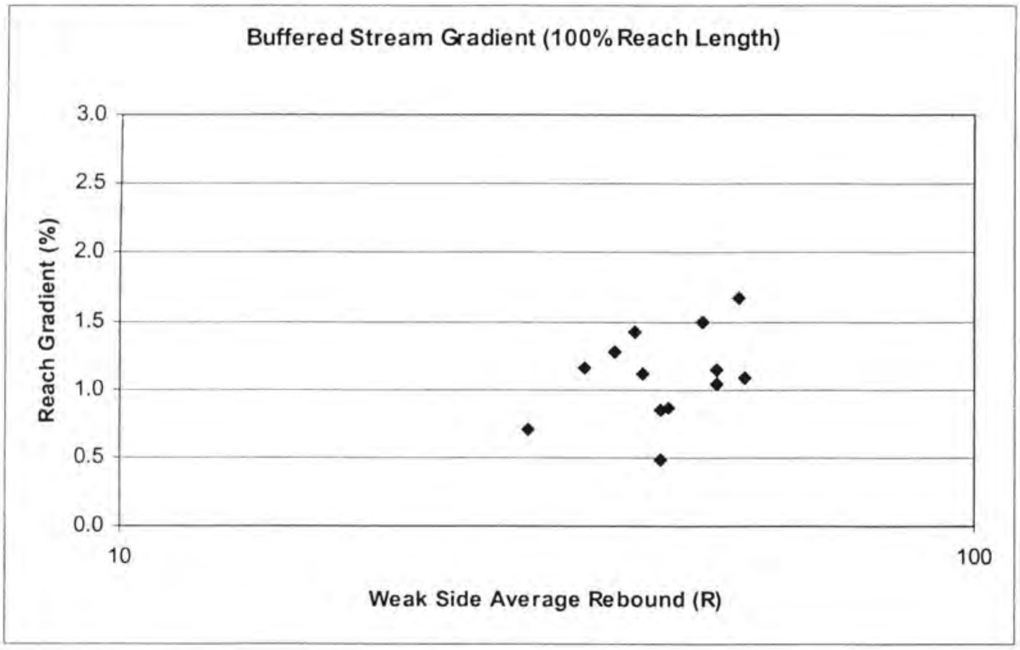

Figure 39. Semi-log graph of average rebound on the weak side of the valley vs. buffered stream gradient at each reach ($r^2 = 0.1261$, $P = 0.2338$).

Moving Average Stream Gradient

Comparing bedrock rebound to the stream gradients calculated with the moving average demonstrates again that no apparent relationship exists between these parameters at Big Creek. The graphs of the moving average gradient versus the average rebound of the strong side of the valley (Figure 40, $r^2 = 0.0478$, $P = 0.5185$) and the average rebound of the weak side of the valley (Figure 41, $r^2 = 0.0804$, $P = 0.3478$) illustrate a lack of correlation.

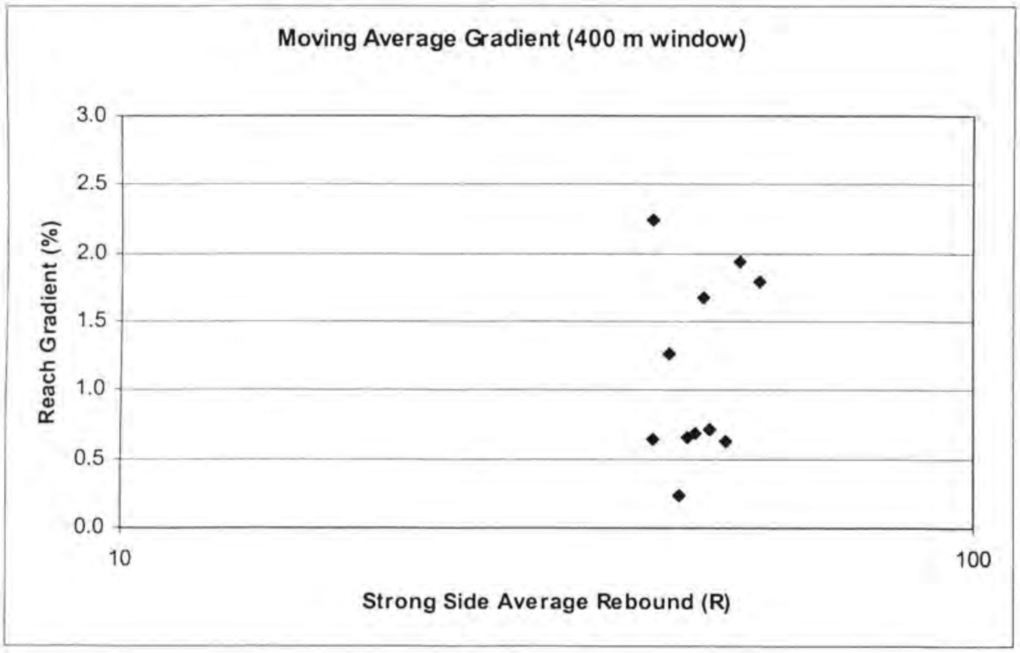

Figure 40. Semi-log graph of average rebound on the strong side of the valley vs. reach gradient calculated with a 400 m moving average window ($r^2 = 0.0478$, $P = 0.5185$).

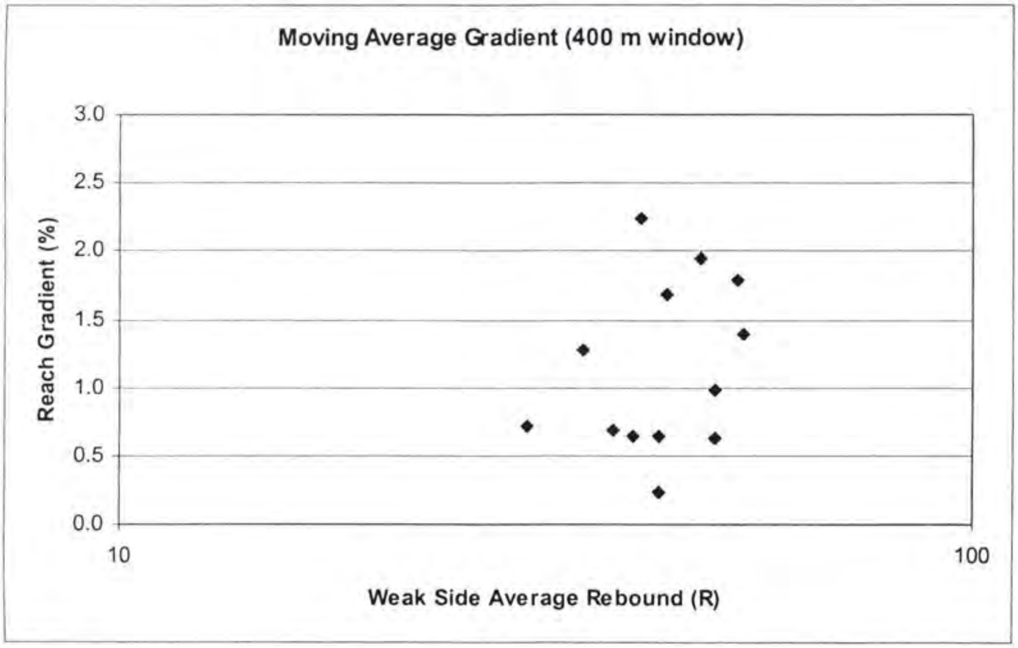

Figure 41. Semi-log graph of average rebound on the weak side of the valley vs. reach gradient calculated with a 400 m moving average window ($r^2 = 0.0804$, $P = 0.3478$).

REFERENCES

Aoki, H., Matsukura, Y., 2004, Relationship between equotip hardness and unconfined compressive strength of intact rock and weathered rock. Chikei, Transactions of the Japanese Geomorphological Union 25(3) 288.

Axelrod, D.I., 1968, Tertiary floras and topographic history of the Snake River basin, Idaho. Geological Society of America Bulletin 79, 713-734.

Basu, A., Aydin, A., 2004, A method for normalization of Schmidt hammer rebound values. International Journal of Rock Mechanics and Mining Sciences 41, 1211-1214.

Burnett, B.N., Meyer, G.A., McFadden, L.D., 2002, Microclimate controls on slope forms and processes, northeastern Arizona. Geological Society of America Abstracts with Programs 34(6), 245.

Day, M.J., 1980, Rock hardness: field assessment and geomorphic importance. Professional Geographer 32(1), 72-81.

Digital Atlas of Idaho, 2005, Available URL: http://imnh.isu.edu/digitalatlas/, accessed July 21, 2005.

Environmental Systems Research Institute, Inc., 2004, ArcMap 9.0 Geographic Information Systems software, Redlands, CA.

Gilbert, G.K., 1877, Report on the geology of the Henry Mountains. US Geographical and Geological Survey of the Rocky Mountain Region, Washington, D.C.

Grant, G.E., Swanson, F.J., 1995, Morphology and processes of valley floors in mountain streams, Western Cascades, Oregon. In: Costa, J.E., et al. (Eds.), Natural and anthropomorphic influences in fluvial geomorphology, Geophysical Monograph 89, American Geophysical Union, pp. 83-101.

Grassland, Soil and Water Research Laboratory, USDA, 2002, Soil and Water Assessment Tool software, Temple, TX.

Hancock, G.S., Anderson, R.S., Whipple, K.X., 1998, Beyond power: Bedrock river incision process and form. In: Tinkler, K., Wohl, E.E. (Eds.), Rivers over rock: Fluvial processes in bedrock channels. American Geophysical Union, Geophysical Monograph 107, 35-60.

Howard, A.D., Seidl, M.A., Dietrich, W.E., 1994, Modeling fluvial erosion on regional to continental scales. Journal of Geophysical Research 99, 13971-13986.

ISRM, 1981, Rock characterization testing and monitoring, ISRM suggested methods. International Society for Rock Mechanics, Pergamon, Oxford Press, pp. 101-102.

Janecke, S.U., 1994, Sedimentation and paleogeography of an Eocene to Oligocene rift zone, Idaho and Montana. Geological Society of America Bulletin 106, 1083-1095.

Janecke, S.U., Hammond, B.F., Snee, L.W., Geissman, J.W., 1997, Rapid extension in an Eocene volcanic arc: Structure and paleogeography of an intra-arc half graben in central Idaho. Geological Society of America Bulletin 109(3), 253-267.

Jordan, B.T., 1994, Emplacement and exhumation of the southeastern Atlanta lobe of the Idaho Batholith and outlying stocks, south-central Idaho. M.S. thesis, Idaho State University, Pocatello, 110 p.

Kahraman, S., 2001, A correlation between P-wave velocity, number of joints, and Schmidt hammer rebound number. International Journal of Rock Mechanics and Mining Sciences 38, 729-733.

Katz, O., Reches, Z., Roegiers, J.C., 2000, Evaluation of mechanical rock properties using a Schmidt hammer. International Journal of Rock Mechanics and Mining Sciences 37, 723-728.

Knight, R.D., 2004, Physics for scientists and engineers: a strategic approach. Pearson, San Francisco, pp. 470-471.

Leonard, B.F., Marvin, R.F., 1982, Temporal evolution of the Thunder Mountain caldera and related features, central Idaho. In: Bonnichsen, B., Breckenridge, R.M. (Eds.), Cenozoic geology of Idaho. Idaho Bureau of Mines and Geology Bulletin 26, 23-41.

Lewis, R.S., Kiilsgaard, T.H., Bennett, E.H., Hall, W.E., 1987, Lithologic and chemical characteristics of the central and southeastern part of the southern lobe of the Idaho batholith. In: Vallier, T.L., Brooks, H.C. (Eds.), Geology of the Blue Mountains region of Oregon, Idaho, and Washington: The Idaho batholith and its border zone. United States Geological Survey Professional Paper 1436, pp. 171-196.

Link, P.K., Janecke, S.U., 1999, Geology of east-central Idaho: Geologic roadlogs for the Big and Little Lost River, Lemhi, and Salmon River Valleys. In: Hughes, S.S., Thackray, G.D. (Eds.), Guidebook to the Geology of Eastern Idaho: Pocatello, Idaho Museum of Natural History, pp. 219-235.

Link, P.K., Reading, R.W., Godfrey, A.E., Prevedal, D., 1999, Topographic development of Southern Idaho: The passage of the Yellowstone-Snake River Plain hotspot. In: Hughes, S.S., Thackray, G.D. (Eds.), Guidebook to the Geology of Eastern

Idaho: Pocatello, Idaho Museum of Natural History, pp. 219-235.

Link, P.K., Winston, D., Lewis, R.S., 2002, Subdivisions of the Mesoproterozoic Yellowjacket Formation and Hoodoo Quartzite, Salmon River Mountains, central Idaho. Geological Society of America Abstracts with Programs 34(4), 18.

Link, P.K., Winston, D., Boyack, D., 2003, Stratigraphy of the Mesoproterozoic Belt Supergroup, Salmon River Mountains, Lemhi County, Idaho. In: Lageson, D.R., Christner, R.B., (Eds.), 2003 Tobacco Root Geological Society field conference at the Belt symposium IV, Northwest Geology 32, 107-123.

Lund, K., Derkey, P.D., Brandt, T.R., Oblad, J.R., 1998, Digital geologic map database of the Payette National Forest and vicinity, Idaho: U.S. Geological Survey Open-File Report 98-219-B, url: http://geology.cr.usgs.gov/pub/open-file-reports/ofr-98-219-b/.

Mackley, R.D., Pederson, J.L., 2004, Large-scale geologic control of the Colorado River's profile through Glen and Grand Canyons, UT and AZ; testing J.W. Powell's hypothesis. Geological Society of America Abstracts with Programs 36(4), 13.

Malde, H.E., 1991, Quaternary geology and structural history of the Snake River Plain, Idaho and Oregon. In: Morrison, R.B. (Ed.), Quaternary nonglacial geology: Conterminous U.S. Geological Society of America, The Geology of North America K2, 252-282.

McCarroll, D., 1991, The Schmidt hammer, weathering, and rock surface roughness. Earth Surface Processes and Landforms 16, 477-480.

McFadden, L.D., Eppes, M.C., Gillespie, A.R., Hallet, B., 2005, Physical weathering in arid landscapes due to diurnal variation in the direction of solar heating. Geological Society of America Bulletin 117(1-2), 161-173.

Meyer, G.A., Leidecker, M.E., 1999, Fluvial terraces along the Middle Fork Salmon River, Idaho, and their relation to glaciation, landslide dams, and incision rates. A preliminary analysis and river-mile guide, In: Hughes, S.S., Thackray, G.D. (Eds.), Guidebook to the Geology of Eastern Idaho: Pocatello, Idaho Museum of Natural History, pp. 219-235.

Montgomery, D.R., Buffington, J.M., 1997, Channel-reach morphology in mountain drainage basins. Geological Society of America Bulletin 109(5), 596-611.

Othberg, K.L., 1994, Geology and geomorphology of the Boise valley and adjoining areas, western Snake River Plain, Idaho. Idaho Geological Survey Bulletin 29, 54 pp.

Sklar, L.S, Dietrich, W.E., 2001, Sediment and rock strength controls on river incision into bedrock. Geology 29(12), 1087-1090.

Sklar, L., Dietrich, W.E., 2004, A mechanistic model for river incision into bedrock by saltating bedload. Water Resources Research 40 (6).

Stewart, D.E., Lewis, R.S., and Link, P.K., 1995-2004, Unpublished maps, Idaho Geological Survey.

Strahler, A.N., 1952, Hypsometric (area-altitude curve) analysis of erosional topography. Geological Society of America Bulletin 63(11), 1117-1141.

Sumner, P., Nel, W., 2002, The effect of rock moisture on Schmidt hammer rebound, tests on rock samples from Marion Island and South Africa. Earth Surface Processes and Landforms 27, 1137-1142.

Sweetkind, D.S., Blackwell, D.D., 1989, Fission-track evidence of the Cenozoic thermal history of the Idaho batholith. Tectonophysics 157, 241-250.

Terzaghi, K., 1962, Stability of steep slopes in hard unweathered rock. Geotechnique 12, 251-270.

Thorne, C.R., 1982, Processes and mechanisms of river bank erosion. In: Hey, R.D., Bathurst, J.C., Thorne, C.R. (Eds.), Gravel-Bed Rivers, John Wiley and Sons, Chichester, pp. 227-271.

Tysdal, R.G., Lund K.I., Evans, K.V., 2003, Geologic map of the western part of the Salmon National Forest, In: Evans, K.V., Green, G.N. (Eds.), Geologic map of the Salmon National Forest and vicinity, East-Central Idaho, U.S. Geological Survey Geologic Investigations Series I-2765.

United States Geological Survey, 2005, available URL: http://edc.usgs.gov/guides/dem.html, accessed June 24, 2005.

Vutukuri, V.S., Lama, R.D., Saluja, S.S., 1974, Handbook on mechanical properties of rocks. Volume 1: Testing techniques and results. Trans Tech Publishers, Bay Village, Ohio, pp. 105-115.

Western Regional Climate Center, 2005, available URL: http://www.wrcc.dri.edu/cgi-bin/cliMAIN.pl?idtayl, accessed July 11, 2005.

Whipple, K.X., Hancock, G.S., Anderson, R.S, 2000, River incision into bedrock: Mechanics and relative efficacy of plucking, abrasion, and cavitation. Geological Society of America Bulletin 112(3), 490-503.

Williams, R.B.G., Robinson, D.A., 1983, The effect of surface texture on the